Enhancing sustainable development of the winter bait fishery for Atlantic menhaden through the use of industry acoustics

Final Report

Award Number: NOAA Grant #NA20NMF4270163
Award Period: December 1, 2020-November 30, 2023

Submitted to:

National Oceanographic and Atmospheric Administration
Fisheries Headquarters Program Office
&
Saltonstall-Kennedy Competitive Grants Program

By:

Geneviève Nesslage, Ph.D.
University of Maryland Center for Environmental Science
Chesapeake Biological Laboratory
Solomons, Maryland

February 13, 2024

2022 Cooperative Atlantic Menhaden Winter Survey Collaborators

Principal Investigator
Geneviève Nesslage (UMCES Chesapeake Biological Laboratory)

Co-Principal Investigators
James Gartland & Robert Latour (Virginia Institute of Marine Science)
Christopher Gurshin (ASA Analysis & Communication, Inc)
Dong Liang (UMCES Chesapeake Biological Laboratory)

Industry Collaborators
Stefan Axelsson & Leif Axelsson (H&L Axelsson Inc.)
Wayne Reichle & Jeff Kaelin (Lund's Fisheries, Inc.)

Federal & State Partners
Michael Jech (NOAA Fisheries Northeast Fisheries Science Center)
Ray Mroch (NOAA Fisheries Southeast Fisheries Science Center Beaufort Laboratory)
Jeffrey Brust (New Jersey Department of Environmental Protection)

Field and Laboratory Scientific Teams
Chief Scientist - Dustin Gregg (Virginia Institute of Marine Science)
Survey Team - Charlie Jordan, Matt Farnham, Chris Bonzek (Virginia Institute of Marine Science)
Ageing Team – Jameson Gregg (Virginia Institute of Marine Science), Amanda Rezek (NOAA Fisheries Southeast Fisheries Science Center Beaufort Laboratory), Jamie Darrow (New Jersey Department of Environmental Protection)

EXECUTIVE SUMMARY

Prior to this study, little information was available to inform sustainable development of winter bait fishing opportunities for Atlantic menhaden (*Brevoortia tyrannus*) by the Mid-Atlantic midwater trawl fleet. Thus, academic, federal, state, and private scientists teamed with fishing industry members to design and implement a cooperative acoustic survey for Atlantic menhaden. The primary goal of this survey was to generate estimates of biomass and characterize size, age, and sex, and maturity of the portion of the Atlantic menhaden stock that overwinters off the coast of New Jersey where the winter Atlantic menhaden bait fishery is concentrated. This survey was funded by the NOAA Saltonstall-Kennedy Competitive Grants Program (Award #NA20NMF4270163), which aims to provide science and technology necessary to support sustainable fisheries development.

The survey was conducted during February 14-24, 2022. We systematically surveyed the primary bait fishing region 13-43 nmi (15-50 mi) offshore of New Jersey from the southern border of Hudson Canyon to the Delaware border using a commercial midwater trawling vessel, the *F/V Dyrsten*, which was equipped with a recordable Simrad ES80 split-beam, hull-mounted 38kHz ES38B transducer and FSV25S (20 kHz) omnidirectional sonar. A subset of schools encountered were ensonified and captured for comparison of acoustic school biomass estimates with school weight measured at port. Biological samples were collected from trawled schools to characterize the age, size, sex, and maturity of fish in each school. Additional samples were collected by the survey team at sea while accompanying fishing operations for five days after the survey and at port throughout the remainder of the winter Atlantic menhaden fishing season. Acoustic data were processed and analyzed to produce estimates of school biomass and to evaluate the utility of industry acoustics in cooperative research. To quantify ageing uncertainty, an exchange of paired hard parts (scales and otoliths) collected from individually sampled fish was conducted among the Virginia Institute of Marine Science (VIMS), NOAA Fisheries Southeast Fisheries Science Center Beaufort Laboratory (Beaufort), and New Jersey Department of Environmental Protection (NJDEP).

Of the 38 schools identified as Atlantic menhaden along survey transects, 12 were ensonified and three were sampled (2,132 fish were sampled for size and 80 for full workups, including paired scale and otolith ages). During post-survey data collection, an additional 155 schools were identified as Atlantic menhaden, 94 were ensonified, and two were sampled (2,005 size samples and 72 full workups). An additional five fishing trips were sampled at port (150 full workups). Throughout acoustic data collection, an additional 73 schools could not be identified to species and were classified as “other fish” or “small pelagic school”; however, the total unidentifiable biomass was 58,661 kg, representing only 3% of the total biomass of Atlantic menhaden ensonified (1,754,563 kg).

Acoustic estimates of school biomass were similar to trawl catch weight of each trawled school as measured at port. All schools sampled during survey and post-survey operations were highly homogeneous schools of Atlantic menhaden. Out of 1,361 mt (3,110,380 lbs) of Atlantic menhaden landed and over 4,299 fish sampled during the 2022 survey and fishing season, only one American shad (*Alosa sapidissima*) was collected in a sampling bucket during post-survey at-sea sampling operations and <30 fish of other species were noted by survey crew during catch processing. Size of Atlantic menhaden sampled was similar across sampling periods.

Both the NOAA Beaufort Laboratory and VIMS agers estimated that most Atlantic menhaden sampled during this project were ages 3 and 4, regardless of whether ages were based on scales or otoliths. Sampled Atlantic menhaden were 56% female and displayed sexual dimorphism such that average weight and length of females (273 mm, 0.32 kg) was larger than that of males (267 mm, 0.30 kg). Most sampled Atlantic menhaden that received full workups were visually identified as being mature (resting stage). The ageing exchange demonstrated low interlab agreement, likely due to the focus on larger, older fish, the early time of year during which samples collected, and the quality of scale samples collected given the gear used. However, the exchange demonstrated the potential for the use of otoliths in future ageing work, and agers are committed to a second exchange in 2024 to identify differences and come to an agreement on best practices for ageing older Atlantic menhaden.

Total biomass of Atlantic menhaden estimated in the study area ranged between 7,963 mt (17,556,115 lbs) using a traditional ratio estimator and 11,005 mt (24,261,843 lbs) using a spatial model that accounted for changes in school detectability due to large changes in water temperature during the survey period that likely affected schooling behavior. In comparison with the 2022 stock assessment, the biomass of overwintering Atlantic menhaden estimated in the study region is a small fraction (approximately 0.22-0.31%) of estimated coastwide total biomass of age 1+ fish. From a management perspective, New Jersey's winter bait fishery quota in a typical year is approximately 680 mt (1.5 million lbs), which represents a small fraction (6%-9%) of the total estimated biomass in the study area.

This study provided fishery-independent field confirmation that Atlantic menhaden are partial migrants such that a portion of the adult stock resides overwinter along the shelf in the Mid-Atlantic region. Given the dense schooling behavior of Atlantic menhaden, we demonstrated that alternative acoustic survey designs that account for the patchy distribution of large schools across the landscape should be employed when surveying for pelagic clupeids like Atlantic menhaden. Our study provides an effective survey design that may prove useful in future monitoring.

CONTENTS

BACKGROUND

Atlantic menhaden (*Brevoortia tyrannus*) supports the largest commercial fishery by weight on the U.S. East Coast (National Marine Fisheries Service 2018). The commercial fishery consists of two main components, namely a reduction fishery (approximately 70% of landings) located primarily in the Chesapeake Bay and nearby coastal waters, and a coastwide bait fishery (approximately 30% of landings). Although most bait fishing for Atlantic menhaden occurs in estuaries and coastal waters, midwater trawl fishermen initiated a new and highly successful winter bait fishery in 2014 along the offshore portion of the Mid-Atlantic shelf from New Jersey to Southern New England. To help determine if development of this winter bait fishery for Atlantic menhaden is sustainable, more information on the size and age structure of the overwintering stock was needed.

Despite the economic and ecological importance of the Atlantic menhaden stock (Garrison et al. 2010, SEDAR 2015, Buchheister et al. 2016), data to support management is sparse, particularly in the northern portion of the range. Most biological samples used to inform stock assessment are obtained from the reduction fishery which, although well sampled, no longer regularly operates across most of the stock's range, which extends from Florida to Nova Scotia (SEDAR 2015). Thus, data collected during the last few decades have been concentrated in the Chesapeake Bay region south of the winter bait fishery during spring through fall. Although biological samples are collected from the winter bait fishery as required in Amendment II to the Atlantic States Marine Fisheries Commission's Atlantic Menhaden Fishery Management Plan (ASMFC 2012), sampling intensity is landings-based and thus limited by catch-based quotas. Another reason little is known about the northern, overwintering portion of the Atlantic menhaden stock is that there is no dedicated survey designed to target Atlantic menhaden. Traditional bottom trawl surveys rarely encounter Atlantic menhaden because fish are highly mobile and school near the surface throughout most of the year. Although Atlantic menhaden schools typically spend most of the day deep below the surface when water temperatures drop in winter (June and Reintjes 1959, Reintjes 1969, Ahrenholz 1991, Smith 1991), agency surveys do not operate during this time or far enough offshore to reliably encounter overwintering Atlantic menhaden. Thus, a need was identified for the development of new methods for surveying overwintering Atlantic menhaden.

To address this challenge, simulation testing of a novel survey design tailored to Atlantic menhaden winter biology and behavior was conducted during 2017-2018 with funding provided by the National Science Foundation, Science Center for Marine Fisheries (award #1266057). This study estimated the accuracy and precision of a hydroacoustic survey for Atlantic menhaden using a combination of bait fishery Vessel Trip Reports, observed bycatch records, and water condition data collected during winter months off the coast of New Jersey. Results suggested that the use of traditional acoustic survey designs would produce biomass estimates with poor precision and accuracy due to patchiness of large Atlantic menhaden schools across the landscape. Instead, the combined use of downward-viewing echosounder and an omni-directional sonar allowed the search range to be expanded along each transect and generated biomass estimates with a coefficient of variation approximately 25% (Liang et al. 2020). This novel acoustic survey design was implemented in winter 2022 as described below by a team of academic, federal, state, and private scientists and fishing industry members with funding provided by the Saltonstall-Kennedy Competitive Grants Program.

The goals of this cooperative survey were to:
1. address industry's need for collection of novel scientific data to support sustainable development of enhanced fishing opportunities,
2. expand the use of cooperative science, and
3. reduce uncertainty in assessment and management of Atlantic menhaden.

The objectives of this cooperative survey were to:
1. estimate overwintering biomass and structure of Atlantic menhaden in the winter bait fishery's primary fishing area,
2. evaluate performance of industry acoustics in estimating Atlantic menhaden biomass,
3. evaluate ageing uncertainty, and
4. effectively communicate and disseminate project findings to menhaden scientists and fishery managers.

METHODS

Survey design and preparation

Atlantic menhaden encountered by the winter bait fishery typically form large sedentary schools that drop below the surface waters during the day and demonstrate reduced vessel avoidance when water temperatures offshore of New Jersey drop to ~4-6ºC. Using a spatially explicit model, the performance of a suite of hydroacoustic survey designs were simulation-tested in order to determine the best approach for surveying Atlantic menhaden during their more sedentary overwintering period and estimate the total transect distance that needed to be surveyed to achieve an acceptable level of precision (Liang et al. 2020). Classical downward-sounding acoustic survey design led to low precision of biomass estimates because Atlantic menhaden form extremely large schools that are patchily distributed across the landscape. Acceptable precision was achieved with a two-stage survey design in which a combination of industry acoustics and midwater trawling was used to estimate stock biomass within the study region. With this design, schools are detected along a series of transects within a wide search area (1,600m on either side of the vessel) using omnidirectional sonar, and a downward-facing echosounder provided *in situ* acoustic-based estimates of school biomass for a subset of schools encountered within the search area. For more details on survey design justification, see Liang et al. 2020.

Prior to survey implementation, a protocol for research involving animals was approved by the UMCES Institutional Animal Care and Use Committee (Protocol F-CBL-21-07), a Scientific Research/Cruise Plan was submitted to UMCES, a Scientific Research Letter of Acknowledgement was obtained from NOAA Fisheries Greater Atlantic Regional Fisheries Office (21003), and a Scientific Collecting Permit was obtained from NJDEP (2022-1903).

Survey implementation

The survey was conducted using a 49 m (160 ft) commercial midwater trawling vessel, the *F/V Dyrsten*, that is owned and operated by H&L Axelsson, Inc. (Fig. 1). The *F/V Dyrsten* utilized a Cosmos Trawl net with an 18-m vertical opening, 51-m horizontal opening, and mesh size of 3.8cm in the cod end. The vessel was equipped with a recordable Simrad ES80 7° split-beam, hull-mounted 38kHz ES38B transducer, and Furuno

Figure 1. F/V Dyrsten, Cape May, NJ.

FSV25S (20 kHz) omnidirectional sonar. Unlike previous Simrad industry-grade echosounders, the ES80 echosounder does not contain a systematic "triangle-waver" error component.

The survey was initially scheduled to begin the first week of February 2022, but was delayed until mid-February due to warm ocean temperatures (Table 1). The ES80 echosounder was calibrated offshore of Cape May, NJ February 11-13 using a wireless calibration system developed at the Northeast Fisheries Science Center to position the tungsten carbide (with 6% cobalt binder) sphere (e.g., 38.1-mm diameter) under the transducers to map the beam pattern and measure the on-axis response using the standard sphere method. Additional details on field calibration can be found in Appendix A.

Table 1. 2022 Cooperative Atlantic Menhaden Winter Survey timeline

Date	Survey event
Feb 11-Feb 13, 2022	At-sea sonar calibration
Feb 14-Feb 15, 2022	Transects 1-2 ("Leg 1")
Feb 16-Feb 19, 2022	Survey suspended due to severe storm
Feb 20-Feb 24, 2022	Transects 3-6 ("Leg 2")
Feb 28-Mar 4, 2022	Additional at-sea samples collected by VIMS during fishing ("Leg 3")
Mar 6-Mar 22, 2022	Additional port samples collected by Lund's Fisheries

Transects 1 and 2 were surveyed February 14-15 during which Atlantic menhaden schools were encountered, and a subset were ensonified, trawled, and sampled (details below). The vessel returned to port to offload and weigh the catch on February 15. The survey was suspended February 16-19 due to a severe winter storm. When the survey resumed February 20-24 to complete Transects 3-6, oceanographic conditions had changed and the dense menhaden schools observed near the ocean floor prior to the storm had dispersed into small schools near the surface.

The survey was completed earlier than expected on February 24. Given additional sea days were available, the VIMS survey team returned to the vessel February 28-March 4 and continued to ensonify and sample additional Atlantic menhaden schools and collect hydrographic data during targeted fishing operations. Once VIMS crew were no longer accompanying the vessel, industry partner Lund's Fisheries collected additional port samples throughout the remainder of the fishing season and delivered them to VIMS for preparation and analysis

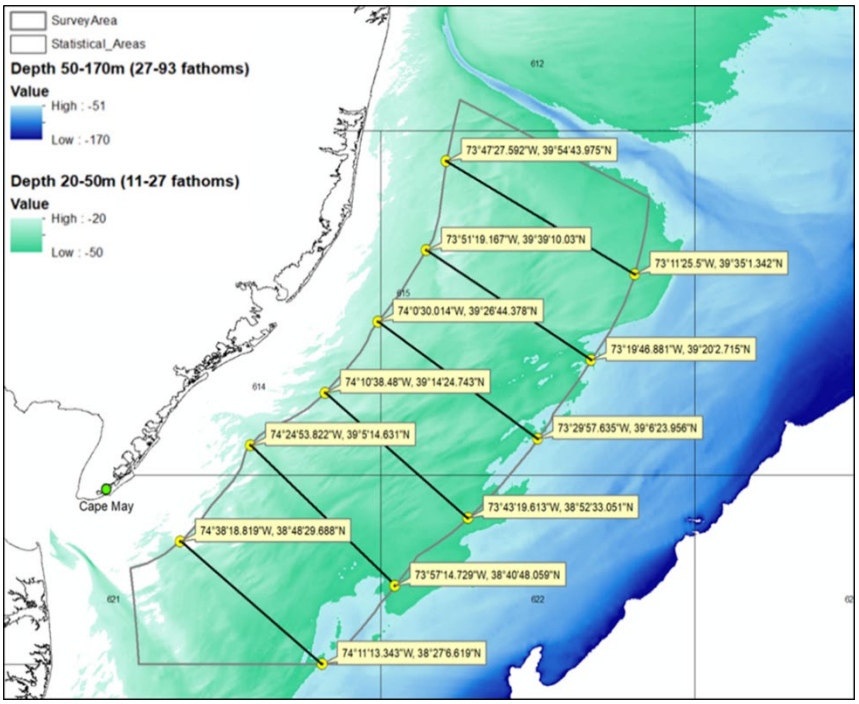

Figure 2. 2022 Cooperative Atlantic Menhaden Winter Survey area (black line) 15-50 miles off the coast of New Jersey. Colors indicate depth (m).

During the survey (February 14-24), six systematic transects with an average length of 58 km were surveyed with approximately 29 km between transects (Fig. 2). Transects were oriented perpendicular to shore beginning at a random starting latitude between 73°44'56.4919"W 40°5'23.5729"N and 73°51'57.8296"W 39°38'15.5024"N. The survey began with the southernmost Transect 1 at the point nearest to shore and proceeded northward (Table 2). The direction of transects alternated such that Transect 1 was run inshore to offshore, Transect 2 was run offshore to inshore, and so on. Transects were of variable length due to the irregular shape of the study area and random start location. GPS coordinates of each transect and the entire survey track were recorded in VIMS's Fisheries Environment for Electronic Data software.

Table 2. Starting and ending coordinates of survey transects.

	Direction	Start Longitude	Start Latitude	End Longitude	End Latitude
Transect 1	Offshore	74°38'18.819"W	38°48'29.688"N	74°11'13.343"W	38°27'6.619"N
Transect 2	Inshore	73°57'14.729"W	38°40'48.059"N	74°24'53.822"W	39°5'14.631"N
Transect 3	Offshore	74°10'38.48"W	39°14'24.743"N	73°43'19.613"W	38°52'33.051"N
Transect 4	Inshore	73°29'57.635"W	39°6'23.956"N	74°0'30.014"W	39°26'44.378"N
Transect 5	Offshore	73°51'19.167"W	39°39'10.03"N	73°19'46.881"W	39°20'2.715"N
Transect 6	Inshore	73°11'25.5"W	39°35'1.342"N	73°47'27.592"W	39°54'43.975"N

All transects were surveyed during daylight hours. The vessel sampled along the transects at approximately 7 knots (3.6 m/s) with the ES80 split-beam echosounder while the omnidirectional sonar was used to search for schools within a distance of 1,600 m on either side of the transect (vessel). The ES80 7° split-beam echosounder mounted to the hull of the vessel collected at the fastest ping rate setting in narrowband ("continuous wave") mode and 0.256-ms pulse duration. The acoustic backscatter from the omnidirectional sonar was scrutinized in real time by experienced fishing captain Stefan Axelsson and Chief Scientist Dustin Gregg. GPS coordinates, heading, and approximate distance from the vessel of all schools identified in real time by the omnidirectional sonar were recorded. If schools were detected, the vessel would break from the planned transects to collect backscatter of the schools encountered (Fig. 3). A unique school ID

number was assigned to each school identified and a log was created with timestamps for corresponding ES80 data files. Before leaving the transect, the vessel marked its location, and, once schools were ensonified, the vessel then proceeded to the closest point on the original transect and resumed searching.

When trawl sets were initiated, GPS coordinates and times (synchronized with the echosounder clock) marking the beginning and end of each tow were recorded in VIMS's Fisheries Environment for Electronic Data software. Trawled catch from each school was pumped into separate tanks and individually weighed dockside by the bait processor for comparison with *in situ* acoustic biomass estimates of each school.

In addition to ensonifying menhaden schools during the day on survey transects, the survey team took the opportunity to collect echosounder data on an additional 30 schools at dusk as schools began to break up and disperse to feed. These data will be used in future analysis of menhaden to explore diel migration patterns, schooling behavior, and target strength.

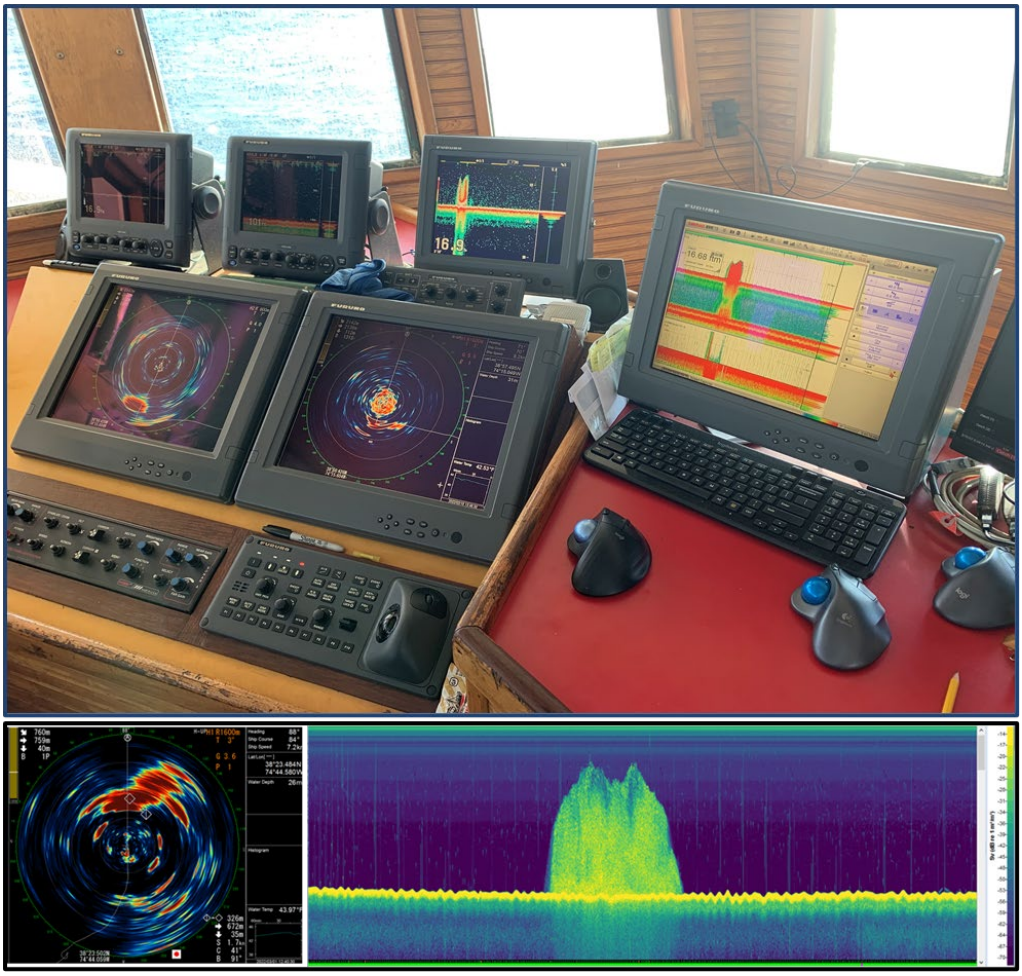

Figure 3. (Top) Instrumentation and sonar displays at helm of 49-m commercial midwater trawling vessel, F/V Dyrsten, equipped with a recordable 38 kHz Simrad ES80 split-beam echosounder and a Furuno FSV25S omnidirectional sonar. (Bottom) Paired Furuno omnidirectional (left) and ES80 echosounder (right) images of ensonified School 49.

Biological samples were collected from each trawled school to provide information on school structure. VIMS scientists subsampled the catch from the net pump using NEFOP's Catch Composition Technique for purse seine and midwater trawl operations, as recommended by the ASMFC Atlantic Menhaden Technical Committee (August 10, 2020 memo). Once the cod end had been brought alongside the vessel, the chief scientist asked the captain for an estimate of pumping time for that haul. The estimated pumping time was divided by 10 to yield the sampling interval (e.g., estimated pumping time = 20 minutes, sampling interval = 2 minutes, yield = 10 baskets of sample).

From each basket collected, 10 individual fish received full processing, which included the following elements: fork length (mm), total length (mm), whole weight (kg), eviscerated weight (kg), macroscopic sex (male/female/unknown), and macroscopic maturity stage (immature/mature-resting/ mature-ripe /mature-spent). A scale patch (~50 scales) was also collected, stored in labeled vials, and frozen. The head was removed and frozen for later extraction and preparation of both sagittal otoliths for ageing. For female menhaden, both ovaries were removed, weighed, and preserved in Normalin for later reproductive evaluation. Once 10 menhaden from each basket had been sampled in this manner, individual length (fork and total) and individual whole weight were recorded for the remaining Atlantic menhaden specimens. Although very little bycatch was encountered, all other species collected during sampling operations were recorded and individual length and individual whole weight data were collected. School number, set number, and GPS location of the set was associated with each biological sample. Sampled menhaden carcasses and bycatch were deposited overboard once data collection was complete.

Hydrographic data were collected at each trawl set location and systematically 10 km apart along each transect to characterize ocean conditions and habitat use. A profile of depth (m), water temperature (ºC), salinity (PSU), and dissolved oxygen concentration (mg/l) was recorded at each location using Hydrolab's Hydras3 LT software.

All biological sampling and water quality data were immediately saved in two locations, the local workstation computer and an onboard server. Upon completion of the cruise, all trawl collection subsampling and hydrographic data were audited at VIMS using a series of custom-built routines designed to effectively and efficiently identify and correct at-sea data entry errors.

School biomass estimation

A summary of acoustic data calibration, processing, and analysis is provided here; complete documentation can be found in Appendix A.

Echoview calibration

Echoview software (version 12.1 or 13, Hobart, Tasmania) was used to process and export acoustic estimates of Atlantic menhaden biomass. ES80 data files of the calibration sphere were used to adjust calibration results from the field. In Echoview, the sound speed was updated based on water temperature in the data file source (surface temperature from the ship's NMEA network) and user-entered salinity estimate. Target strength of the sphere was determined from single echo detections within the region in the echogram corresponding to the echo traces of the sphere (Appendix A Figs. 3-1 and 3-2). Single echo detection criteria selected in Echoview are given in Appendix A Table 3-1. Single echo detections were also analyzed after filtering out single echoes greater than 0.5° off the acoustic axis.

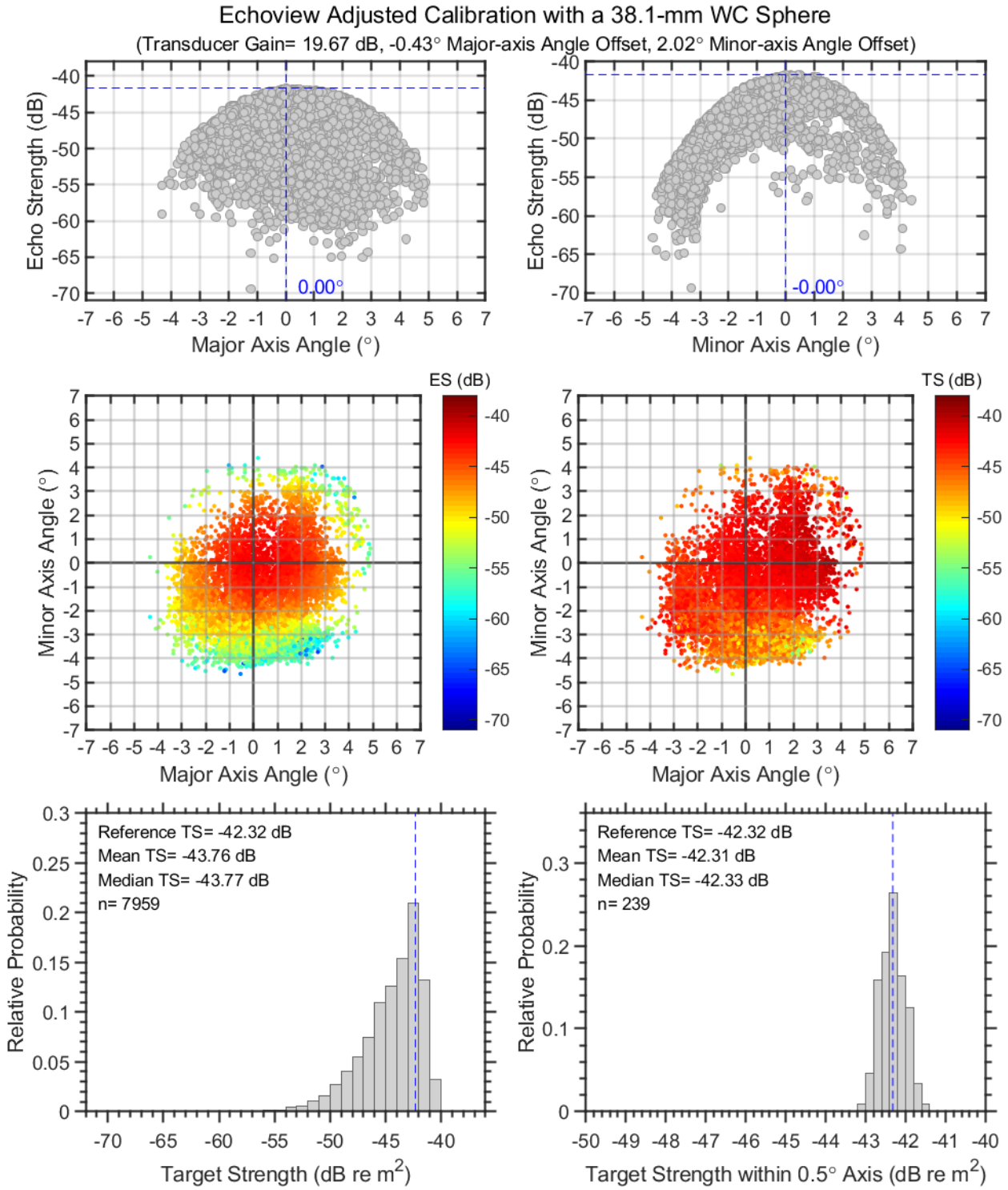

Figure. 4. TOP and MIDDLE: Angular target strength plots of 38.1 mm Tungsten Carbide sphere with on-axis adjustments of transducer gain to 19.67 dB and major and minor axis angle offsets of -0.43° and 2.02°; BOTTOM: target strength histograms of all (left) and on-axis (right) single echo detections.

The target strength of the sphere under field conditions prior to field calibration adjustments to angles (Appendix A Figure 3-3) and after angular offsets were applied (Appendix A Figure 3-4) indicated further improvement was possible. Based on all single echo detections in Echoview, the echo strength peaked at a major axis angle offset of -0.43° and minor axis angle offset at 2.02° (Fig. 4; also Appendix A Figure 3-5). The transducer gain was adjusted to 19.67 dB such that the mean target strength of on-axis single echo detections matched the reference target strength of -42.31 dB re m^2. After the transducer gain was adjusted, a new S_a correction factor of 1.2652 dB was determined based on the on-axis sphere targets and equation 4.9 from Demer (2015). The adjusted transducer gain and S_a correction factor from the post-hoc analysis of the calibration data in Echoview was updated in the Echoview calibration supplement file.

Echogram processing

ES80 data files corresponding to schools identified in real time by the captain and chief scientist from the omnidirectional sonar were processed. The survey generated 2,788 files (878 GB) in raw ES80 data files that were timestamped at the start of each recording. Not all schools detected in the omnidirectional sonar imagery and assigned a school number (i.e., ID #) were observed or passed over with the ES80 split-beam echosounder due to various reasons, including school evasion of vessel, schools being located too high in the water columns, and potential misidentification of schools. Details on ES80 raw files processed can be found in Appendix A.

The *F/V Dyrsten* has a draft estimated to be approximately 4.3 m (14 ft) with no fish/water cargo and 5.2 m (17 ft) under full load. The transducer is mounted 1.8 m (6 ft) below the keel. For purposes of processing data and approximating the water depth, the transducer was assumed to be at a water depth of 6.5 m. The transducer was mounted securely in reverse direction where the forward arrow on the transducer was pointed to the stern. To compensate for this, a beam rotation of 180° was used during processing. The Hydrolab profile measurements were used to estimate representative average water quality conditions during each leg of the survey. The differences on sound speed estimates for each leg were negligible, and the final calibration file was updated for sound speed for each trip taken during the survey and post-survey data collection periods.

Several echograms were examined that contained small pelagic fish backscatter and large benthic Atlantic menhaden school backscatter. Minimum S_v (volume backscattering strength, dB re m^2 m^{-3}) threshold curves for selected fish backscatter versus water column background S_v following methods of Jech and Michaels (2006) would indicate a minimum S_v threshold could have been set between -50 dB and -60 dB. However, Rudstam et al. (2009) suggests setting the minimum S_v threshold to be equivalent to the minimum target strength (TS, , dB re m^2) of interest. Assuming the minimum TS of interest and minimum single echo detection criterion to be -50 dB, then the TS uncompensated for beam pattern would be -56 dB, which converts to approximately -63 dB assuming sound speed of 1475 m/s and 55 m in range. Given the minimum TS threshold of -63 dB and -66 dB minimum S_v threshold used by Jech and Michaels (2006) for Atlantic herring (*Clupea harengus*), the minimum S_v threshold used in this study was a conservative nominal value of -64 dB. Sv backscatter was filtered by masking the upper water column and removing the impulse noise spikes (Fig. 5, Appendix A Figs. 4-1 and 4-2). Noise may have been due to other depth sensors or the omnidirectional sonar equipped on the vessel.

To convert to fish per m^3 or m^2, TS was back-transformed from a dB value to a linear quantity called the backscattering cross-section ($\sigma_{bs} = 10^{(TS/10)}$). The TS representative of a single Atlantic

menhaden to use for this study does carry with it a degree of uncertainty given the lack of species-specific experimental data, model estimates, and *in situ* estimates. Exploratory analysis of the echograms containing Atlantic menhaden during this survey indicated that schools were too dense to obtain an *in situ* TS estimate. Instead, TS was estimated based on total length (TL; Simmonds and MacLennan 2008) as was done by Lucca and Warren (2018), who used a generalized TS-TL equation to acoustically estimate distribution and abundance of Atlantic menhaden in estuarine waters of Long Island, New York. Thus, the mean TS (-32.2 dB re 1 m^2) of Atlantic menhaden at 38 kHz used in this study was estimated following equation:

$$TS = 19.1Log_{10}(TL) + 0.9Log_{10}(f, kHz) - 62 \quad \text{(Eq. 1)}$$

where TS = target strength (dB re 1 m^2), TL = total length (cm), and f = acoustic frequency (kiloHertz, kHz).

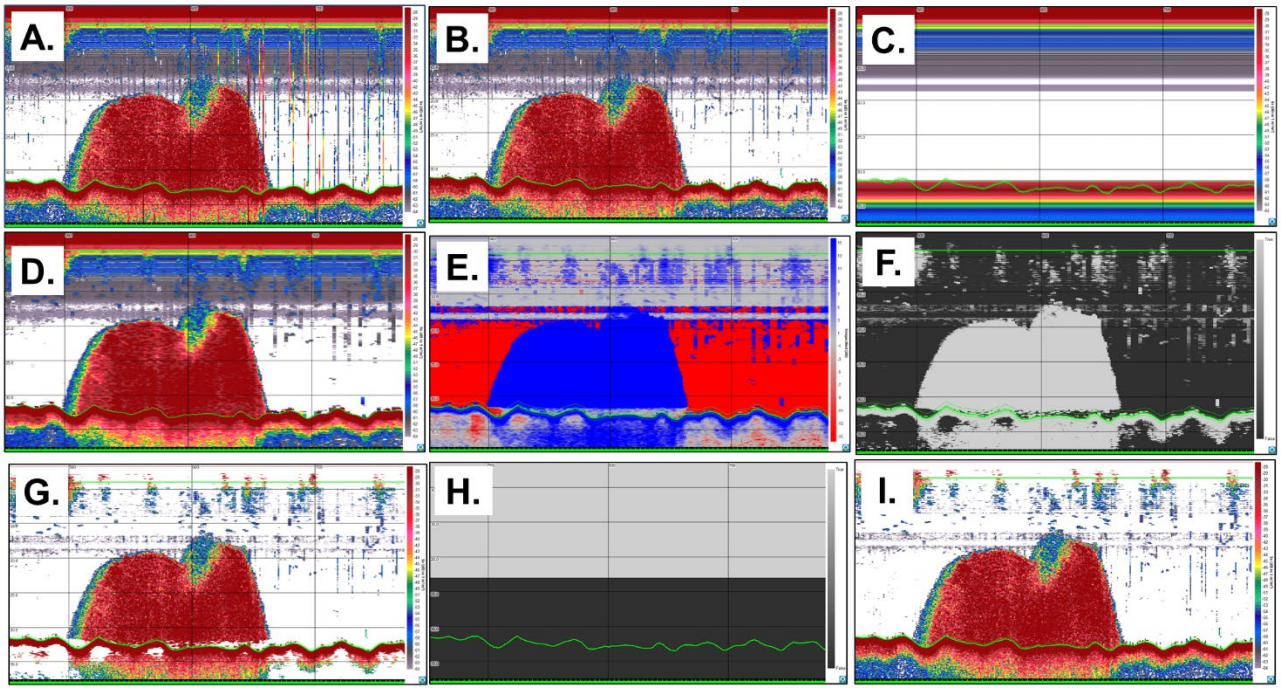

Figure 5. Step by step echogram processing: A. Raw S_v. B. Impulse noise removed. C. Resampled (median of 2000 ping × 3 sample window and matched S_v pings. D. Smoothed 3×3 S_v. E. Signal-to-Noise Ratio (SNR). F. Mask |SNR| > 3 dB. G. Filtered Sv mask to water column. H. Upper (23 m) water column mask. I. Filtered S_v.

Volumetric fish density of each classified echogram region (number of fish per cubic meter) was calculated as $10^{(Sv\_mean/10)}/(10^{(meanTS/10)})$. Volumetric biomass density of each classified echogram region (kilograms per cubic meter) was calculated as volumetric fish density multiplied by mean weight from this study (0.285 kg; Appendix A Table 6.1). Given the difference in shape between schools located near the ocean floor and schools located off bottom, we used the equation for a dome to estimate the volume of all schools with a minimum altitude <=0 and we used the equation for an ellipsoid to calculate the volume of all schools with a minimum altitude >0; altitude of each school was based on minimum altitude of the school region's bottom boundary referenced to the

back step off bottom, which allowed minimum altitude to be <0. Volumetric biomass density was then multiplied by school volume to estimate the biomass of each school (kg). Only conservative estimates that excluded echoes related to side lobe or multiple scattering contributions, ensonified and likely to be menhaden were included. Given logistical constraints, we were unable to re-ensonify the trawled area to estimate trawl efficiency as originally planned. Therefore, we assumed 100% trawl efficiency when estimating biomass. Additional details on school density, volume, and biomass calculations can be found in Appendix A.

Schools were identified as Atlantic menhaden either through direct sampling, visual sighting at surface, or via shoaling behavior (formation of extremely large, dense schools; e.g., Fig. 5). Schools that could not be identified in this way were categorized as "other fish" (e.g., medium to large individual fish echo traces) or "small pelagic school" (e.g., small, less coherent regions of weaker S_v in the mid- to upper water column) based on visual scrutiny of the location, morphology and magnitude of the S_v echogram region.

School biological structure

Size, age, sex, and maturity composition of five Atlantic menhaden schools sampled at-sea and the five fishery trips sampled at port was characterized. Ageing methods are described below and in Appendix D. Samples were examined for differences in composition by data collection period: fishery-independent samples collected during the survey, post-survey at-sea fishery-dependent samples, and post-survey fishery-dependent port samples. Using all size samples collected, weight-at-length and total length vs fork length relationships were quantified. Size-at-age relationships were characterized using both scale- (Beaufort) and otolith-based (VIMS) ages to reflect differences among reads for each hard part using the part with which each lab was most familiar.

Study area biomass estimation

This survey followed a transect design such that six transects were selected using systematic random sampling. The actual survey protocol slightly deviated from the original design due to a severe storm such that Transects 3 to 6 ("leg 2") were surveyed 5 days after Transects 1 and 2 ("leg 1"), and the planned trawling of acoustically identified schools during the latter half of the survey was mostly not possible due to high mobility of the population and its location near the surface. Thus, we used acoustic estimates of school biomass and associated hydrographic data to inform a spatial simulation model to estimate the range of total biomass in the region during the study period. This model-based approach examined a suite of alternative biomass estimators, including a ratio estimator appropriate for random sampling along transects with unequal lengths as well as three other approaches that accounted for the potential changes in detectability between the two legs of the survey due to different ocean conditions. To characterize ocean conditions, hydrographic data were exported to a Geographical Information System and interpolated into a raster estimating the contemporary environmental conditions at the centroid of the schools across the study area using inverse distance weighting (R Core Team (2003) Version 4.3.1 and ArcMap 10.8.1).

Species distribution modeling

A species distribution model was developed to estimate the changes in detectability driven by the change in seascape conditions, mainly the temperature changes possibly due to warm eddy and/or storm effects. We assumed that differences observed in schooling intensity and average biomass (i.e., detectability of whole schools) during transects 3-6 (i.e., leg 2 of the survey) were entirely due

to temperature changes, and these changes did not reflect the actual changes in the spatial distribution of the population. The model used other environmental predictors and geographical coordinates to capture residual spatial trends in the population distribution.

The species distribution model was formulated hierarchically for both school location and biomass. Each school was represented as a point location at the horizontal centroid of the school location. Given the relatively small size of the school to the entire study area, this approximation should have a limited impact on biomass estimation. Models varied by whether or not certain environmental variables were used as predictors of school location and biomass, and the spatial autocorrelation process within a marked point pattern model (Diggle et al. 2010). The schooling distribution follows a log-Gaussian Cox process, while the observed biomass follows a log-Gaussian Geostatistical model. We considered shared spatial random effects between the two model components to enable joint estimation of the spatial process governing both the schooling density and the biomass (Conn et al. 2017, Pennino et al. 2019).

We initially considered all environmental covariates such as bathymetry, salinity, temperature, and dissolved oxygen. The variance inflation factor was computed to identify multi-collinearity between the environmental covariates (Fox 2015). Models for spatially auto-correlated random effects followed a Matérn covariance function and were implemented via a computationally efficient approximation (Lindgren et al. 2011, Simpson et al. 2016b). The Geostatistical model was approximated using the Stochastic Partial Differential Equation approach (Lindgren et al. 2011) and implemented using the Integrated Nested Laplace Approximation method (INLA, Rue et al. 2009). We used marginal log-likelihood, as well as mean square errors (MSE) in school intensity and log biomass preschool to estimate the predictive performance of each model.

Detectability estimation

A relative detectability for the leg 2 sampling was estimated by first predicting the schooling density and average biomass per school at leg 2 transects, based on a hypothetical temperature distribution that was similar in range to the temperature during the leg 1 sampling, accounting for the temperature-driven differences of detectability. These model-based predictions of school intensity and biomass were then compared with the model predictions based on the actual observed temperature. The additional number of schools as well as the increase in log average biomass were estimated. These estimated impacts of relative detectability were applied to the actual biomass and schooling data and expanded using a design-based or ratio-based estimator to the entire study area (Thompson 2012). The design-based uncertainty for these estimates was also quantified using the standard deviation and the ratio-based estimates methods (Thompson 2012). Additional details can be found in Appendix C.

Statistical inference was based on approximated Monte Carlo sampling implemented in INLA. All analyses were conducted in R using packages R-INLA (Rue et al. 2009), terra (Hijmans 2023), and sf (Pebesma 2018). To incorporate the uncertainty of both the design-based estimation and the detectability, the design-based errors were randomly sampled from the model-based adjusted transect-specific biomass. Normal approximation was assumed for the design-based error estimates. A Monte Carlo integration was then applied across the approximate posterior sample of adjusted biomass estimates to derive the 90% credible sets for the biomass. This was necessary because the model estimates were highly right-skewed and posterior moments were not robust to outliers and could generate unrealistic uncertainty estimates.

Ageing uncertainty

An ageing exchange of scales and otolith samples was conducted post-survey to quantify ageing uncertainty. The exchange involved project collaborators with ageing programs, namely VIMS, NJDEP, and NOAA Beaufort Laboratory. These three labs were chosen because Beaufort Laboratory is responsible for ageing all port samples used to inform the Atlantic menhaden stock assessment, VIMS was a collaborator on survey implementation and their staff are experienced at ageing Atlantic menhaden otoliths collected in their fishery-independent surveys, and NJDEP was interested in having their ageing team learn to age Atlantic menhaden. Thus, these three labs represented a wide range of different experience levels and expertise in ageing Atlantic menhaden using different methods.

The objectives of the ageing exchange were to:

1) quantify intralab and interlab paired age agreement, when possible,
2) quantify scale vs otolith paired age agreement, and
3) identify patterns, if present, in paired age agreement by sex and size.

Although validated ages were not available to assess accuracy (age estimates compared with true ages), intralab and interlab estimates of precision (repeatability of age estimates by the same or among different readers), and bias (systematic differences in age estimates) can be used to improve ageing methodology, ensure greater consistency among ageing programs, and inform stock assessment uncertainty (Campana et al. 1995, Morison et al. 2005).

Data collection

A total of 81 samples were selected for full data collection, including sex, maturity, eviscerated weight, and age (both scale- and otolith-based reads) during the survey. An additional 72 samples were fully processed from the post-survey sampling conducted by VIMS at-sea. Once the VIMS team had returned to land, Lund's Fisheries continued port sampling throughout the remainder of the winter menhaden fishing season, collecting an additional 150 fish at port (three 10-fish samples/trip collected over five additional trips), and all 150 samples received full workups.

Sample processing

All samples collected in the field for full workups were first transported to VIMS for processing using standard VIMS survey protocols and procedures. VIMS fish ageing protocols were established from procedures developed by NEFSC, Old Dominion University, and VIMS validated and published research developed by NEFSC, Old Dominion University, and VIMS (Bonzek et al. 2017, VanderKooy 2020). VIMS standard ageing protocols have been verified, collaborated, and referenced annually at the ASMFC Fish Ageing QA/QC Workshop (ASMFC 2023).

Scale samples were thawed and lightly scrubbed in a soap and water solution to remove debris and excess slime. Six of the cleanest, undamaged scales from each scale patch were selected, thoroughly dried, and pressed between two glass microscope slides. Many samples included regenerated scales. When possible, replacement scales were found, but some samples included a few regenerated samples on the slides. One sample (Specimen ID #75) contained all regenerated samples with no replacements and was omitted from analysis. Both sagittal otoliths from each sample were extracted, thoroughly dried, and cleaned as necessary.

Ageing methods

Each ageing lab followed their own standard protocols for ageing Atlantic menhaden as described below. VIMS prepared scale samples and evaluated them using a microfiche reader using VIMS Atlantic menhaden protocols (Appendix D). Paired whole otoliths were evaluated in water under a stereo dissecting microscope at 50x magnification with transmitted light. One reader, Jameson Gregg, read each hard part twice using VIMS protocols for scale (June and Roithmayr 1960) and otolith ageing (Deegan and Thompson 1987, Warlen 1988, Warlen 1992, Ahrenholz 1994) of menhaden. In cases where the two reads differed, info on size or location and date of capture was used to inform the final age assignment based on expected timing of mark formation. Upon completion, all samples were mailed to NJDEP.

At NJDEP, two readers, Jamie Darrow (Reader 1) and Alissa Wilson (Reader 2), read each hard part once. Beaufort Laboratory ageing protocols were used to age scales and VIMS protocols were used to age otoliths as detailed in the attached protocols. Prepared scale samples were evaluated using a Microfiche reader. Paired whole otoliths were evaluated in water under a stereo dissecting microscope using reflected light. Upon completion, all samples were mailed to Beaufort.

At Beaufort, one reader, Amanda Rezek, read each hard part once. Prepared scale samples were evaluated using a stereo microscope (10X magnification) with transmitted light and cellSens imaging software to measure. Scales were aged using Beaufort Laboratory scale ageing protocols (attached). Paired whole otoliths were evaluated in 70% ethanol under a stereo dissecting microscope (20X magnification) with transmitted light using VIMS ageing protocols. Upon completion, all samples were archived at Beaufort Laboratory for use in future studies.

Statistical Analyses

Of the 303 samples for which full workups were conducted, 302 were suitable for inclusion in the ageing comparison. However, agers noticed that many of the scales were damaged and difficulty to read due to the physical stress of fish caught in the mid-water trawl net used for this survey. In the absence of validated ages, ageing agreement was evaluated. For labs that aged each hard part more than once (VIMS and NJDEP), consistency between two reads by the same reader, and among two different readers was quantified. For the two interlab comparisons, the most experienced ager at the NJDEP lab (Darrow – Reader 1) and VIMS's second read were used.

To quantify ageing agreement within and among ageing labs, the following indices were calculated: percent agreement (PA), average percent error (APE), and Chang's average coefficient of variation (ACV). To evaluate bias within and among ageing labs, the following tests of symmetry were conducted: McNemar's (McNemar; McNemar 1947) and Evans & Hoenig (EvansHoenig; Evans and Hoenig 1998). Although frequently used in other ageing studies, Bowker's test of symmetry (Bowker 1948) was not used here given the overall large number of samples, high variability in age reads, and pattern of decreasing sample size with age would likely generate false positives indicating bias when it is not actually present (Nesslage et al. 2022). Age-bias plots were generated for each comparison and for each comparison with results separated by the sex of each sample. All indices were calculated and tests of symmetry performed using the FSA package (Ogle DH 2023) for R Version 0.9.4 (R Core Team 2023).

RESULTS

Survey data collection

In general, schools were more mobile during the survey periods than anticipated due to warmer than expected water temperatures. Thus, some schools were spotted but fled the vessel, some schools fled or dispersed after initial ensonification (goal had been two perpendicular pre-fishing passes), and some schools remained sedentary enough to be both ensonified and trawled.

Along the six survey transects, a total of 38 schools were identified as Atlantic menhaden with the omnidirectional sonar, 12 were ensonified with the ES80 echosounder, and three were sampled (Fig. 6). Of these, 23 schools were spotted, 8 ensonified, and three sampled prior to the storm. Post-storm, the 15 schools observed on the omnidirectional sonar (and sometimes visually identified from the vessel) were often too near the surface to be detected by the ES80. Although 4 additional schools were ensonified post-storm, no additional schools were sedentary or low enough in the water column to be sampled.

Table 3. Schools or trips/hauls sampled and samples collected pre- and post-survey.

	Schools/trips sampled	Fork length, total length, whole weight	Sex, maturity, eviscerated weight, age (scale & otolith)
Survey (at-sea)	3 schools	2,132	80
Post-survey (at-sea)	2 schools	2,005	72
Post-survey (port)	5 trips/7 hauls	150	150
Total		4,287	302

Post-survey data collection

Additional samples were collected at sea by the VIMS team during targeted fishing operations both inside and outside the study area for five days after completion of the survey. An additional 155 schools were spotted and 94 schools were ensonified (Fig. 6). Two extremely large schools were sampled post-survey as well, providing an additional 2,005 menhaden size samples (Table 3). Of those samples, 72 were sampled for additional data, including sex, maturity, eviscerated weight, and age (both scale- and otolith-based reads). Additional hydrographic data were collected post-survey to document ocean temperature change, which likely influenced menhaden schooling behavior. Once the VIMS team had returned to land, Lund's Fisheries continued port sampling throughout the remainder of the winter menhaden fishing season, collecting an additional 150 fish at port (three 10-fish samples/trip collected over five additional trips). All 150 port samples received full workups.

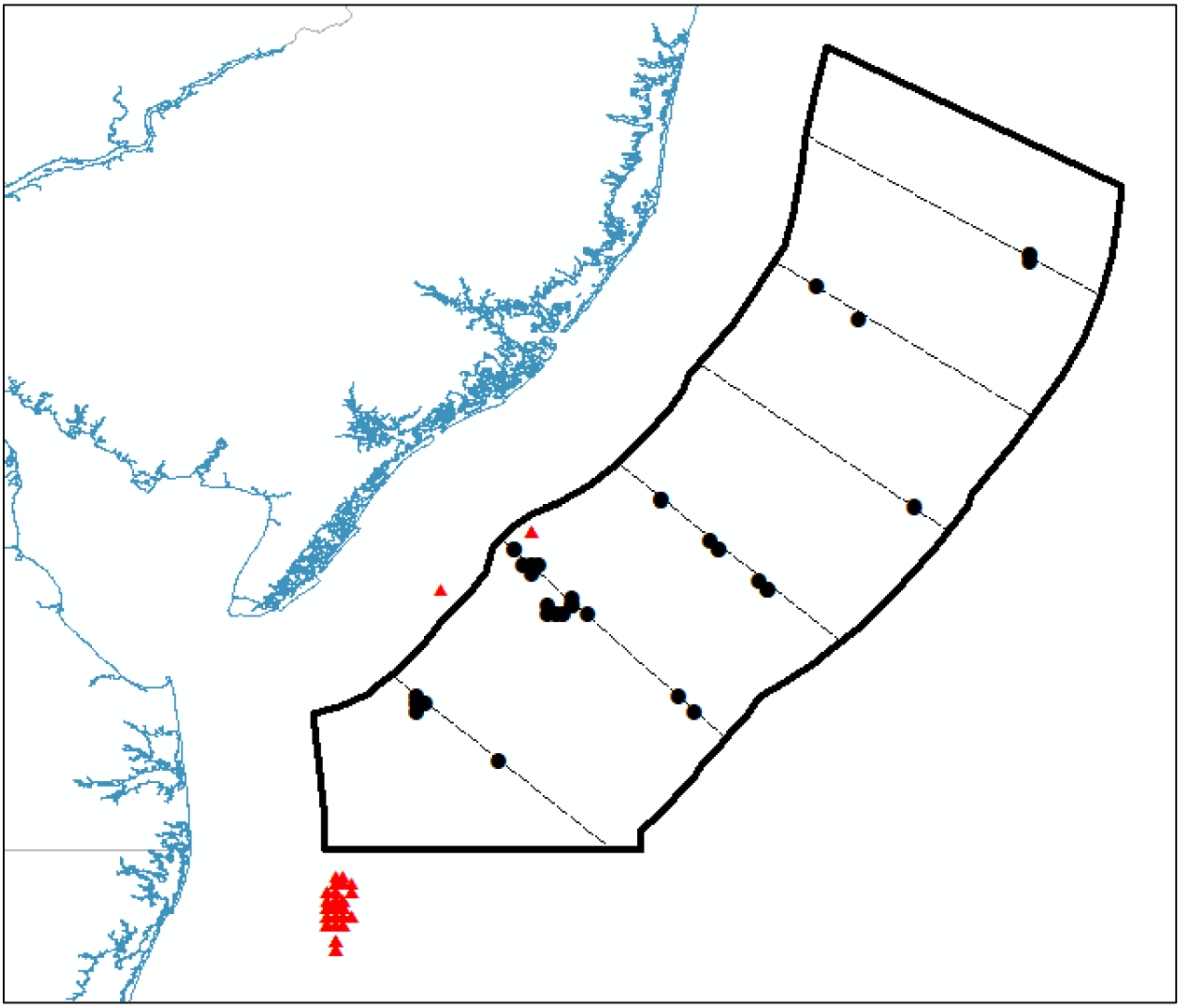

Figure 6. Schools encountered during survey (black circles) along survey transects (dashed lines) in the survey area (black outline), and schools encountered during at-sea sampling post-survey (red triangles).

School biomass

Biomass estimates for all Atlantic menhaden schools ensonified, both during and after the survey period, and their average depth can be found in Appendix B. During Leg 1 of the survey (Transects 1-2), more and larger schools were ensonified than during Leg 2 (Transects 3-6; Table 4). The maximum school ensonified during Leg 1 was 47,291 kg vs 54 kg during Leg 2. The difference between survey Legs may reflect behavioral response of Atlantic menhaden due to large changes in ocean conditions as described below. The 84 schools ensonified post-survey were more similar in depth and size to those ensonified during Leg 1 of the survey, as were ocean conditions.

Table 4. Summary of school biomass by data collection period.

Data Collection Period	Number of ensonified schools	School mean depth (m)	School biomass (kg) Mean	School biomass (kg) Sum
Survey - Leg 1	20	25.7	47,291	945,811
Survey - Leg 2	3	20.1	54	162
Post Survey - Leg 3	84	26.1	23,662	1,987,620

Acoustically derived biomass estimates and trawl catch weights obtained dockside by individually weighing each school were largely similar in agreement (Fig. 7).

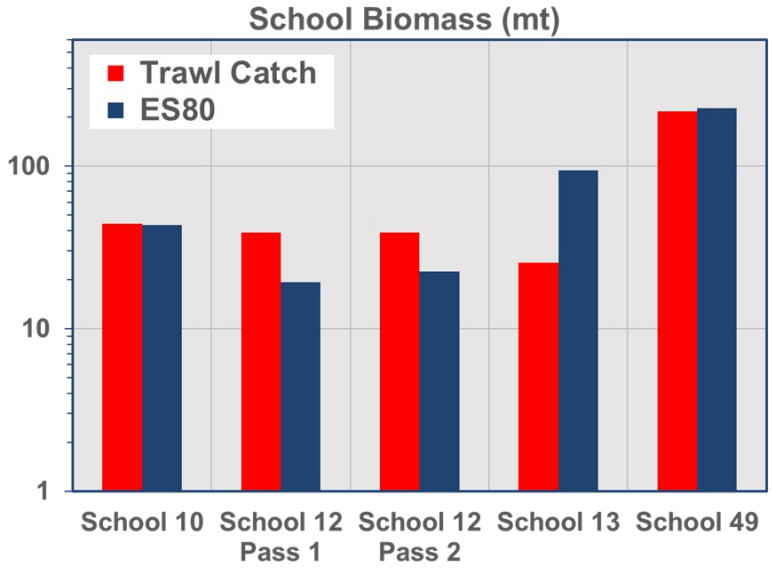

Figure 7. Atlantic Menhaden school biomass estimates by midwater trawl (dockside weigh-out at Lund's Fisheries in Cape May, NJ) and Simrad ES80 split-beam echosounder. Acoustically-derived density was scaled to biomass (metric tons) based on the ideal dome volume (school height, school length). Note that schools 10, 12, and 13 were ensonified and harvested during the survey period in the survey area, whereas school 49 was ensonified and harvested during the post-survey period just south of the survey area.

During the survey, an additional 49 schools were spotted on the omnidirectional sonar, but could not be identified to species; three were categorized as "other fish" and 46 were categorized as "small pelagic school"). Post-survey, an additional 24 schools were spotted on the omnidirectional sonar, but could not be identified to species (five "other fish" and 19 "small pelagic school"). During this project, the total biomass ensonified that could not be identified to species was relatively small (58,661 kg), only 3% of the total biomass of Atlantic menhaden ensonified (1,754,563 kg).

School biological structure

All schools identified as Atlantic menhaden by the captain and crew with omnidirectional sonar and subsequently sampled during survey and post-survey operations were confirmed to be highly homogeneous schools of Atlantic menhaden. Schools sampled were almost entirely composed of Atlantic menhaden. Out of >3 million pounds of Atlantic menhaden landed and over 4,299 fish

sampled during the 2022 survey and fishing season, only one American shad (*Alosa sapidissima*) was collected in a sampled bucket during post-survey sampling operations. Throughout all survey and post-survey sampling conducted by VIMS scientists, other species were noted when observed in the chute or bycatch grate, recorded in the cruise notes, and given sampling workups for inclusion in the biosamples database when it was safe to collect them. This additional bycatch included one Atlantic mackerel (*Scomber scombrus*), one Atlantic herring (*Clupea harengus*), one spiny dogfish (*Squalus acanthias*) and 10 striped bass, all collected post-survey. An additional 10-15 striped bass were caught but released during catch processing. VIMS survey crew also noted very small operational discards of Atlantic menhaden during mid-water trawling operations.

Size of Atlantic menhaden sampled was similar (Fig. 8) across sampling periods: during the survey (fishery-independent), after the survey at sea (fishery-dependent), or at port (fishery-dependent). Average weight of Atlantic menhaden encountered during February-March off the coast of New Jersey was 0.291 kg and average fork length was 265.7 mm.

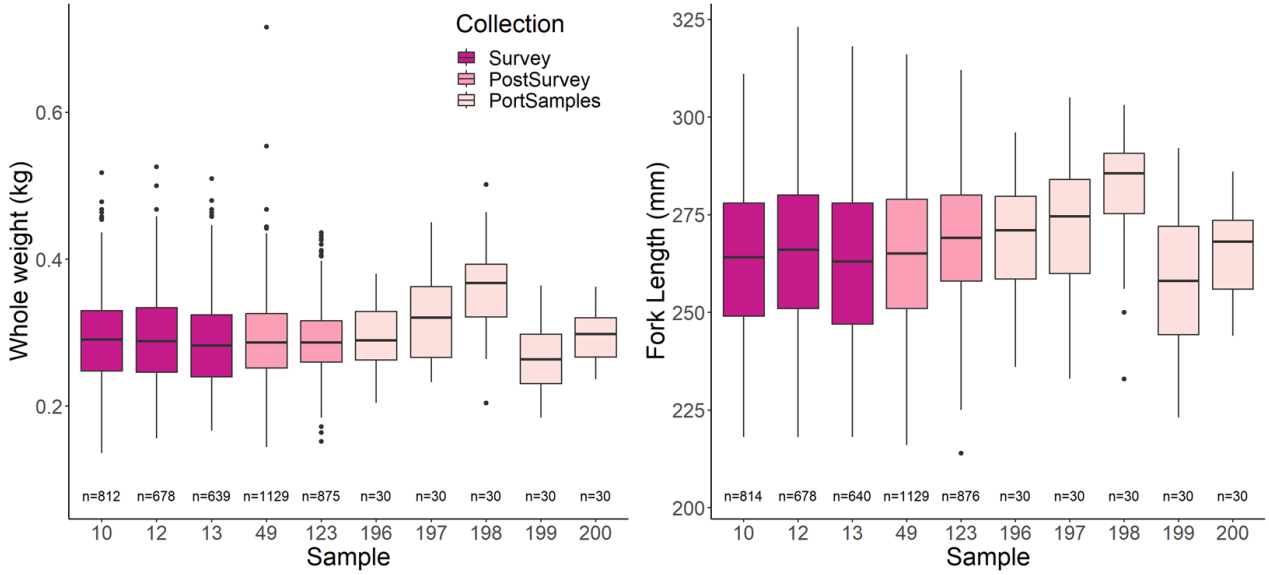

Figure 8. Distribution of weight (kg; LEFT) and fork length (mm; RIGHT) from samples collected during survey, post-survey and port sampling. Survey and post-survey sample x-axis labels represent the number assigned to the school sampled; port samples x-axis labels represent trips sampled.

Relationships between total length and fork length and weight and length of Atlantic menhaden sampled at sea were similar to previously published analyses of port samples collected primarily from the reduction fishery (Figs. 9-10; Smith et al. 2008).

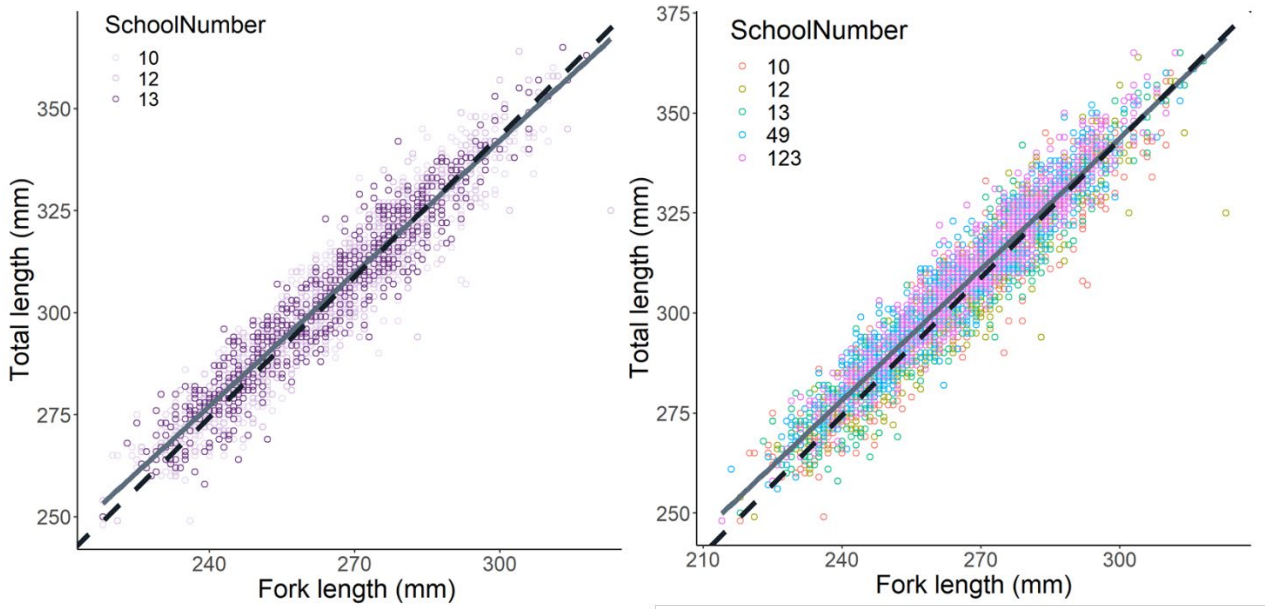

Figure 9. Relationship between total length (mm) and fork length (mm) for Atlantic menhaden sampled during the survey (LEFT) and both survey and post-survey at-sea sampling (RIGHT). Dashed black line represents 2022 data and solid gray line represents reduction fishery port sampling-based relationship published by Smith (2008).

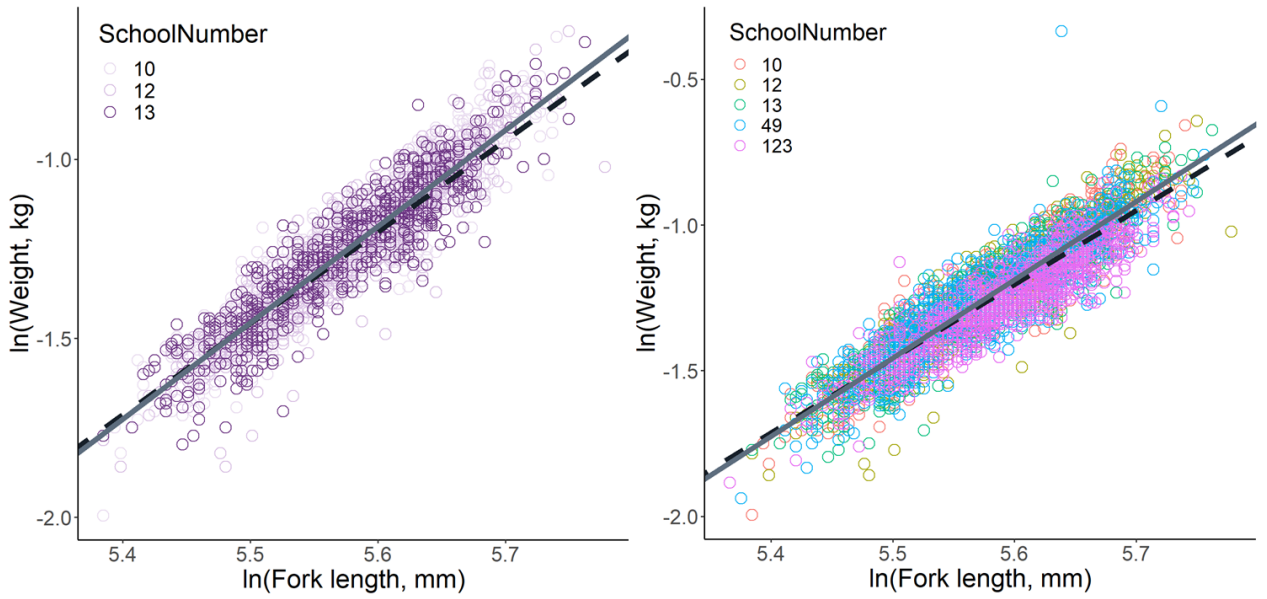

Figure 10. Relationship between the natural log of weight (kg) and the natural log of fork length (mm) for Atlantic menhaden sampled during the survey (LEFT) and both survey and post-survey at-sea sampling (RIGHT). Dashed black line represents 2022 data and solid gray line represents reduction fishery port sampling-based relationship published by Smith (2008).

Atlantic menhaden sampled were 56% female and displayed sexual dimorphism (Fig. 11) such that average weight and length of females (273 mm, 0.32 kg) was larger than that of males (267 mm, 0.30 kg).

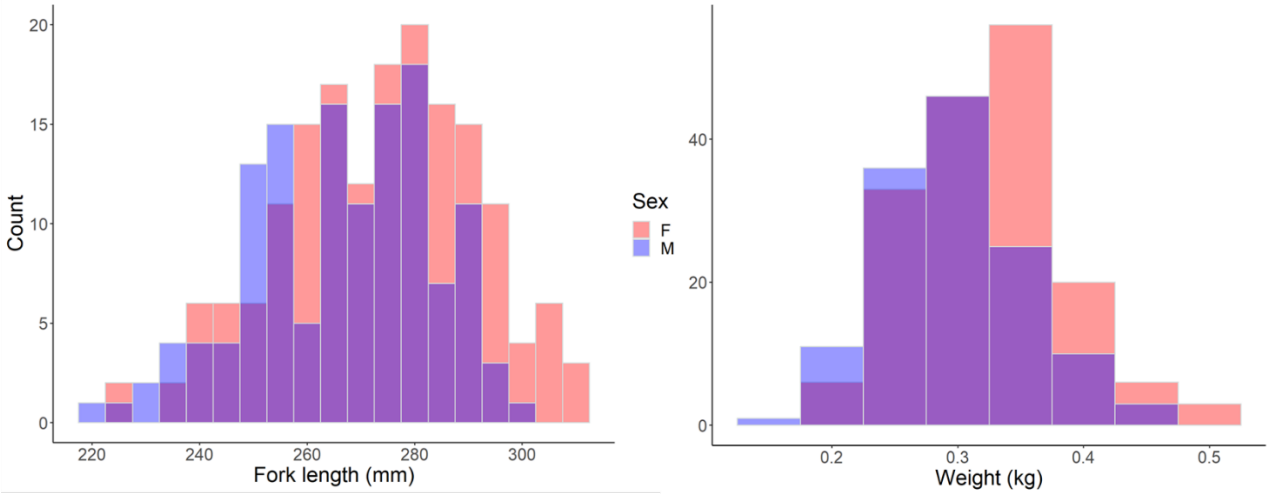

Figure 11. Fork length (mm) and weight (kg) distribution of Atlantic menhaden across all samples collected at-sea and port. "F" denotes female and "M" denotes male.

Most Atlantic menhaden sampled that received full workups were visually identified as being mature (resting), but some were identified as spent, ripe, or immature (Fig. 12). Thus, the survey and post-survey fishing operations did not appear to be sampling on active spawning aggregations.

Both Beaufort Lab and VIMS estimated that most Atlantic menhaden sampled during this project were ages 3 and 4, regardless of whether ages were based on scales or otoliths. Ages ranged from age 2 to age 6 for Beaufort Lab scale-based age estimates and age 2 to age 5 for VIMS otolith-based ages (Fig. 13).

Length-at-age relationships generated from this survey were similar to stock assessment input assumptions (Fig. 14); however, weight-at-age in our survey exhibited an asymptote not observed in the weight-at-age matrix used in the stock assessment (ASMFC 2022). The ASMFC Atlantic Menhaden Technical Committee is exploring these discrepancies for the 2025 stock assessment.

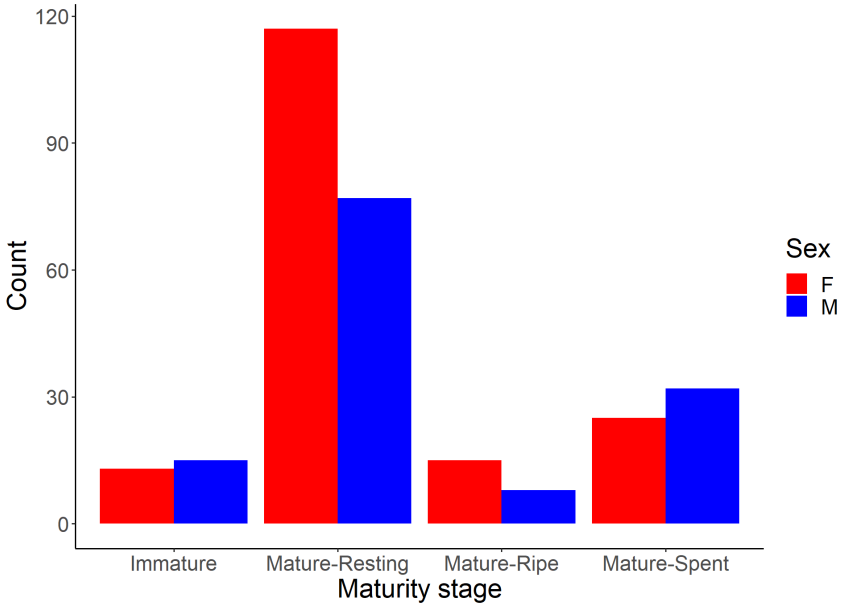

Figure 12. Proportion of all Atlantic menhaden samples receiving full work ups categorized by sex and maturity stage (visual identification). "F" denotes female and "M" denotes male.

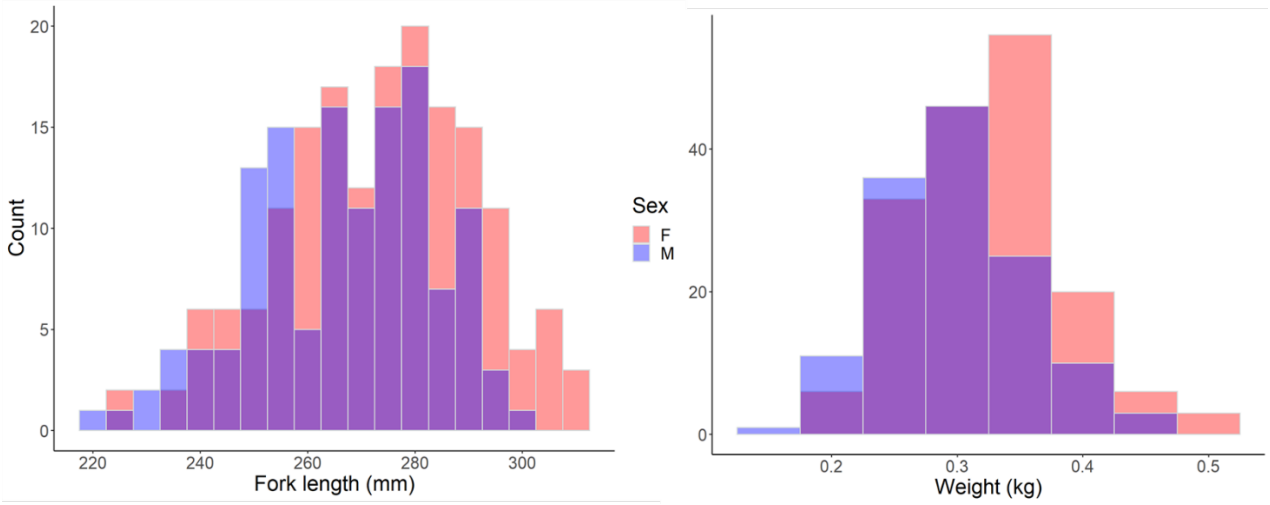

Figure 13. Proportion of all Atlantic menhaden samples receiving full work ups by age and sex determined by Beaufort Lab reading scales (LEFT) and VIMS readings otoliths (RIGHT). "F" denotes female and "M" denotes male.

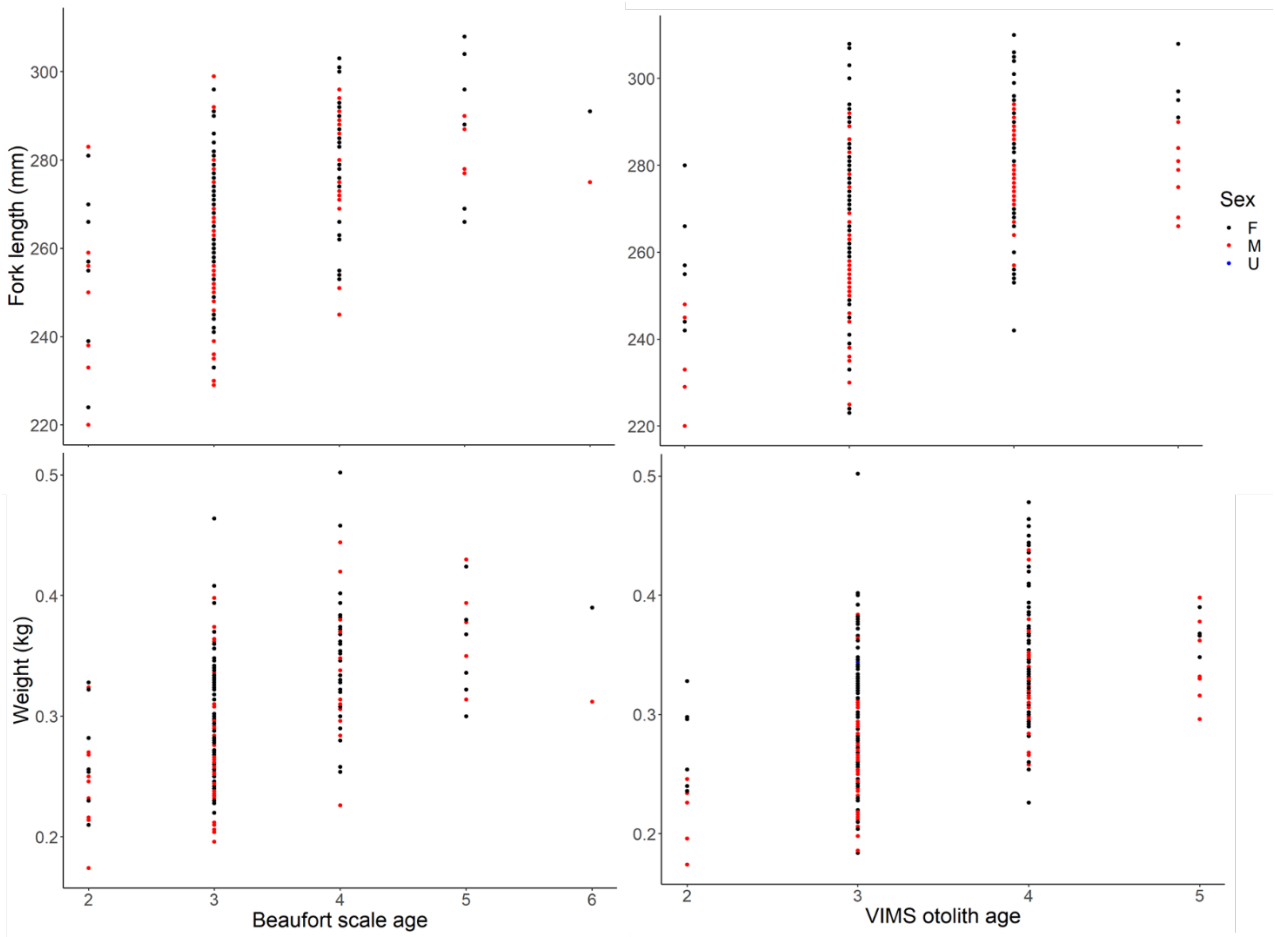

Figure 14. (TOP) Fork length (mm) at age for Atlantic menhaden as estimated by Beaufort Lab using scales (LEFT) and VIMS using otoliths (RIGHT) by sex. (BOTTOM) Weight (kg) at age for Atlantic menhaden as estimated by Beaufort Lab using scales (LEFT) and VIMS using otoliths (RIGHT) by sex. "F" denotes female and "M" denotes male.

Hydrography

Hydrographic data collection at sea indicated that oceanographic conditions underwent large, detectable changes during the survey period that may be linked to observed changes in schooling behavior of Atlantic menhaden. During the first leg of the survey (Transects 1-2), Atlantic menhaden were easily detectable and identifiable as they formed extremely large, dense schools near the sea floor (e.g., Fig. 5). The vessel returned to port to offload and remained off the water for three days due to a severe storm (Table 1). When survey operations resumed for Transects 3-6, median bottom water condition was 0.63°C warmer and 0.31 ppt more saline than when surveying Transects 1-2 (Fig. 15). Atlantic menhaden were no longer found to be forming extremely large, dense schools, but were instead dispersed into small schools at or near the sea surface, making it difficult or impossible to ensonify and sample as described above. The change in ocean conditions was likely due to a warm eddy that formed just prior to the start of the survey, causing warmer and more saline waters to diffuse into the region during the course of our survey (Fig. 16; personal communication, Drs. Glen Gawarkiewicz and Avijit Gangopadhyay), possibly influenced as well by the severe storm of February 16-19.

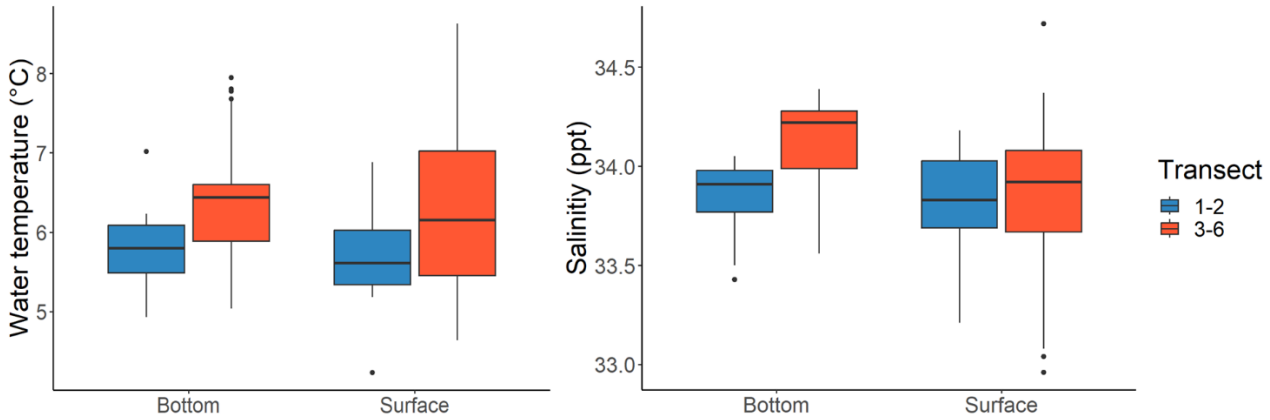

Figure 15. Average water temperature (°C; LEFT) and salinity (ppt; RIGHT) at bottom and surface of water column during the first survey trip (Transects 1-2) and second survey trip (Transects 3-6).

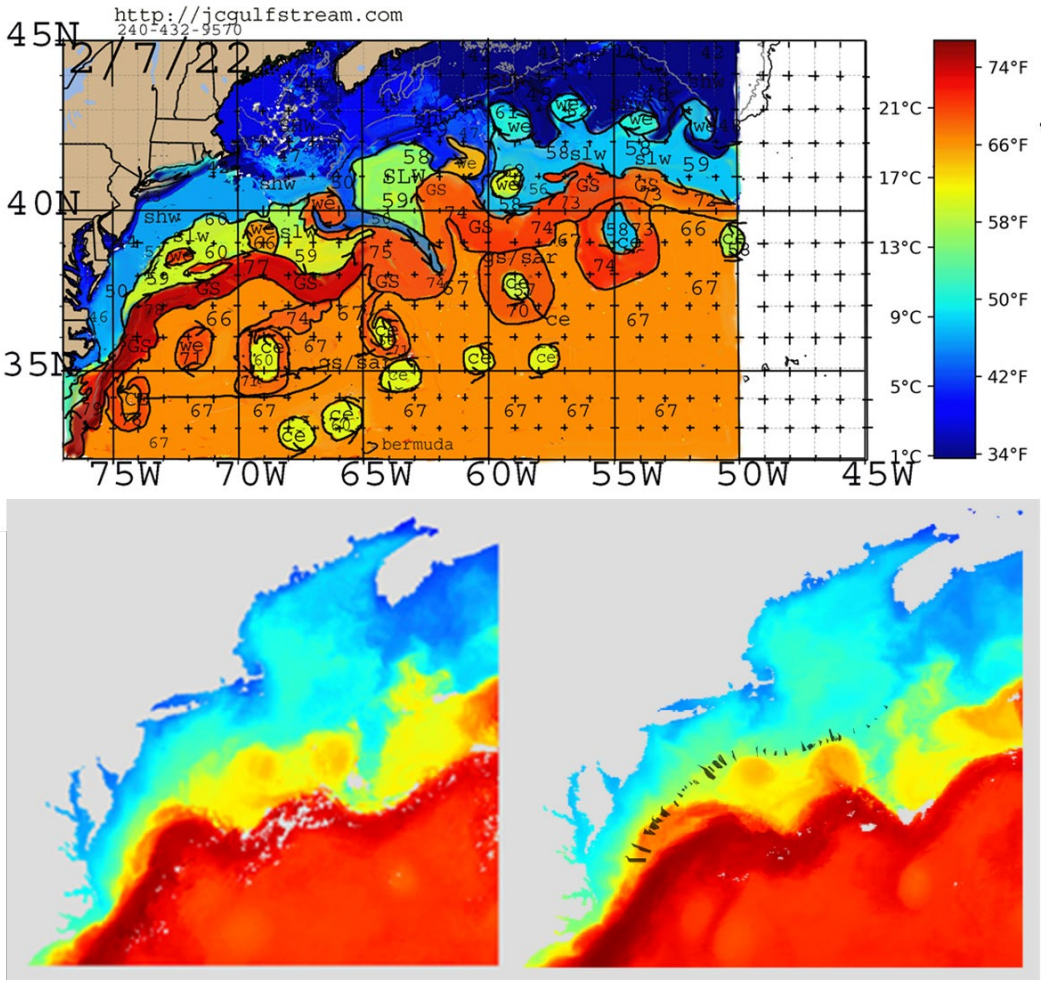

Figure 16. (TOP) Satellite-derived sea surface temperature maps confirming presence of an offshore warm eddy prior to the start of the survey (February 7, 2022; courtesy Dr. Avijit Gangopadhyay, jcgulfstream.com). (BOTTOM) Likely diffusion of warm eddy warmer waters onto the shelf off New Jersey during the survey period (courtesy Sarah Salois, NOAA Cooperative Research Branch, Squid Squad Weekly Viewer). Black markings denote canyon locations.

Regional stock biomass

Salinity was associated with the largest variance inflation factor (>10) and removed from further modeling (Fox 2015). Twenty-four models were built using the remaining environmental covariates and spatial random effects. Marginal likelihood was estimated for each model to measure their predictive capability (Appendix C Table 1). Two models generated extreme marginal log-likelihood. The corresponding residual mean squared errors (RMSE) were large, which indicated numerical issues within INLA. The model with only a fixed effect of temperature and shared spatial random effects between the log intensity and average biomass (Appendix C Figure 1) was best in terms of marginal likelihood, along with a small residual Mean Square Error (MSE). According to the best-fitting model, the temperature had a statistically significant and negative linear effect on both the schooling intensity and the average log biomass per school (Appendix C Table 2).

The adjusted temperature in leg 2 (transects 3-6) had a similar range as the observed temperature in leg 1, but still exhibited the spatial pattern of the actual temperature observed during the survey (Fig. 17). Large uncertainty exists regarding the temperature effects on detectability (Fig. 18), possibly due to the small sample size (n=23). More and larger schools on average were expected under the adjusted (and lower) temperature. The relative magnitude of changes in both school intensity and average biomass depends on the assumed changes in the temperature.

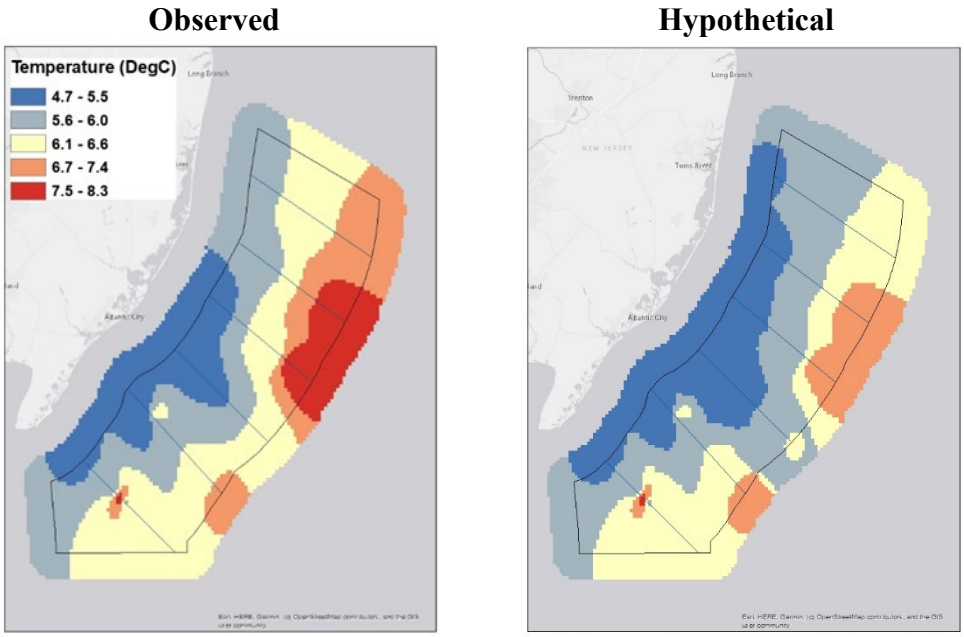

Figure 17. Interpolated water temperature contemporary to the survey in the study area, along with the hypothetical water temperature when the northern area (leg 2, transects 3-6) was adjusted to maintain the same range as the southern area (leg 1, transects 1-2).

Biomass estimates ranged between 8,000 and 11,000 metric tons in the study area (Figure 19, Table 5). Ratio estimates based on the transect area generated 15%-20% lower biomass estimates than the design-based estimates because the design-based estimator expanded to the whole area based on the number of transects, whereas the ratio estimator expanded based on the ratio of biomass per unit area. The design-based estimator of uncertainty was large because it was based on random sampling, which did not fully incorporate the systematic nature of the sampling. The ratio-based

uncertainty estimates were more reasonable. Detectability adjustment led to at most an 18% increase in design-based estimates and a 38% increase in ratio-based estimates.

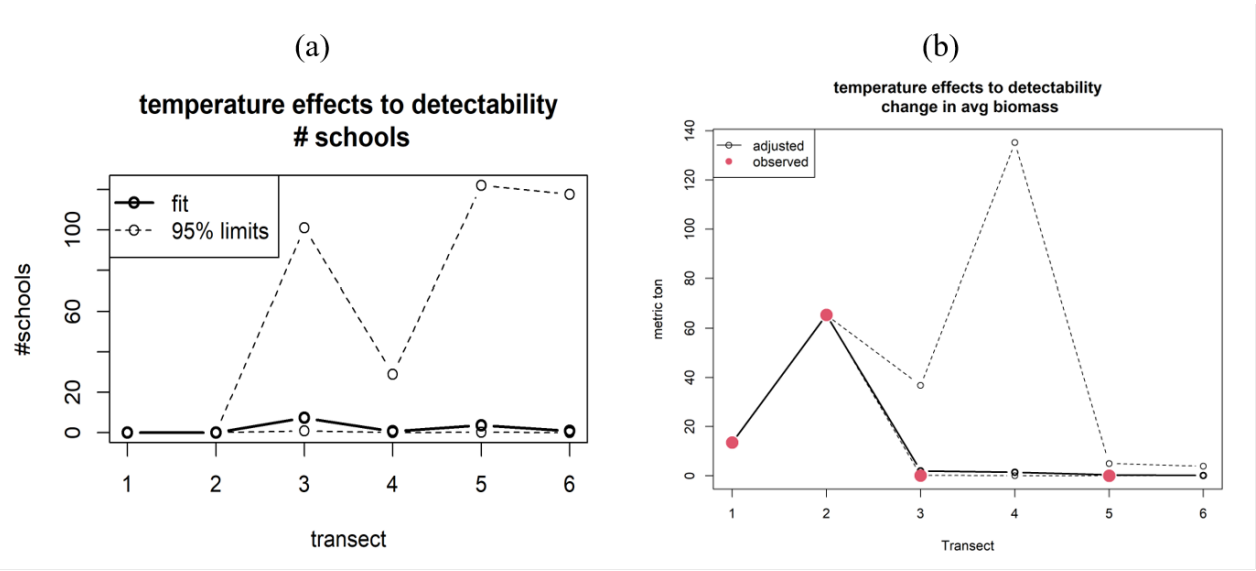

Figure 18. Estimates of temperature effects on (a) school intensity measured as the expected additional number of schools on each transect; and (b) the average biomass per school observed and after the hypothetical temperature change.

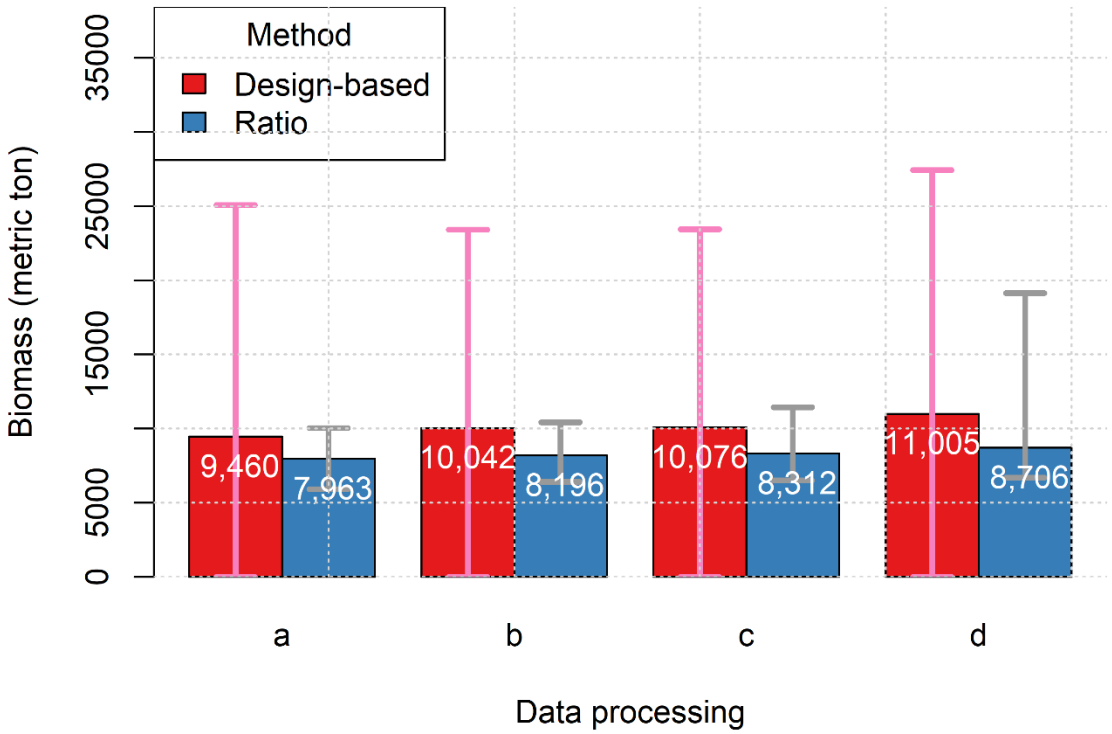

Figure 19. Biomass estimates (mt) for the study area in terms of posterior median and 90% credit sets according to expansion estimators and detectability adjustment: a) no adjustment, b-d) temperature adjustment to school intensity (b), average biomass (c), and both (d).

Table 5. Biomass estimates for the study area (mt) in terms of posterior median and 90% credit sets according to detectability adjustment and expansion estimators.

	Design-based			Ratio-estimate		
Detectability Adjustment	Estimate	Lower	Upper	Estimate	Lower	Upper
No adjustment	9,460	0	25,065	7,963	5,902	10,024
Adjusted school number	10,042	0	23,422	8,196	6,410	10,432
Adjusted school size	10,076	0	23,441	8,312	6,505	11,434
Adjusted size and number	11,005	0	27,441	8,706	6,703	19,137

Ageing uncertainty

The ageing exchange demonstrated low interlab agreement and intralab precision was high for VIMS and low for NJDEP. VIMS demonstrated high agreement among reads (Table 6, Appendix D Figs. 1-2) for both scales (PA=89%) and otoliths (PA=92%), although scale-based reads were slightly biased such that second reads of scales tended to be older than first reads. Agreement between the two NJDEP readers was low for otoliths (PA=36%), and very low for scales (PA=2%; Table 2, Fig. 2); both sets of intralab NJDEP age comparisons demonstrated significant bias.

Among labs, there was greater agreement in paired ages between VIMS and Beaufort (Appendix D Fig. 3) for both scales (PA=66%) and otoliths (PA=59%) than between VIMS and NJDEP (Appendix D Fig. 4) or between Beaufort and NJDEP (Appendix D Fig. 5), which ranged in PA from 36-48% (Table 6). VIMS Read 2 age determinations were consistently older than that of Beaufort's for younger fish and vice versa for older fish. Although ACV for otolith-based age comparisons between VIMS Read 2 and Beaufort was greater than seven, the overall difference among reads was statistically unbiased (Appendix D Fig. 3). NJDEP Reader 1 age determinations were typically older than that of VIMS Read 2 and Beaufort regardless of hard part examined (Appendix D Figs. 4-5).

VIMS demonstrated good agreement between paired scale and otolith ages (PA=82%; Fig. 20). Paired age agreement between hard parts was lower for Beaufort (54%) and NJDEP (PA=41%). Scale-otolith comparisons for both VIMS and NJDEP were biased, but Beaufort was not. When comparing scale- vs otolith-based age determinations, all three labs demonstrated a pattern of assigning an older age to younger fish and a younger age to older fish when aging scales.

Table 6. Ageing comparison indices of agreement and tests of symmetry. R=Read (VIMS) or Reader (NJDEP), PA= percent agreement, APE = average percent error, ACV = Average Coefficient of Variation, McNemar = p-value for McNemar's test of symmetry, EvansHoenig = p-value for Evans and Hoenig test of symmetry. Gray shading indicates either ACV > 7 (indicating low precision), or test of symmetry p-value was significant (α = 0.05; indicating bias).

Lab	Hard Part	Comparison	PA	APE	ACV	McNemar	EvansHoenig
VIMS	Scales	R1 vs R2	89%	1.64	2.32	*0.00026*	*0.00026*
NJDEP	Scales	R1 vs R2	2%	42.61	*60.26*	*0.00000*	*0.00000*
Interlab	Scales	VIMS R2 vs NJDEP R1	44%	8.27	*11.70*	*0.00000*	*0.00000*
Interlab	Scales	Beafort vs VIMS R2	66%	5.52	*7.80*	*0.00013*	*0.00058*
Interlab	Scales	Beafort vs NJDEP R1	36%	10.59	*14.97*	*0.00000*	*0.00000*
VIMS	Otoliths	R1 vs R2	92%	1.32	1.87	0.41422	0.68321
NJDEP	Otoliths	R1 vs R2	36%	12.03	*17.02*	*0.00000*	*0.00000*
Interlab	Otoliths	VIMS R2 vs NJDEP R1	48%	8.72	*12.34*	*0.00000*	*0.00000*
Interlab	Otoliths	Beafort vs VIMS R2	59%	6.64	*9.38*	0.08897	0.17260
Interlab	Otoliths	Beafort vs NJDEP R1	45%	9.47	*13.40*	*0.00000*	*0.00000*
VIMS	Both	R2 Scales vs Otoliths	82%	2.72	3.85	*0.00000*	*0.00000*
NJDEP	Both	R1 Scales vs Otoliths	41%	9.04	*12.78*	*0.00097*	*0.00182*
Beaufort	Both	Scales vs Otoliths	54%	8.00	*11.32*	0.16339	0.44192

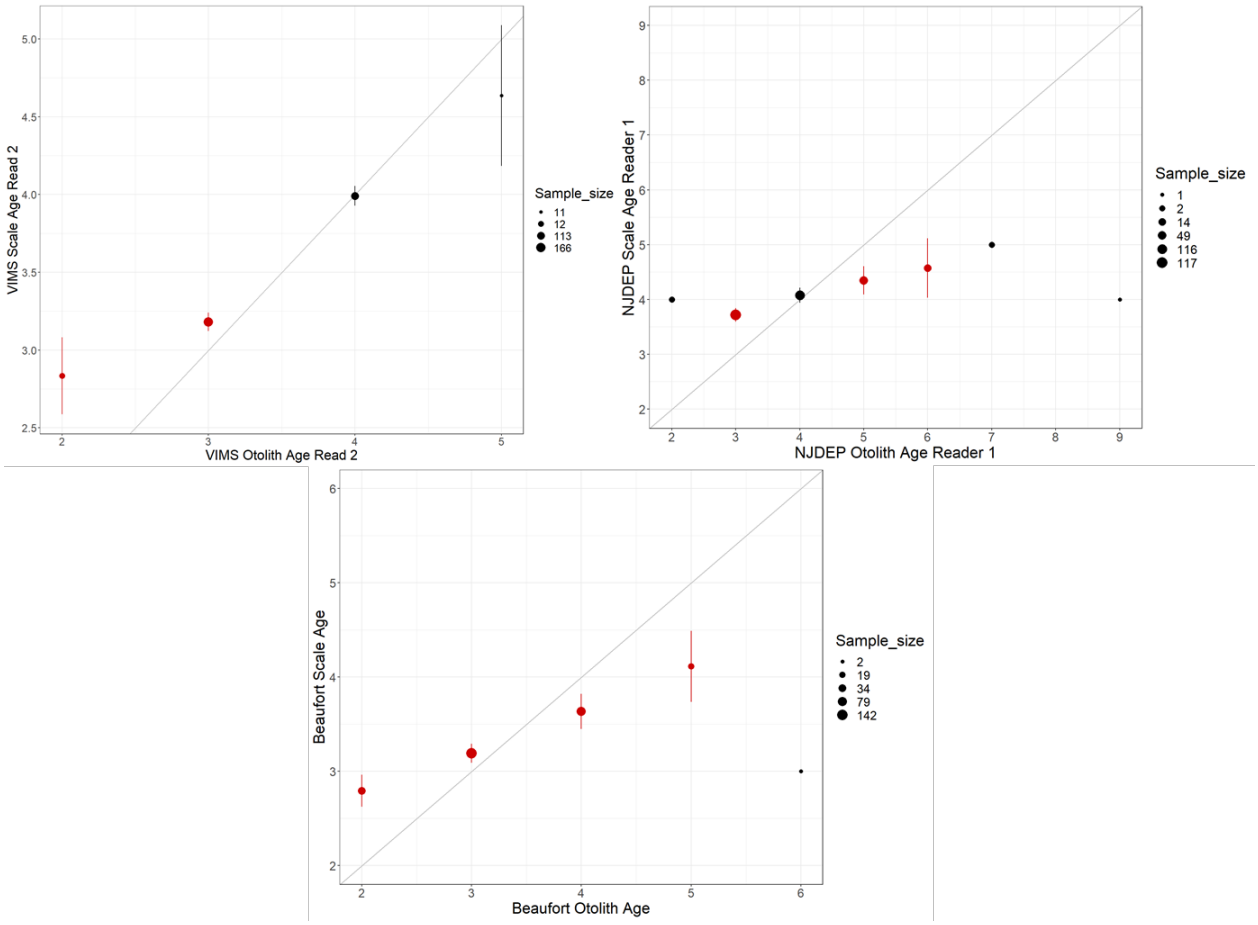

Figure 20. Scale vs otolith paired age comparisons for VIMS Read 2 (top left), NJDEP Reader 2 (top right), and Beaufort (bottom). Solid symbols and bars represent mean and 95% confidence intervals, respectively, for the y-axis age relative to the x-axis age. Red solid symbols indicate the difference among reads was significantly different from 0. The dashed line represents the 1:1 relationship.

MANAGEMENT IMPLICATIONS

Estimating regional biomass and structure

This study provided field confirmation that a portion of the adult Atlantic menhaden stock does indeed overwinter in the offshore Mid-Atlantic region. Until recently, scientists assumed that most spawning-age Atlantic menhaden migrate south in winter to congregate offshore of Cape Hatteras based on historical tagging data and frequent fall encounters of the reduction fishery with large schools of fish ages 3+ passing through coastal areas from Chesapeake Bay to North Carolina (Nicholson 1978). However, re-analysis of historical tagging data indicated Atlantic menhaden are partial migrants and that a portion of each local population remains resident coastwide in winter (Liljestrand 2017, Liljestrand et al. 2019a, b). Also, analysis of long-term (1977-1987, 2000-2013) ichthyoplankton survey data provided evidence of the year-round presence of spawning Atlantic menhaden across the Mid-Atlantic (Simpson et al. 2016a, Simpson et al. 2017). This study provides updated fishery-independent and fishery-dependent data to corroborate previous studies demonstrating that Atlantic menhaden are partial migrants.

Our study can also help provide context for stock assessment model estimates of spawner biomass not encountered by the reduction fishery or inshore fishery-independent surveys. We estimated that biomass in the study region ranged between 7,963 and 11,005 mt (Table 7). Thus total biomass of overwintering Atlantic menhaden in the study region is a small fraction (approximately 0.22-0.31%) of coastwide total biomass of age 1+ fish estimated by the stock assessment (ASMFC 2022). Although efficiency of the midwater trawling gear used in this study has not been quantified, our assumption of 100% trawl efficiency is unrealistic. Other published estimates of mid-water trawl efficiency range from 1-80% (Williams et al. 2015). Thus, our biomass estimates are conservative and likely underestimate school size as well as overall biomass in the study region.

This study also has implications for the development of future surveys that target Atlantic menhaden. Conclusions drawn from simulation studies (Liang et al. 2020) proved correct in that a traditional acoustic survey design employing only a downward-facing echosounder collecting data only below the vessel along the transect will not be successful in estimating regional biomass of Atlantic menhaden. Given the dense schooling behavior of Atlantic menhaden, alternative survey designs that account for the patchy distribution of schools across the landscape should be employed when surveying for pelagic clupeids across a large geographic region. Our study provides an effective survey design that may prove useful in future monitoring. We also found that Atlantic menhaden schooling behavior was highly dependent on water temperature; thus, future winter surveys should incorporate real-time oceanographic condition monitoring tools to determine the most appropriate time to survey.

The estimates of regional Atlantic menhaden stock biomass generated by this study should also be useful in informing management of New Jersey's Atlantic menhaden bait fishery. New Jersey's winter bait fishery quota in a typical year is approximately 680 mt (1.5 million lbs), which represents a small fraction (6%-9%) of the estimated biomass in the study area (Table 7). Also, visual inspection of fish examined for maturity stage indicated that most of the Atlantic menhaden encountered were not actively spawning, which suggests the fishery in 2022 was not targeting spawning aggregations. Biomass estimates and life history information from this study can provide valuable context for future management actions and help ensure sustainable development of the fishery in this region.

Although we only sampled a relatively small number of schools (i.e., independent sample collections), most of the Atlantic menhaden encountered in winter were larger and older than fish typically encountered in the reduction fishery and inshore surveys used to inform the stock assessment. Information on size-at-age for older, larger Atlantic menhaden is rare, and we anticipate that data collected from this survey will help inform future stock assessment assumptions regarding growth.

Use of industry acoustics

By employing advanced echosounder and sonar equipment already present on an active fishing vessel, we were able to explore the utility of industry-series acoustic technology in cooperative research. Additional post-survey calibration and processing of ES80 files was required relative to the use of scientific-grade sonar. Thus, future acoustic studies that plan to use commercial sonar should anticipate substantial additional processing time and expense.

Despite these complications, we found the ES80 produced estimates of Atlantic menhaden school biomass that were similar to weigh-outs of individual schools at the dock. Acoustically derived biomass estimates and trawl catch weights obtained dockside by individually weighing each school were largely similar in magnitude (Fig. 7). Therefore, there is potential for the use of industry sonar to provide reasonable estimates of Atlantic menhaden biomass across a larger survey without the need to capture and weigh each school encountered. Obtaining CT or MRI digital scans of a subset of sampled fish to inform species-specific TS values would substantially reduce the uncertainty of abundance and biomass estimates generated by this and any future acoustic surveys targeting Atlantic menhaden.

Table 7. Atlantic menhaden biomass estimates for the study area relative to a suite of stock assessment and management metrics in both metric tons and pounds.

	Metric tons	Pounds
Study area biomass estimate min	**7,963**	**17,556,115**
Study area biomass estimate max	**11,005**	**24,261,843**
Coastwide age 1+ biomass from 2022 assessment	3,594,979	7,925,562,603
2022 NJ winter bait landings	1,411	3,110,380
2022 NJ winter trawl quota	1,361	3,000,000
More typical NJ winter trawl quota	~680	~1,500,000
NJ bait quota (all gears)	25,691	56,637,857
Coastwide 2022 bait landings	60,100	132,497,662
Coastwide 2022 reduction landings	134,000	295,419,080
Coastwide 2021 bait landings	North: 41,170 South: 17,830	North: 90,764,205 South: 39,308,375
Coastwide 2021 reduction landings	North: 59,620 South: 77,070	North: 131,439,444 South: 169,910,063

Evaluating ageing uncertainty

We found overall low agreement among ageing labs in this study, likely due to the focus on larger, older fish, the early time of year during which samples collected, and the quality of the samples collected given the gear used. Interlab agreement among the VIMS, NJDEP, and Beaufort ageing labs in this study was much lower than that of the 2015 Atlantic Menhaden scale ageing exchange (ASMFC 2015). In the 2015 study, scale age agreement was >80% among all three labs compared with percent agreement in this study which ranged from 36%-66% (Table 6). Similarly, ACV was low among the three labs in the 2015 study, but consistently exceeded the threshold of 7 in this study (range 7.8-14.97). Systematic differences among labs were also identified in this study with the high proportion of significant tests of symmetry for interlab comparisons vs the lack of bias evident in the previous ageing exchange.

The findings of this ageing exchange were presented at the ASMFC ageing workshop November 14-15, 2023 in Beaufort, NC. Due to significant disagreement among ageing labs, samples from this survey will be further examined by workshop participants in a second exchange in 2024 to refine Atlantic menhaden ageing protocols and determine best practices. VIMS, NJDEP, and Beaufort Laboratory will also repeat the ageing exchange from this study to further refine best practices for larger Atlantic menhaden encountered early in the year. This second survey exchange will also include Maryland Department of Natural Resources age and growth lab given their long history of and interest in ageing Atlantic menhaden.

DATA ARCHIVES

All raw echosounder and calibration data have been submitted to the archives at the National Centers for Environmental Information (URL pending). All scales and otoliths collected for this survey have been archived at the Beaufort Laboratory for use in future ageing studies.

ACKNOWLEDGEMENTS

Funding for this project was provided by the NOAA Saltonstall-Kennedy Program under award #NA20NMF4270163. Special thanks to New Jersey Department of Environmental Conservation and the states of Delaware, North Carolina, and South Carolina for ensuring adequate Atlantic menhaden quota was available to conduct the survey. We thank the captains and crew of the *F/V Dyrsten* and the staff at Lund's Fisheries in Cape May, NJ for their enthusiastic participation and support. We thank Eban Charles for assistance with data analysis and Mike Wilberg for data analysis advice. We thank Sarah Salois, Glen Gawarkiewicz, and Avijit Gangopadhyay for sharing data and advice on interpreting oceanographic conditions during our survey. Finally, we thank the Atlantic States Marine Fisheries Commission's Atlantic Menhaden Management Board for support of this project, the ASMFC Atlantic Menhaden Technical Committee for initial review and constructive feedback on survey design.

REFERENCES

Ahrenholz, D. 1994. Confidence of otolith ageing through the juvenile stage for Atlantic menhaden (Brevoortia tyrannus). Fishery Bull. **93**:209-216.

Ahrenholz, D. W. 1991. Population biology and life history of the North American menhadens, Brevoortia spp. Marine Fisheries Review **53**:3-19.

ASMFC. 2012. Amendment 2 to the Interstate Fishery Management Plan for Atlantic Menhaden. Arlington, VA.

ASMFC. 2015. Atlantic Menhaden Ageing Workshop Report. ASMFC, Arlington, VA.

ASMFC. 2022. Atlantic Menhaden Stock Assessment Update. Arlington, VA.

ASMFC. 2023. Report of the Quality Assurance/Quality Control Fish Ageing Workshop St. Petersburg, Florida March 7-9, 2023. Arlington, VA.

Bonzek, C. F., J. Gartland, D. J. Gauthier, and R. J. Latour. 2017. Northeast Area Monitoring and Assessment Program (NEAMAP) 2016 data collection and analysis in support of single and multispecies stock assessments in the Mid-Atlantic: Northeast Area Monitoring and Assessment Program Near Shore Trawl Survey. Virginia Institute of Marine Science, William & Mary. https://doi.org/10.25773/7206-KM61.

Bowker, A. H. 1948. A test for symmetry in contingency tables. Journal of the American statistical Association **43**:572-574.

Buchheister, A., T. J. Miller, E. D. Houde, D. H. Secor, and R. J. Latour. 2016. Spatial and temporal dynamics of Atlantic menhaden (Brevoortia tyrannus) recruitment in the

Northwest Atlantic Ocean. ICES Journal of Marine Science **73**:1147-1159.
Campana, S. E., M. C. Annand, and J. I. McMillan. 1995. Graphical and statistical methods for determining the consistency of age determinations. Transactions of the American Fisheries Society **124**:131-138.
Conn, P. B., J. T. Thorson, and D. S. Johnson. 2017. Confronting preferential sampling when analysing population distributions: diagnosis and model-based triage. Methods in Ecology and Evolution **8**:1535-1546.
Deegan, L. A., and B. A. Thompson. 1987. Growth Rate and Life History Events of Young-of-the-Year Gulf Menhaden as Determined from Otoliths. Transactions of the American Fisheries Society **116**:663-667.
Demer, D. 2015. Calibration of acoustic instruments. ICES Cooperative Research Report No. 326. 133 pp.
Diggle, P. J., R. Menezes, and T.-l. Su. 2010. Geostatistical inference under preferential sampling. Journal of the Royal Statistical Society Series C: Applied Statistics **59**:191-232.
Evans, G. T., and J. M. Hoenig. 1998. Testing and viewing symmetry in contingency tables, with application to readers of fish ages. Biometrics:620-629.
Fox, J. 2015. Applied regression analysis and generalized linear models. Sage Publications.
Garrison, L. P., J. S. Link, D. P. Kilduff, M. D. Cieri, B. Muffley, D. S. Vaughan, A. Sharov, B. Mahmoudi, and R. J. Latour. 2010. An expansion of the MSVPA approach for quantifying predator–prey interactions in exploited fish communities. ICES Journal of Marine Science **67**:856-870.
Hijmans, R. J. 2023. terra: Spatial Data Analysis. CRAN, Vienna, Austria.
Jech, J. M., and W. L. Michaels. 2006. A multifrequency method to classify and evaluate fisheries acoustics data. Canadian Journal of Fisheries and Aquatic Sciences **63**:2225-2235.
June, F. C., and J. W. Reintjes. 1959. Age and size composition of the menhaden catch along the Atlantic coast of the United States, 1952-55: with a brief review of the commercial fishery. US Department of Interior, Fish and Wildlife Service.
June, F. C., and C. M. Roithmayr. 1960. Determining age of Atlantic menhaden from their scales. US Fish and Wildlife Service.
Liang, D., G. M. Nesslage, and M. J. Wilberg. 2020. A spatial simulation approach to hydroacoustic survey design: A case study for Atlantic menhaden. Fisheries Research **222**:105402.
Liljestrand, E. M. 2017. Mortality and movement of adult Atlantic menhaden during 1966-1969 estimated from mark-recapture models. Master's Thesis. University of Maryland Center for Environmental Science Chesapeake Biological Laboratory.
Liljestrand, E. M., M. J. Wilberg, and A. M. Schueller. 2019a. Estimation of movement and mortality of Atlantic menhaden during 1966–1969 using a Bayesian multi-state mark-recovery model. Fisheries Research **210**:204-213.
Liljestrand, E. M., M. J. Wilberg, and A. M. Schueller. 2019b. Multi-state dead recovery mark-recovery model performance for estimating movement and mortality rates. Fisheries Research **210**:214-223.
Lindgren, F., H. Rue, and J. Lindström. 2011. An explicit link between Gaussian fields and Gaussian Markov random fields: the stochastic partial differential equation approach. Journal of the Royal Statistical Society: Series B (Statistical Methodology) **73**:423-498.
Lucca, B. M., and J. D. Warren. 2018. Acoustically measured distribution and abundance of Atlantic menhaden (*Brevoortia tyrannus*) in a shallow estuary in Long Island, NY. Estuaries and coasts **41**:1436-1447.

McNemar, Q. 1947. Note on the sampling error of the difference between correlated proportions or percentages. Psychometrika **12**:153-157.

Morison, A., J. Burnett, W. McCurdy, and E. Moksness. 2005. Quality issues in the use of otoliths for fish age estimation. Marine and Freshwater Research **56**:773-782.

National Marine Fisheries Service. 2018. Fisheries of the United States, 2017. U.S. Department of Commerce, NOAA Current Fishery Statistics No. 2017. Available at: https://www.fisheries.noaa.gov/national/sustainable-fisheries/fisheries-united-states#current-report.

Nesslage, G., A. M. Schueller, A. R. Rezek, and R. M. Mroch III. 2022. Influence of sample size and number of age classes on characterization of ageing error in paired-age comparisons. Fisheries Research **249**:106255.

Nicholson, W. R. 1978. Movements and population structure of Atlantic menhaden indicated by tag returns. Estuaries **1**:141-150.

Ogle DH, D. J., Wheeler AP, Dinno A 2023. FSA: Simple Fisheries Stock Assessment Methods. R package version 0.9.5, https://fishr-core-team.github.io/FSA/.

Pebesma, E. J. 2018. Simple features for R: standardized support for spatial vector data. R Journal **10**:439.

Pennino, M. G., I. Paradinas, J. B. Illian, F. Muñoz, J. M. Bellido, A. López-Quílez, and D. Conesa. 2019. Accounting for preferential sampling in species distribution models. Ecology and evolution **9**:653-663.

R Core Team. 2023. R: A language and environment for statistical computing. R Foundation for Statistical Computing, Vienna, Austria. URL https://www.R-project.org/.

Reintjes, J. W. 1969. Synopsis of biological data on the Atlantic menhaden, Brevoortia tyrannus. US Bureau of Commercial Fisheries.

Rudstam, L. G., S. L. Parker-Stetter, P. J. Sullivan, and D. M. Warner. 2009. Towards a standard operating procedure for fishery acoustic surveys in the Laurentian Great Lakes, North America. ICES Journal of Marine Science **66**:1391-1397.

Rue, H., S. Martino, and N. Chopin. 2009. Approximate Bayesian inference for latent Gaussian models by using integrated nested Laplace approximations. Journal of the Royal Statistical Society Series B: Statistical Methodology **71**:319-392.

SEDAR. 2015. SEDAR 40 – Atlantic Menhaden Stock Assessment Report. SEDAR, North Charleston SC. 643 pp. available online at: http://www.sefsc.noaa.gov/sedar/Sedar_Workshops.jsp?WorkshopNum=40. North Charleston, SC

Simmonds, J., and D. N. MacLennan. 2008. Fisheries acoustics: theory and practice. John Wiley & Sons.

Simpson, C., H. Bi, D. Liang, M. Wilberg, A. Schueller, G. Nesslage, and H. Walsh. 2017. Spawning locations and larval dispersal of Atlantic menhaden during 1977-2013. ICES Journal of Marine Science **74**:1574-1586.

Simpson, C., M. Wilberg, H. Bi, A. Schueller, G. Nesslage, and H. Walsh. 2016a. Trends in relative abundance and early life survival of Atlantic menhaden during 1977-2013 from long-term ichthyoplankton programs. Transactions of the American Fisheries Society **145**:1139-1151.

Simpson, D., J. B. Illian, F. Lindgren, S. H. Sørbye, and H. Rue. 2016b. Going off grid: Computationally efficient inference for log-Gaussian Cox processes. Biometrika **103**:49-70.

Smith, J. W. 1991. The Atlantic and gulf menhaden purse seine fisheries: Origins, Harvesting technologies, biostatistical monitoring, recent trends in fisheries statistics, and forecasting.

Marine Fisheries Review **53**:28-41.
Smith, J. W., W. B. O'Bier, and N. A. McNeill. 2008. Length and weight relationships for Atlantic menhaden (*Brevoortia tyrannus*). Journal of the North Carolina Academy of Science **124**:102-105.
Team, R. C. 2003. R: A Language and Environment for Statistical Computing R Foundation for Statistical Computing, Vienna, Austria. https://www.R-project.org.
Thompson, S. K. 2012. Sampling. John Wiley & Sons.
VanderKooy, S. 2020. A practical handbook for determining the ages of Gulf of Mexico and Atlantic coast fishes. Gulf States Marine Fisheries Commission: Ocean Springs, MS, USA.
Warlen, S. M. 1988. Age and growth of larval gulf menhaden, Brevoortia patronus, in the northern Gulf of Mexico. Fishery Bulletin **86**:77-90.
Warlen, S. M. 1992. Age, Growth, and Size Distribution of Larval Atlantic Menhaden off North Carolina. Transactions of the American Fisheries Society **121**:588-598.
Williams, K., J. K. Horne, and A. E. Punt. 2015. Examining influences of environmental, trawl gear, and fish population factors on midwater trawl performance using acoustic methods. Fisheries Research **164**:94-101.

Appendix A

Acoustic Survey Estimates of Atlantic Menhaden

Acoustic Survey Estimates of Atlantic Menhaden

Enhancing Sustainable Development of the Winter Bait Fishery for Atlantic Menhaden through the Use of Industry Acoustics (NOAA-NMFS-FHQ-2020-2006111)

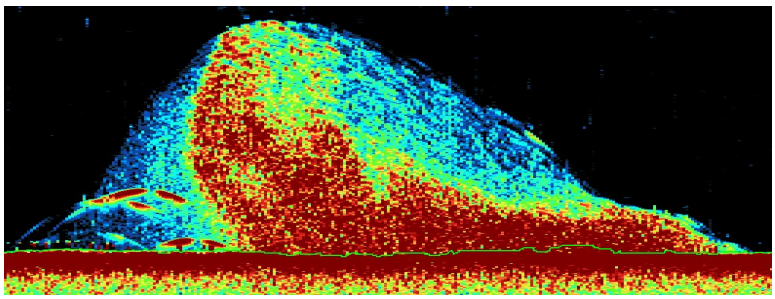

Prepared For
GENEVIÈVE NESSLAGE, PH.D.
Chesapeake Biological Laboratory
University of Maryland Center for Environmental Science
P. O. Box 38
Solomons, MD 20688

Prepared By
NORMANDEAU ASSOCIATES, INC.
30 International Drive, Suite 6
Portsmouth, NH 03801
www.normandeau.com

NORMANDEAU ASSOCIATES
ENVIRONMENTAL CONSULTANTS

September 26, 2023

Normandeau Project No. 24579.0

TABLE OF CONTENTS

LIST OF TABLES

LIST OF FIGURES

ACRONYMS AND ABBREVIATIONS

°C	Celsius
dB	decibels
NOAA	National Oceanic and Atmospheric Administration
Sa	Area backscattering strength (dB re m2/m2)
Sv	Volume backscattering strength
S-K	Saltonstall-Kennedy
TS	target strength (dB re 1 m^2)
UMCES	University of Maryland Center for Environmental Science

1 INTRODUCTION

1.1 Background

National Oceanic and Atmospheric Administration ("NOAA") Fisheries awarded a FY2020 Saltonstall-Kennedy ("S-K") Grant to University of Maryland Center for Environmental Science ("UMCES") for collaborative research project titled *Enhancing sustainable development of the winter bait fishery for Atlantic menhaden through the use of industry acoustics* (NOAA-NMFS-FHQ-2020-2006111; "the Project"). The Project addresses S-K Priority #2 for "Science or Technology that Promotes Sustainable U.S. Seafood Production and Harvesting" by providing scientific information necessary to support sustainable development of the winter bait fishery for Atlantic Menhaden and maximize fishing opportunities for the Mid-Atlantic midwater trawl fleet. While Atlantic Menhaden stocks have supported a successful winter bait fishery since 2014, historically low catch-based quotas have limited fishing opportunities despite recent stock assessments indicate that total spawning stock biomass has doubled in the last two decades, the stock is not overfished and overfishing is not occurring. Before alternative quotas can be established, estimates of the biomass and size structure of the overwintering stock believed to be elusive to traditional bottom trawl surveys are needed. The Project sought to fill that data gap by conducting an adaptive acoustic survey for Atlantic Menhaden along approximately 400 kilometers of transects approximately 24–32 km (15–20 miles) offshore from the Hudson Canyon to the New Jersey/Delaware border based on simulations for an optimal survey design (Liang et al 2020). After delays related to COVID-19 pandemic and warm winter water temperatures, this survey was completed between February 14 and March 3, 2022. February 14–15 and February 20–March 3, 2022.

Normandeau Associates, Inc. ("Normandeau") received a subaward to collaborate with UMCES on this Project. Normandeau's role in the Project is to process and analyze data collected from the *F/V Dyrsten's* Simrad ES80 split-beam echosounder for purposes of estimating Atlantic Menhaden abundance and biomass. This report documents the echogram processing methods and estimates of school biomass based on the ES80 echosounder data.

1.2 Objectives

The Project's objectives were to:

1. Estimate overwintering biomass and structure of Atlantic Menhaden in the winter bait fishery's primary fishing area,
2. Evaluate performance of industry acoustics in estimating Atlantic Menhaden biomass,
3. Evaluate ageing uncertainty, and
4. Effectively communicate and disseminate project findings to scientists and fishery managers.

This report presents the methods and results addressing Research Objective #2 above. The specific objective of this report is to:

- Estimate biomass and abundance of Atlantic Menhaden schools from volume backscatter collected by a Simrad ES80 echosounder and compare acoustic and trawl abundance/biomass estimates from coincidental data to assess relative performance.

2 OVERVIEW OF THE SURVEY DESIGN

The acoustic survey design was based on spatial simulations to account for challenges of patchy distributions that pelagic schooling species like Atlantic Menhaden display (Liang et al. 2020). This acoustic survey was designed to target Atlantic Menhaden during cold winter months when their behavior easier to acoustically survey. Once water temperatures drop below 6°C, Atlantic Menhaden form recognizable schools near the bottom and exhibit sedentary behavior, which make them easier to classify and minimizes bias associated with vessel avoidance and double counting. The survey was conducted in an area approximately 24–80 km (15–50 miles) off the coast of New Jersy in water depths of 20–50 m, where a winter bait fishery typically operates, and Atlantic Menhaden bycatch is concentrated. Based on anticipated school size and patchiness, this area was acoustically sampled along six transects with an average length of 54 km spaced 24–32 km apart and perpendicular to the coast (Figure 1-1).

The research vessel used for this survey was a 49-m commercial midwater trawling vessel, *F/V Dyrsten,* which was equipped with a recordable 38-kHz Simrad ES80 split-beam echosounder, Furono FSV25S omnidirectional sonar, midwater water trawl (net dimensions of 18 m high, 51 m wide and 3.25-cm mesh), and other navigation systems (Figure 1-2). Unlike previous Simrad industry-grade echosounders, the ES80 echosounder does not contain a systematic "triangle-waver" error component. A Hydrolab MS5 multi-sonde was used to measure depth profiles of water temperature (°C), salinity (PSU) and dissolved oxygen (mg/L) at the start and end of each transect and every 10 km along the transect.

Once the survey began, the vessel sampled along the transects at approximately 7 knots (3.6 m/s) with the ES80 split-beam echosounder while the omnidirectional sonar was used to search for schools within a distance of 1,600 m on either side of the transect (vessel). The ES80 split-beam echosounder collected at the fastest ping rate setting in narrowband ("continuous wave") mode and 0.256-ms pulse duration. The acoustic backscatter from the omnidirectional sonar was scrutinized in real time by the captain and if schools were detected, the vessel would break from the planned transects to collect backscatter of the schools and on occasion fished with the midwater trawl. Five schools were fished with the midwater trawl to collect biological samples. A unique school ID number was assigned to each school (discrete or close aggregation) identified in real time by the omnidirectional sonar and a log was created with timestamps for corresponding ES80 data files.

The survey cruise was completed over several periods (legs):

- February 11, 2022 – Calibration
- February 14–15, 2022 – Leg 1 (Transects 1–2)
- February 20–22, 2022 – Leg 2 (Transects 4–6)
- February 23–22, 2022 – Leg 2 transit and opportunistic sampling
- February 28–March 3, 2022 – Leg 3 (opportunistic during fishing)

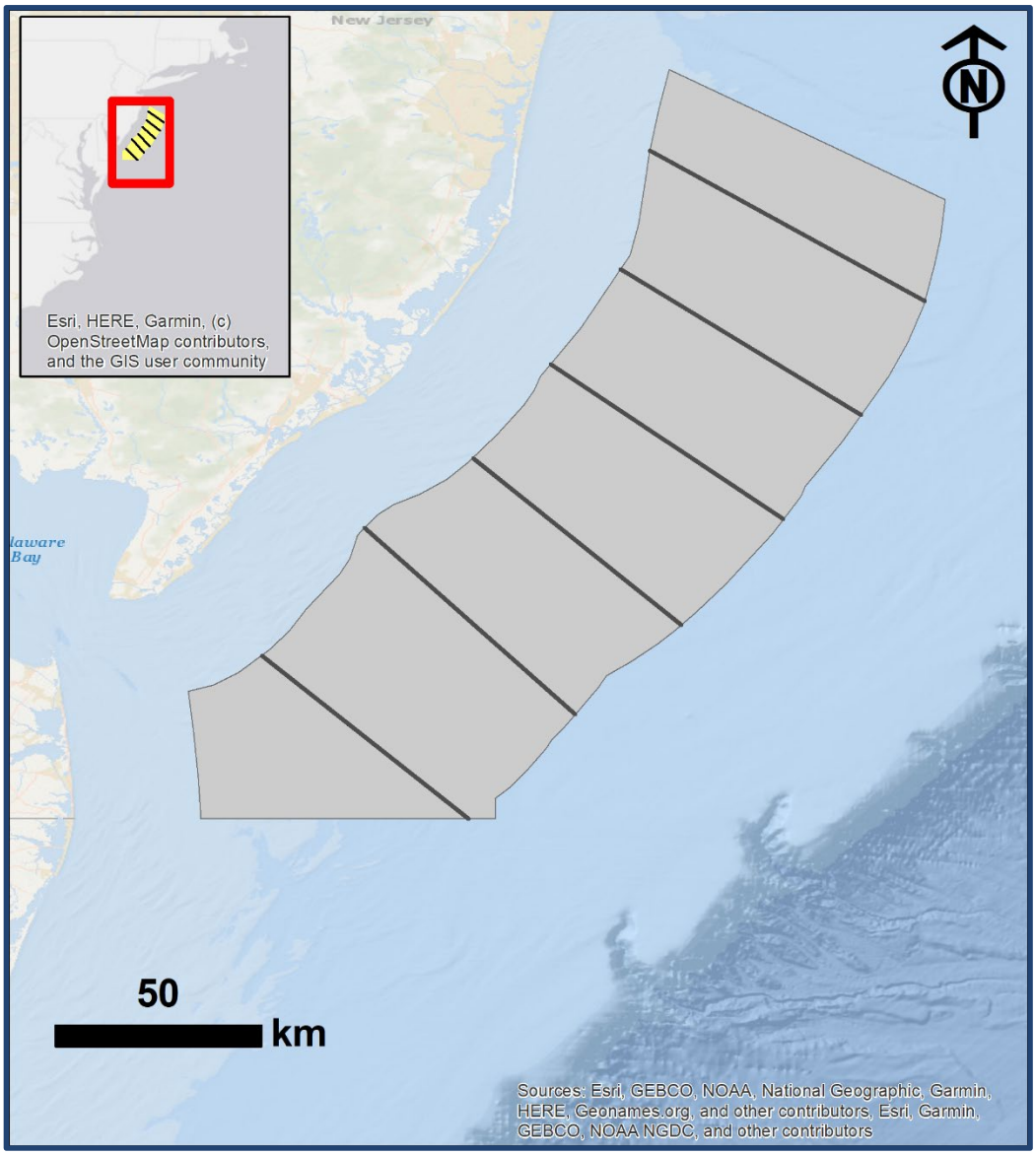

Figure 1-1 **The primary bait fishery region 24–80 km offshore of the New Jersey coast was surveyed systematically over six transects perpendicular to the coast and spaced 23 km apart (~400 km total).**

Figure 1-2 **(Top) 49-m commercial midwater trawling vessel, *F/V Dyrsten*, equipped with a recordable 38 kHz Simrad ES80 split-beam echosounder and a Furuno FSV25S omnidirectional sonar. (Bottom) Instrumentation and sonar displays at the helm.**

3 CALIBRATION

3.1 Field Calibration

The Simrad ES80 echosounder with a 7° split-beam 38-kHz ES38B transducer mounted to the hull of the 48.8-m commercial mid-water trawler *F/V Dyrsten*, was calibrated by the standard sphere method (Foote et al. 1987, Demer 2015) off the southern New Jersey shore on 11 February 2022. A solid 38.1-mm tungsten carbide (with 6% cobalt binder) sphere was used as the standard target for calibration. The sphere was attached by monofilament line to a wireless calibration system developed by the Northeast Fisheries Science Center ("NEFSC"). The calibration sphere was lowered under the transducer to a range of approximately 8.3 to 11.9 m with weights added to the line approximately 2 m below the sphere to provide additional stability in the currents (Figure 3-1). The calibration system communicated wirelessly with the downriggers via control circuitry that was housed in waterproof Pelican cases (one case per downrigger). Open-source JAVA software called EchoCal was used written to control the downriggers from a laptop PC. The user used a digital joystick to instruct EchoCal where to position the calibration sphere to map the beam pattern and measure on-axis response.

The reference target strength of the sphere was estimated by NOAA/SWFSC/AST (2022) as -42.31 dB re m^2 at nominal environmental conditions (water temperature = 5.75°C; salinity = 35 PSU; pressure = 2 atmospheres [20.3 dbar]) during the field calibration (Appendix A). Using the default transducer gain setting of 23 dB, the mean target strength of the sphere was -49.48 dB re m^2 but more peculiar was the angular dependence of the TS estimates (increases with off-axis angle that is more exaggerated in the minor-axis angle (Figure 3-2). In the field, the calibration was adjusted by setting the major-axis angle offset to -0.10°, minor-axis angle offset to 2.0°, transducer gain of 20.1 dB and S_a correction factor to 0.8318 dB, which resulted in the single echo detections of the sphere to have a mean TS of -44.72 dB re m^2.

3.2 Echoview Calibration

Since Echoview software (version 12.1 or 13, Hobart, Tasmania) was used to process and export acoustic estimates of Atlantic Menhaden biomass, the ES80 data files of the calibration sphere were used to adjust calibration results from the field. In Echoview, the sound speed was updated based on water temperature in the data file source (surface temperature from the ship's NMEA network) and user-entered salinity estimate. Target strength of the sphere was determined from single echo detections within region in the echogram corresponding to the echo traces of the sphere (Figure 3-1). Single echo detection criteria selected in Echoview are given in Table 1-1. Single echo detections were also analyzed after filtering out single echoes greater than 0.5° off the acoustic axis following the on-axis definition by Demer et al. (2015). The target strength of the sphere under field conditions prior to field calibration adjustments to angles (Figure 3-3) and after angular offsets were applied (Figure 3-4) indicate further improvement was possible. Based on all single echo detections in Echoview, the echo strength peaked at a major axis angle offset of -0.43° and minor axis angle offset at 2.02° (Figure 3-5). The transducer gain was adjusted to 19.67 dB such that the mean target strength of on-axis single echo detections matched the reference target strength of -42.31 dB re m^2. After the transducer gain was adjusted, a new S_a correction factor of 1.2652 dB was determined based on the on-axis sphere targets and equation 4.9 from Demer et al. (2015). The adjusted transducer gain and S_a correction factor from the post-hoc analysis of the calibration data in Echoview was updated in the Echoview calibration supplement file (*Dyrsten-cal_11February2022-Final20221220.ecs*).

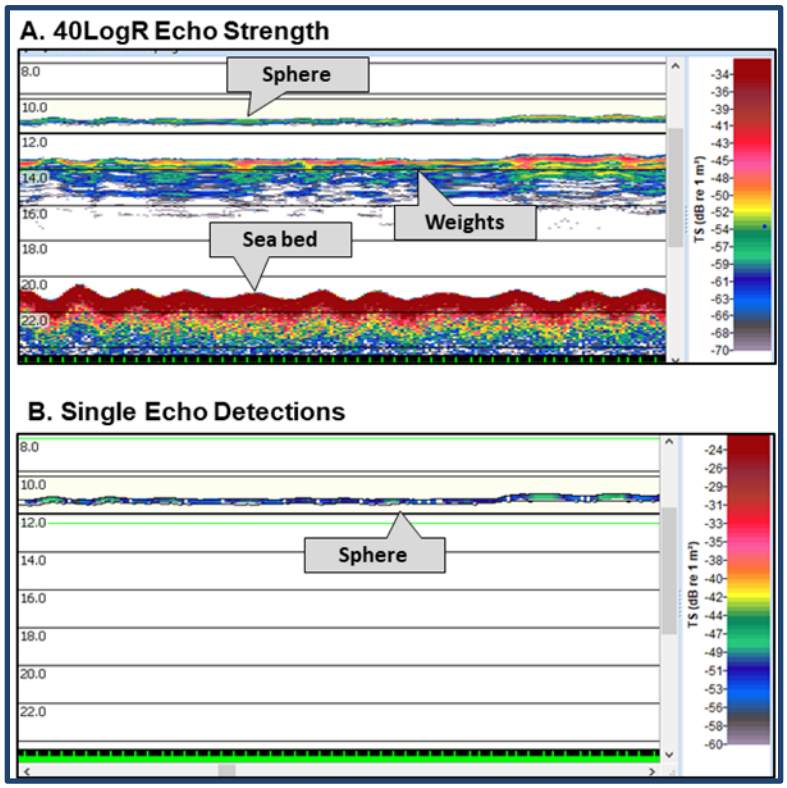

Figure 3-1 **(A) Raw echo strength (40Log R) ES80 amplitudes during calibration on 11 February 2022, (B) single echo detections sphere near 11 m.**

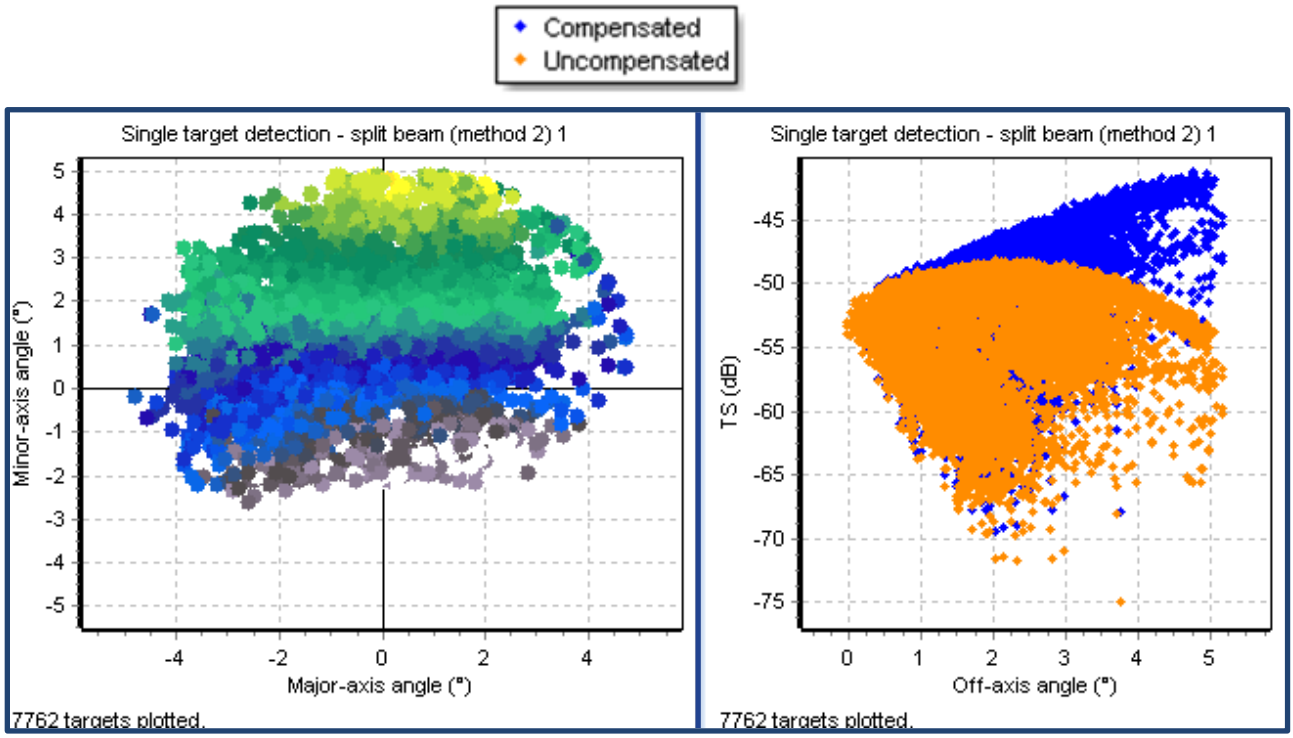

Figure 3-2 Angular TS compensation plots of 38.1 mm Tungsten Carbide sphere with default Transducer Gain at 23 dB.

Table 3-1 Single echo detection criteria used in Echoview software settings.

Parameter	Value Setting
Echoview algorithm	Split Beam Method 2
TS threshold	-70 dB
Pulse length determination level	6 dB
Minimum normalized pulse length	0.5 dB
Maximum normalized pulse length	2.0 dB
Beam compensation model	Simrad LOBE
Maximum beam compensation	12 dB
Minor-axis angles	1°
Major-axis angles	1°

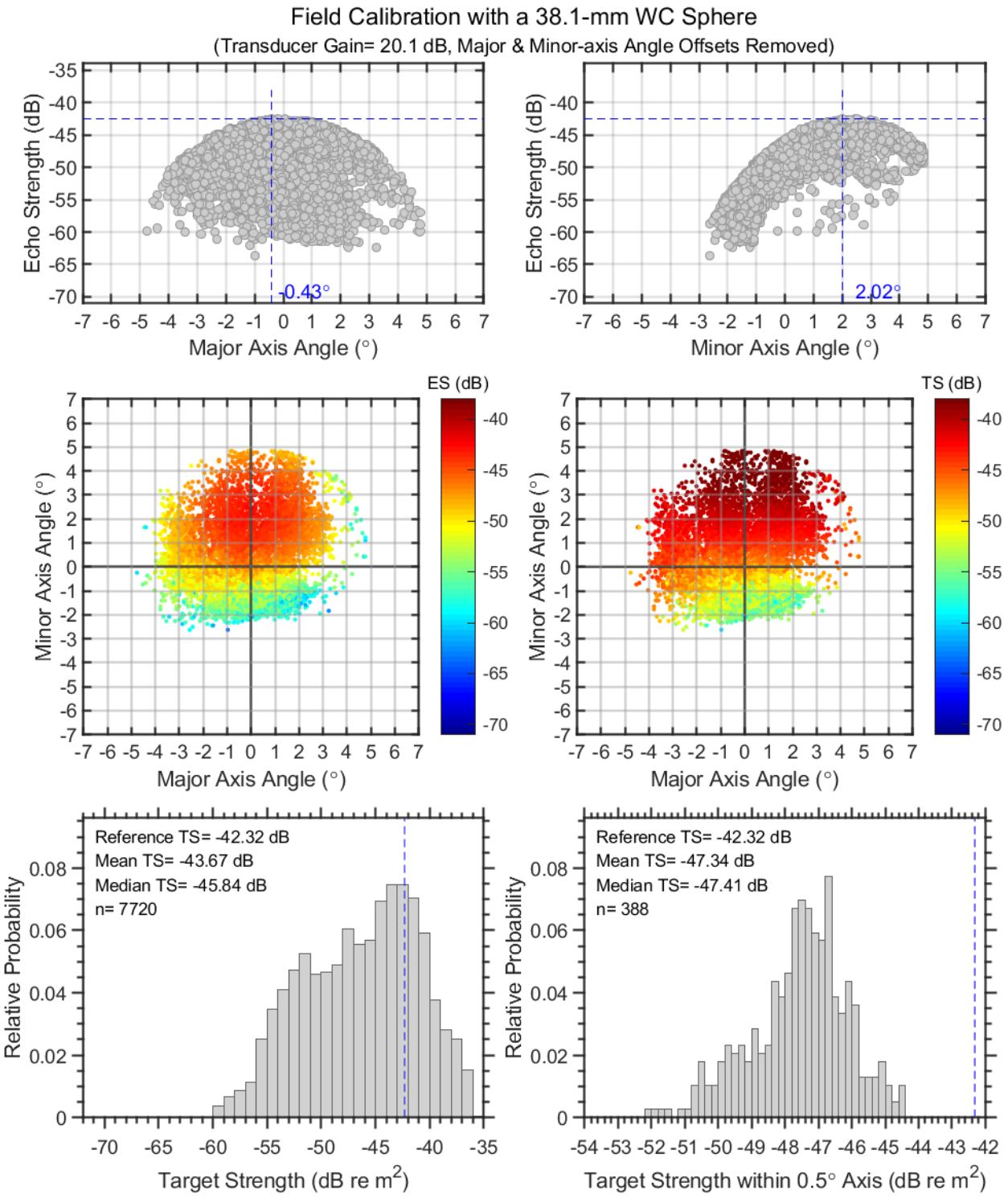

Figure 3-3 **TOP and MIDDLE: Angular target strength plots of a 38.1-mm Tungsten Carbide sphere with field-calibrated transducer gain of 20.1 dB and major and minor axis angle offsets from field calibrations removed; BOTTOM: target strength histograms of all (left) and on-axis (right) single echo detections.**

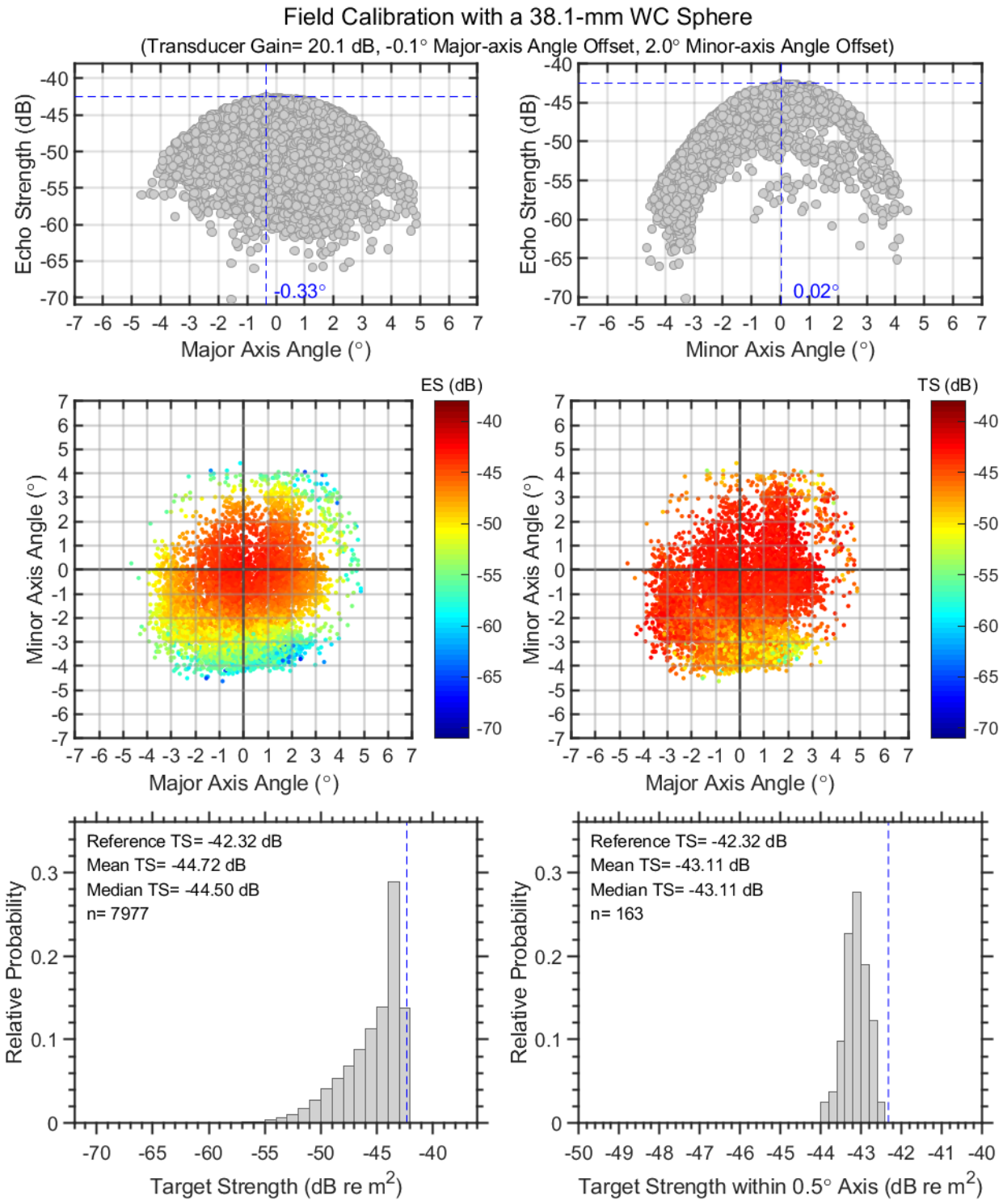

Figure 3-4 **TOP and MIDDLE: Angular target strength plots of a 38.1-mm Tungsten Carbide sphere with field-calibrated transducer gain of 20.1dB and major and minor axis angle offsets applied; BOTTOM: target strength histograms of all (left) and on-axis (right) single echo detections.**

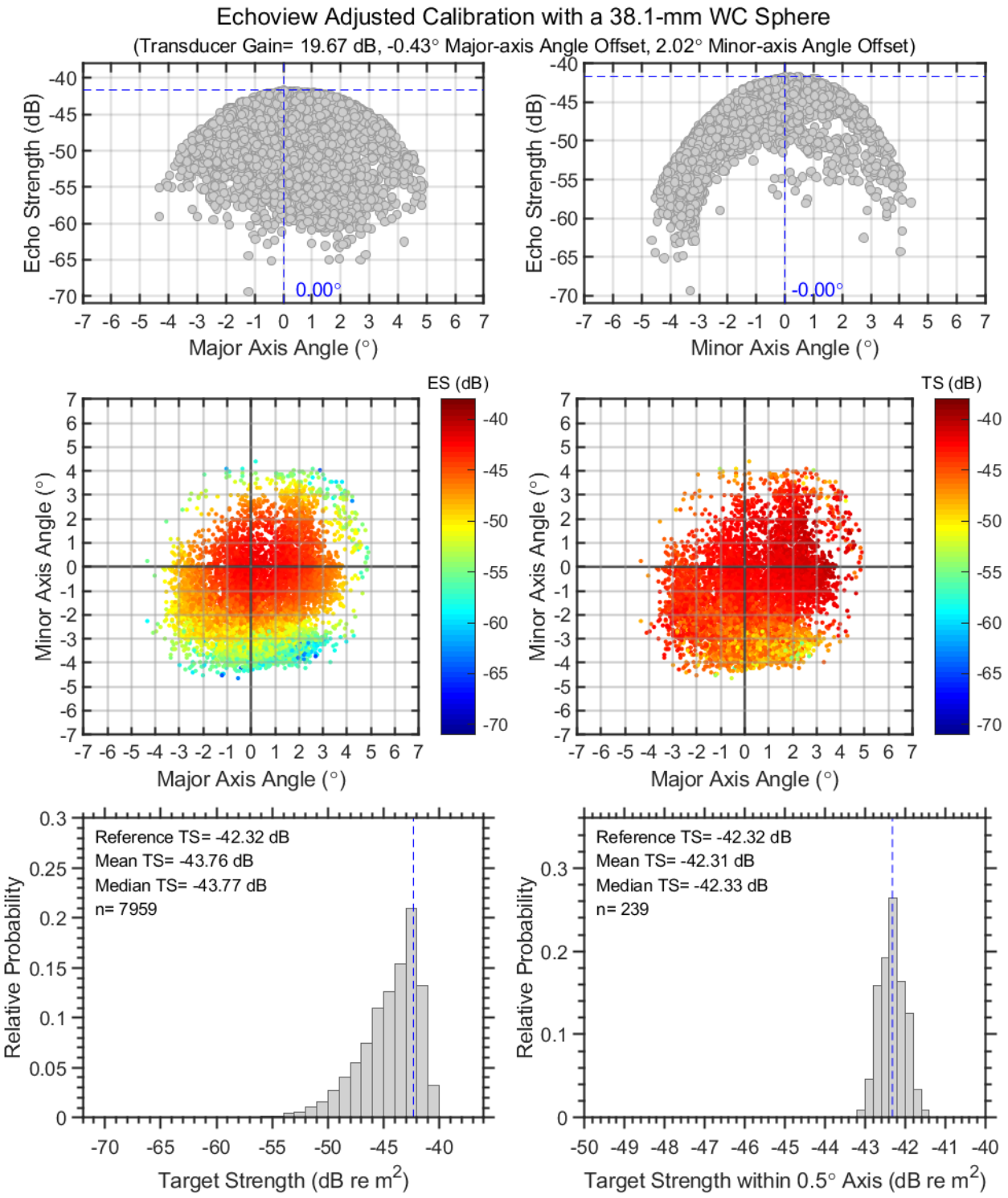

Figure 3-5 **TOP and MIDDLE: Angular target strength plots of 38.1 mm Tungsten Carbide sphere with on-axis adjustments of transducer gain to 19.67 dB and major and minor axis angle offsets of -0.43° and 2.02° ; BOTTOM: target strength histograms of all (left) and on-axis (right) single echo detections.**

4 ECHOGRAM PROCESSING

4.1 ES80 Data

4.1.1 ES80 Raw Data File Structure

The survey generated 2,788 files (878 GB) in raw ES80 data files that were timestamped at the start of each recording. File names also were saved with prefixes exemplified as follows:

- TS1_1* = transect 1, segment 1
- PREF1_1* = pre-fishing school number 1, pass 1 (i.e., ES80 data collected on the first pass over school ID 1 before it was fished)
- FISH1_1* = pass 1 of school ID 1 while fishing
- POSF1_1* = post-fishing school number 1, pass 1 (i.e., ES80 data collected on the first pass over school ID 1 after it was fished)
- TS0 = used during transit between transects, to and from port, and ancillary searching for schools after the vessel completed surveying the six transects.

4.1.2 ES80 Processed Data

The primary objective was to process the ES80 data files corresponding to schools identified in real time by the captain and technician from the omnidirectional sonar. Not all schools detected in the omnidirectional sonar imagery and assigned a school number (i.e., ID #) were observed or passed over with the ES80 split-beam echosounder. Video recordings of the omnidirectional sonar were made but synchronization and/or school morphometric analysis was outside of the scope of this report. A log was maintained to record ES80 data files corresponding with observed co-located schools, which composed the list of data processed here. The data processed included ES80 data files corresponding to the five schools fished (IDs 10, 12, 13, 49 and 123). School ID 123 was observed in Leg 3, which followed a storm event and when schools became less dense and coherent (i.e., School ID 123 represented multiple discrete schools in the echogram).

The data processed as described above are itemized in Table 4-1 through Table 4-5.

4.2 Echoview Settings and Configurations

4.2.1 Transducer Location and Orientation

The *F/V Dyrsten* has a draft estimated to be approximately 4.3 m (14 ft) with no fish/water cargo and 5.2 m (17 ft) under full load. The transducer is mounted 1.8 m (6 ft) below the keel. For purposes of processing data and approximating the water depth, the transducer was assumed to be at a water depth of 6.5 m. The transducer was mounted securely in reverse direction where the forward arrow on the transducer was pointed to the stern. To compensate for this, a beam rotation of 180° was used during processing.

4.2.2 Timestamp and Clock Synchronization

Timestamps in the ES80 data were GMT zone (EST+5 hours). However, the clock for the ES80 data collection computer and times ES80 files were offset (fast) by approximately 58 minutes. Actual EST can be adjusted as GMT- 4:02. Notes and logged observations with timestamps corresponding to the omnidirectional sonar or fishing may be variably off from the observed times in the ES80 echograms because of time elapsed to transit to and over the schools.

4.2.3 Environmental Settings and Calibration Files

The Hydrolab profile measurements were used to estimate representative average water quality conditions during each leg of the survey. The differences on sound speed estimates for each leg were negligible (Table 4-1). The final calibration file (*Dyrsten-cal_11February2022-Final20221220.ecs*) was updated for sound speed in each leg (*Dyrsten-cal_Leg1.ecs*, *Dyrsten-cal_Leg2.ecs,* and *Dyrsten-cal_Leg3.ecs*).

4.2.4 Minimum S_v Threshold

Several echograms were examined that contained small pelagic fish backscatter and large benthic Atlantic Menhaden school backscatter. Minimum S_v Threshold curves for selected fish backscatter versus water column background S_v following methods of Jech and Michaels (2006) would indicate a minimum S_v threshold could have been set between -50 dB and -60 dB. However, Rudstam et al. (2009) suggests setting the minimum S_v threshold to be equivalent to the minimum TS of interest. Assuming the minimum TS of interest and minimum single echo detection criterion to be -50 dB, then the TS uncompensated for beam pattern would be -56 dB, which converts to approximately -63 dB assuming sound speed of 1475 m/s and 55 m in range. Given the minimum TS threshold of -63 dB and -66 dB minimum Sv threshold used by Jech and Michaels (2006) for Atlantic Herring (*Clupea harengus*), the minimum S_v threshold used in this study was a conservative nominal value of -64 dB.

4.3 Echoview Processing Steps

Final steps toward establishing an Echoview template to batch process the echograms and export volume and area backscattering data required to optimize several data flow steps. Figure 4-1 shows an example echogram of Atlantic Menhaden schools (Schools 2 and 3) that shows the long ring down from the transducer, which contaminates the upper water column down just past 20 m water depth, and how the echogram was cleaned. Figure 4-2 illustrates these steps.

Table 4-1 ES80 raw files with real-time school identifications during Leg 1 as documented in *ES80 File Guide.xlsx*.

No.	Filename	Sampling Type	Comment
1	Schools_PREF11_1-D20220215-T174356.raw	Pre-fishing pass	
2	Schools_PREF14_1-D20220215-T223025.raw	Pre-fishing pass	
3	Schools_PREF19_1-D20220215-T232246.raw	Pre-fishing pass	
4	Schools_PREF2_1-D20220214-T145605.raw	Pre-fishing pass	File started recording mid passage over a school; no raw files immediately prior to this file
5	Schools_PREF21_1-D20220215-T232704.raw	Pre-fishing pass	Empty (no regions)
6	Schools_PREF3_1-D20220214-T145830.raw	Pre-fishing pass	
7	Schools_PREF4_2-D20220214-T152458.raw	Pre-fishing pass	
8	Schools_TS2_10-D20220215-T234606.raw	Transect 2 (Segment 10)	
9	Schools_PREF18_1-D20220215-T223419	Pre-fishing pass	

Table 4-2 ES80 raw files with real-time school identifications during Leg 2 as documented in *ES80 File Guide.xlsx*.

No.	Filename	Sampling Type	Comment
1	Schools_PREF27_1-D20220220-T183757.raw	Pre-fishing pass	Empty (no regions)
2	Schools_PREF33_1-D20220220-T211238.raw	Pre-fishing pass	
3	Schools_PREF38_1-D20220221-T201049.raw	Pre-fishing pass	
4	Schools_TS0_2-D20220220-T165655.raw	Transect Crossover	No apparent school or related backscatter in echogram
5	Schools_TS3_4-D20220220-T194134.raw	Transect 3 segment 4	

Table 4-3 Echoview files with real-time school identifications associated with ES80 raw files of fished schools (10, 12, 13, 49, 123).

No.	Filename	Sampling Type	Raw Files	School ID (Pass)	Comment
1	FSchools_FISH10_1-D20220215-T162130.EV	FISH	FISH10_1-D20220215-T162130.raw FISH10_1-D20220215-T162316.raw FISH10_1-D20220215-T162558.raw FISH10_1-D20220215-T163220.raw	10-1	16:26:20 16:29:37
2	FSchools_FISH12_1-D20220215-T181907.EV	FISH	FISH12_1-D20220215-T181907.raw	12-1	18:22:25
3	FSchools_FISH12_2-D20220215-T183841.EV	FISH	FISH12_2-D20220215-T183841.raw FISH12_2-D20220215-T184249.raw	12-2	18:41:08
4	FSchools_FISH13_1-D20220215-T200734.EV	FISH	FISH13_1-D20220215-T200734.raw FISH13_1-D20220215-T203359.raw FISH13_1-D20220215-T203630.raw FISH13_1-D20220215-T204516.raw FISH13_1-D20220215-T205402.raw	13-1	20:09:55 20:43:38 20:53:23
5	Schools_TS0_13-D20220301-T133900.EV	TS0	TS0_13-D20220301-T133900.raw	49	13:41:53
6	FSchools_FISH123_1-D20220303-T162416.EV	FISH	FISH123_1-D20220303-T162416.raw	123-1	16:24:17
7	FSchools_FISH123_1-D20220303-T164028.EV	FISH	FISH123_1-D20220303-T164028.raw FISH123_1-D20220303-T164311.raw	123-1	16:42:59
8	FSchools_FISH123_1-D20220303-T165225.EV	FISH	FISH123_1-D20220303-T165225.raw	123-1	16:53:59
9	FSchools_ FISH123_1-D20220303-T165555.EV	FISH	FISH123_1-D20220303-T165555.raw	123-1	16:57:34
10	FSchools_ FISH123_1-D20220303-T171703.EV	FISH	FISH123_1-D20220303-T171703.raw FISH123_1-D20220303-T171944.raw FISH123_1-D20220303-T172226.raw	123-1	17:17:57 17:19:38
11	FSchools_FISH123_1-D20220303-T172704.EV	FISH	FISH123_1-D20220303-T172704.raw	123-1	Smpelagic schools, no clear large menhaden schools
12	FSchools_FISH123_2-D20220303-T174800.EV	FISH	FISH123_2-D20220303-T174800.raw FISH123_2-D20220303-T175040.raw FISH123_2-D20220303-T175320.raw FISH123_2-D20220303-T175456.raw	123-2	17:49:32 SPelagic 17:51:30 Menh 17:54:04 OtherFish 17:57:03sPelagic
13	FSchools_FISH123_2-D20220303-T180536.EV	FISH	FISH123_2-D20220303-T180536.raw FISH123_2-D20220303-T180816.raw FISH123_2-D20220303-T181058.raw FISH123_2-D20220303-T181338.raw	123-2	18:06:06 Menh 18:06:45 Menh 18:06:45 Menh 18:07:06 Menh
14	FSchools_FISH123_2-D20220303-T182141.EV	FISH	FISH123_2-D20220303-T182141.raw	123-2	18:22:31 Menh

Table 4-4 ES80 raw files with real-time school identifications during Leg 3 as documented in *ES80 File Guide.xlsx*.

No.	Note	Filename	School Number	Recorded ES80 Time	Field Comment
1		TS0_11-D20220301-T001218.raw	44	0:15:00	
2		TS0_11-D20220301-T001218.raw	45	0:17:45	
3		TS0_11-D20220301-T001946.raw	46	0:20:30	
4		TS0_13-D20220301-T133900.raw	49	13:41:45	PREF PASS IN TS0_13
5		TS0_14-D20220301-T213020.raw	59	21:31:08	
6		TS0_14-D20220301-T213020.raw	60	21:32:55	ES80 IN TS0_14 FILE AT 15:35
7		TS0_14-D20220301-T213020.raw	61	21:33:56	ES80 DATA ON TS0_14 AT 15:34
8		TS0_14-D20220301-T213603.raw	62	21:36:15	ES80 IN TS0_14 AT 13:35
9		TS0_14-D20220301-T213603.raw	63	21:36:58	ES80 IN TS0_14 AT 15:37 - DISPERSED AS WE WENT OVER
10		TS0_17-D20220303-T135611.raw	67	13:57:50	
11		TS0_17-D20220303-T135848.raw	68	13:59:00	
12	1	TS0_17-D20220303-T140622.raw	76	14:07:20	
13	1	TS0_17-D20220303-T140622.raw	77	14:08:00	
14	2	TS0_17-D20220303-T140859.raw	78	14:11:20	
15		TS0_17-D20220303-T141510.raw	79	14:16:00	
16		TS0_17-D20220303-T142157.raw	82	14:22:30	
17		TS0_17-D20220303-T142434.raw	83	14:24:50	
18		TS0_17-D20220303-T150226.raw	89	15:02:40	
19		TS0_17-D20220303-T150226.raw	90	15:04:35	
20		TS0_17-D20220303-T150738.raw	97	15:07:40	
21		TS0_17-D20220303-T151014.raw	98	15:10:45	
22		TS0_17-D20220303-T151014.raw	99	15:12:30	
23		TS0_17-D20220303-T151014.raw	101	15:12:30	
24		TS0_17-D20220303-T151337.raw	102	15:15:30	
25		TS0_17-D20220303-T151613.raw	106	15:16:15	
26		TS0_17-D20220303-T151613.raw	107	15:17:33	
27		TS0_17-D20220303-T151849.raw	108	15:19:05	
28		TS0_17-D20220303-T152229.raw	111	15:23:00	
29		TS0_17-D20220303-T152400.raw	112	15:26:10	
30		TS0_17-D20220303-T152637.raw	113	15:27:56	
31		TS0_17-D20220303-T152637.raw	114	15:28:18	
32		TS0_17-D20220303-T153358.raw	115	15:35:25	
33		TS0_17-D20220303-T153634.raw	116	15:37:10	
34		TS0_17-D20220303-T153911.raw	117	15:39:15	EVADED AS WE APPROACHED - VERY LIGHT FISH BACKSCATTER ON ECHOGRAM UP HIGH
35		TS0_17-D20220303-T153911.raw	119	15:41:20	
36		TS0_17-D20220303-T154148.raw	120	15:42:10	
37		TS0_17-D20220303-T154659.raw	126	15:49:05	ONLY GOT A SMALL PIECE
38		TS0_17-D20220303-T154935.raw	127	15:51:20	
39		TS0_17-D20220303-T155212.raw	128	15:52:30	

No.	Note	Filename	School Number	Recorded ES80 Time	Field Comment
40		TS0_18-D20220303-T212855.raw	129	21:30:05	
41		TS0_18-D20220303-T213134.raw	130	21:31:36	
42		TS0_18-D20220303-T213134.raw	132	21:33:35	
43		TS0_18-D20220303-T213413.raw	134	21:35:15	SURFACE SCHOOL ON ES80
44		TS0_18-D20220303-T213653.raw	135	21:36:55	
45		TS0_18-D20220303-T213844.raw	136	21:39:30	STRIPERS SEEN ON ES80 RIGHT AFTER THE SCHOOL
46		TS0_18-D20220303-T214124.raw	137	21:42:30	STRIPERS FEEDING ON SCHOOL ON ES80 - VERY CLEAR
47		TS0_18-D20220303-T214124.raw	138	21:43:50	SCATTERED SCHOOL, SAWN SOME SINGLE TARGETS - COULD BE MENHADEN OR STRIPER
48		TS0_18-D20220303-T222142.raw	139	22:21:40	COUNTING LOOSE JOINING SPOTS AS ONE - MANY STRIPERS SEEN AROUND THIS SCHOOL AND ON ES80
49		TS0_18-D20220303-T222422.raw	141	22:24:44	
50		TS0_18-D20220303-T222532.raw	142	22:27:33	
51		TS0_18-D20220303-T222811.raw	143	22:28:38	
52		TS0_18-D20220303-T222811.raw	145	22:30:45	
53	3	TS0_18-D20220303-T223051.raw	147	22:33:26	
54		TS0_18-D20220303-T223609.raw	149	22:36:10	
55		TS0_18-D20220303-T223851.raw	150	22:40:50	LOOSE SPOTS ON SONAR - BREAKING AS WE APPROACH, BUT SHOWED A SMALL SCHOOL TIGHT TO THE BOTTOM
56	4	TS0_18-D20220303-T224132.raw	151	22:42:10	DIDNT SHOW ON ES80 BUT RAN OVER - MAYBE SURFACE SCHOOL? - CAN BARELY SEE FISH MARKS BELOW NEARFIELD ON ES80 RECORDING POST
57		TS0_18-D20220303-T224412.raw	152	22:44:32	SPLIT AS WE APPROACHED - FISH SURE LOOK ON THE MOVE ON ES80 SIGNATURE
58	5	TS0_18-D20220303-T224501.raw	154	22:45:40	ALL SECTIONS OF SCHOOL WAY MORE THAN 400T - JUST HUGE - STRIPERS SEEN ON ES80 ON MANY OF THE SCHOOLS IN THIS AREA - SEEN HERE CHARGING INTO THE SCHOOL
59		TS0_18-D20220303-T224741.raw	155	22:49:25	
60		TS0_18-D20220303-T225242.raw	158	22:54:00	
61	6	TS0_18-D20220303-T225242.raw	160	22:55:18	

1 Schools were truncated, added TS0_17-D20220303-T141135.raw
2 Concatenated with TS0_17-D20220303-T140622.raw to avoid truncated schools
3 Schools were truncated, added TS0_18-D20220303-T223334.raw
4 No menhaden or other schools (excluded from further analysis)
5 Concatenated with TS0_18-D20220303-T224412.raw to avoid truncated schools
6 Schools were truncated, added TS0_18-D20220303-T225523.raw

Table 4-5 Echoview and ES80 raw files included in the processed data containing real-time school identifications during Leg 3 as documented in *ES80 File Guide.xlsx*.

No.	EV Filename	Raw Files
1	Schools_TS0_11-D20220301-T001218.EV	TS0_11-D20220301-T001218.raw
2	Schools_TS0_11-D20220301-T001946.EV	TS0_11-D20220301-T001946.raw
3	Schools_TS0_13-D20220301-T133900.EV	TS0_13-D20220301-T133900.raw
4	Schools_TS0_14-D20220301-T213020.EV	TS0_14-D20220301-T213020.raw
5	Schools_TS0_14-D20220301-T213603.EV	TS0_14-D20220301-T213603.raw
6	Schools_TS0_17-D20220303-T135611.EV	TS0_17-D20220303-T135611.raw
7	Schools_TS0_17-D20220303-T135848.EV	TS0_17-D20220303-T135848.raw
8	Schools_TS0_17-D20220303-T140622.EV	TS0_17-D20220303-T140622.raw TS0_17-D20220303-T141135.raw TS0_17-D20220303-T140859.raw
9	Schools_TS0_17-D20220303-T141510.EV	TS0_17-D20220303-T141510.raw
10	Schools_TS0_17-D20220303-T142157.EV	TS0_17-D20220303-T142157.raw
11	Schools_TS0_17-D20220303-T142434.EV	TS0_17-D20220303-T142434.raw
12	Schools_TS0_17-D20220303-T150226.EV	TS0_17-D20220303-T150226.raw
13	Schools_TS0_17-D20220303-T150738.EV	TS0_17-D20220303-T150738.raw
14	Schools_TS0_17-D20220303-T151014.EV	TS0_17-D20220303-T151014.raw
15	Schools_TS0_17-D20220303-T151337.EV	TS0_17-D20220303-T151337.raw
16	Schools_TS0_17-D20220303-T151613.EV	TS0_17-D20220303-T151613.raw
17	Schools_TS0_17-D20220303-T151849.EV	TS0_17-D20220303-T151849.raw
18	Schools_TS0_17-D20220303-T152229.EV	TS0_17-D20220303-T152229.raw
19	Schools_TS0_17-D20220303-T152400.EV	TS0_17-D20220303-T152400.raw
20	Schools_TS0_17-D20220303-T152637.EV	TS0_17-D20220303-T152637.raw
21	Schools_TS0_17-D20220303-T153358.EV	TS0_17-D20220303-T153358.raw
22	Schools_TS0_17-D20220303-T153634.EV	TS0_17-D20220303-T153634.raw
23	Schools_TS0_17-D20220303-T153911.EV	TS0_17-D20220303-T153911.raw
24	Schools_TS0_17-D20220303-T154148.EV	TS0_17-D20220303-T154148.raw
25	Schools_TS0_17-D20220303-T154659.EV	TS0_17-D20220303-T154659.raw
26	Schools_TS0_17-D20220303-T154935.EV	TS0_17-D20220303-T154935.raw
27	Schools_TS0_17-D20220303-T155212.EV	TS0_17-D20220303-T155212.raw
28	Schools_TS0_18-D20220303-T212855.EV	TS0_18-D20220303-T212855.raw
29	Schools_TS0_18-D20220303-T213134.EV	TS0_18-D20220303-T213134.raw
30	Schools_TS0_18-D20220303-T213413.EV	TS0_18-D20220303-T213413.raw
31	Schools_TS0_18-D20220303-T213653.EV	TS0_18-D20220303-T213653.raw
32	Schools_TS0_18-D20220303-T213844.EV	TS0_18-D20220303-T213844.raw
33	Schools_TS0_18-D20220303-T214124.EV	TS0_18-D20220303-T214124.raw
34	Schools_TS0_18-D20220303-T222142.EV	TS0_18-D20220303-T222142.raw
35	Schools_TS0_18-D20220303-T222422.EV	TS0_18-D20220303-T222422.raw
36	Schools_TS0_18-D20220303-T222532.EV	TS0_18-D20220303-T222532.raw
37	Schools_TS0_18-D20220303-T222811.EV	TS0_18-D20220303-T222811.raw
38	Schools_TS0_18-D20220303-T223051.EV	TS0_18-D20220303-T223051.raw TS0_18-D20220303-T223334.raw
39	Schools_TS0_18-D20220303-T223609.EV	TS0_18-D20220303-T223609.raw
40	Schools_TS0_18-D20220303-T223851.EV	TS0_18-D20220303-T223851.raw
41	Schools_TS0_18-D20220303-T224412.EV	TS0_18-D20220303-T224412.raw TS0_18-D20220303-T224501.raw
42	Schools_TS0_18-D20220303-T224741.EV	TS0_18-D20220303-T224741.raw
43	Schools_TS0_18-D20220303-T225242.EV	TS0_18-D20220303-T225242.raw TS0_18-D20220303-T225523.raw

Table 4-6 Mean maximum depth, and depth-averaged water temperature and salinity from profile[1] measurements taken by a Hydrolab MS5 multi-parameter sonde during each survey leg.

Leg	Dates (including transit)	Transects	Number of Profiles	Maximum Depth (m)	Mean Depth-averaged Temperature (°C)	Mean Depth-averaged Salinity (PSU)	Sound Speed[2] (m/s)
1	13–15 Feb 2022	1–2	17	50.6	6.0	33.8	1473.5
2	19–25 Feb 2022	3–6	30	51.3	6.3	34.0	1475.0
3	27 Feb–3 Mar 2022		6	32.7	6.4	33.7	1475.0
All	13 Feb–4 Mar 2022		53	51.3	6.2	33.9	1474.5

1 Profile measurements excluded data above the nominal transducer depth (6.5 m).

2 Sound speed was estimated from temperature and salinity assuming depth = 25 m (MacKenzie 1981).

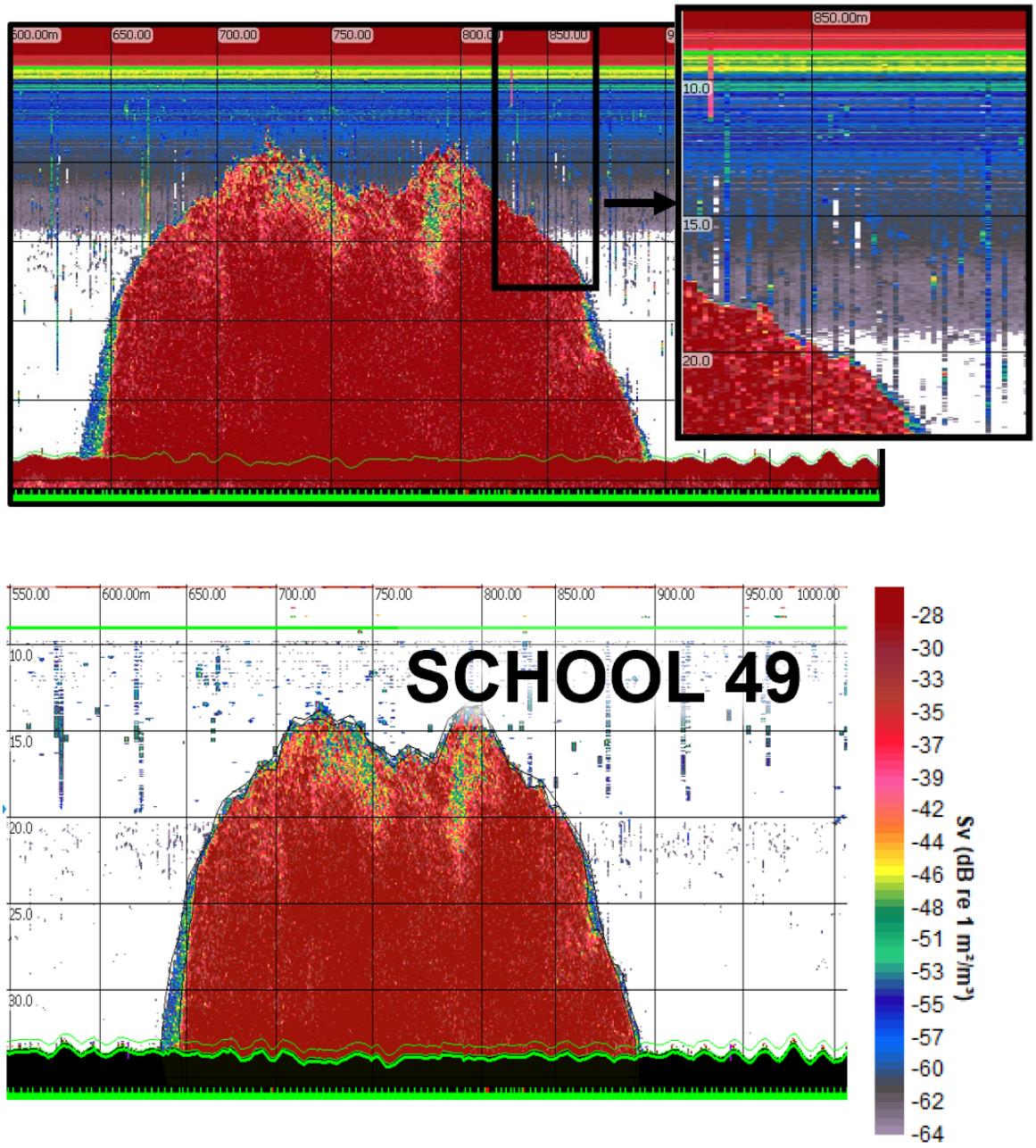

Figure 4-1 **Example of Sv backscatter of School 49 in ES80 raw data. (TOP) shows apparent noise ringing down to approximately 20 m and random impulse noise. (BOTOM) Filtered Sv backscatter after masking the upper water column and remove the impulse noise spikes.**

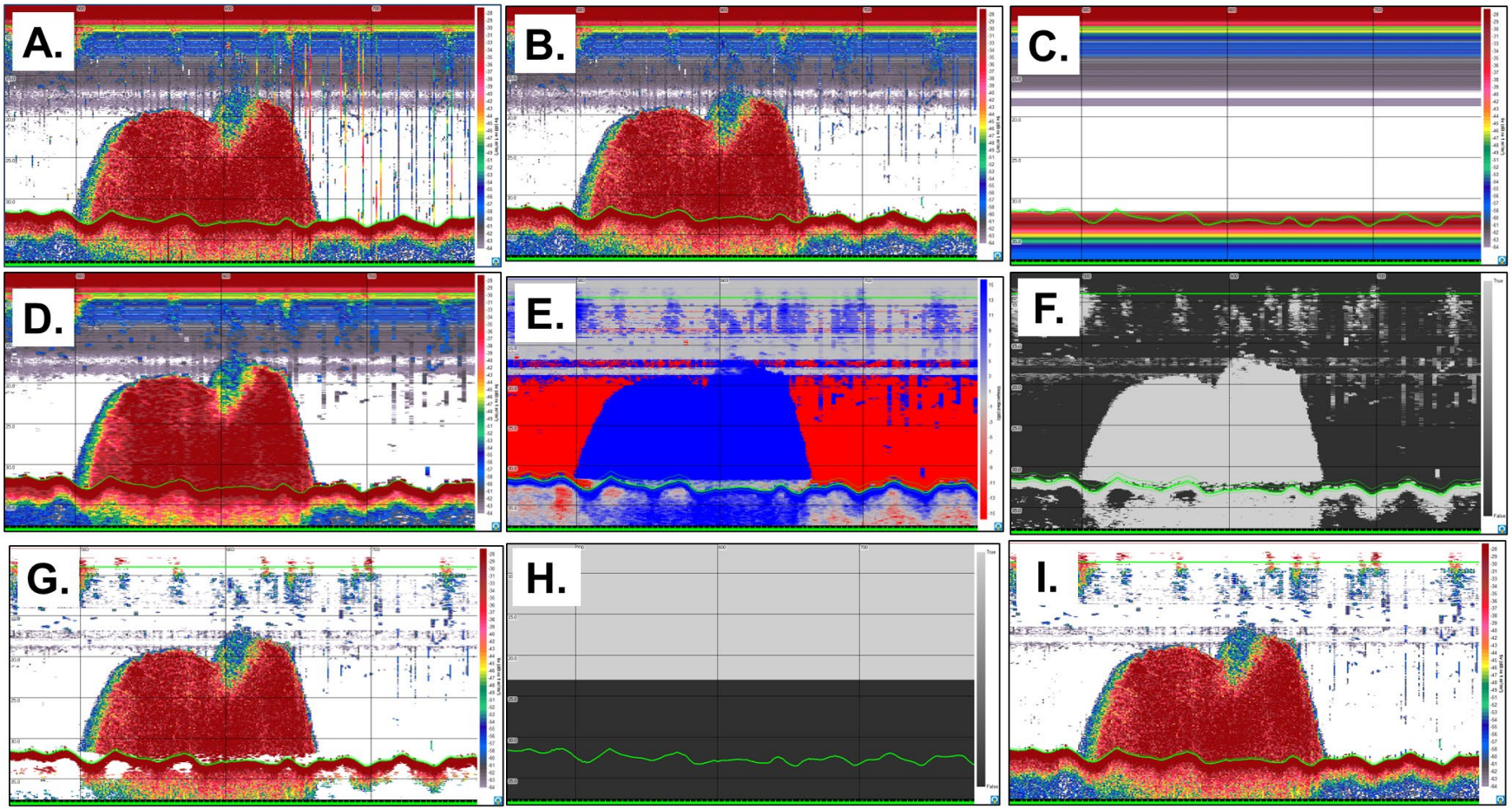

Figure 4-2 **Step by Step Echogram Processing: A. Raw S_v. B. Impulse noise removed (Ryan et al. 2015). C. Resampled (median of 2000 ping × 3 sample window and matched S_v pings. D. Smoothed 3×3 S_v. E. Signal-to-Noise Ratio (SNR). F. Mask |SNR| > 3 dB. G. Filtered Sv Mask to water column. H. Upper (23 m) water column mask. I. Filtered S_v.**

5 TARGET STRENGTH AND INDIVIDUAL BODY SIZE

5.1 Target Strength

Target strength is important in estimating volumetric and areal density of Atlantic Menhaden from the mean volume backscattering and area backscattering coefficients, respectively. To convert to fish per m^3 or m^2, TS was back-transformed from a dB value to a linear quantity called the backscattering cross-section ($\sigma_{bs} = 10^{(TS/10)}$); however, TS is often used to characterize the acoustic quantity representative of a target or fish. The TS representative of a single Atlantic Menhaden to use for this study does carry with it a degree of uncertainty given the lack of specific-specific experimental data, model estimates, and *in situ* estimates. Exploratory analysis of the echograms containing Atlantic Menhaden during this survey indicated that schools were too dense to obtain an *in situ* TS estimate. Instead, TS was estimated based on total length (TL), which is an established method in acoustic surveys (Simmonds and McLennan 2005).

Without species-specific TS data or equations for Atlantic Menhaden, Lucca and Warren (2018) used a generalized TS-TL equation (Emmrich et al. 2012, Love 1971) to acoustically estimate distribution and abundance of Atlantic Menhaden in estuarine waters of Long Island, New York. The mean TS (-32.2 dB re 1 m^2) of Atlantic Menhaden at 38 kHz used in this study was estimated following equation:

$$TS = 19.1\text{Log}_{10}(TL) + 0.9\text{Log}_{10}(f, kHz) - 62 \quad \text{(Eq. 1)}$$

where TS = target strength (dB re 1 m^2),
TL = total length (cm), and
f = acoustic frequency (kiloHertz, kHz)

In another study, Lucca and Warren (2019) made fishery-independent observations of adult Atlantic Menhaden in coastal waters south of New York where they used an alternative TS-TL equation for 120-kHz data based on models of other clupeids but without specific details on its derivation:

$$TS = 20.40\text{Log}_{10}(TL) - 68.88 \quad \text{(Eq. 2}$$

If Equation 2 was applied to the 38-kHz ES80 in this study, the mean TS would be -38.59 dB re 1 m^2, which would increase abundance by over four-fold. However, Lucca and Warren (2019) determined mean *in situ* TS at 120 kHz was -32.8 dB re 1 m^2 at Atlantic Beach and -35.7 dB re 1 m^2 at Hempstead. To further advance acoustic surveys of Atlantic Menhaden, TS measurements and models specific to the species is area of research for improving the uncertainty of abundance and biomass.

5.2 Individual Body Size

Length measurements among the five midwater trawl catches from all legs of the survey were similar, and as such, all individual measurements from biological samples were pooled. The mean TL was 30.5 cm and mean fork length (FL) was 26.5 cm using the following equation developed from measurements taken in this study:

$$TL\ (mm) = 1.091988\ (FL, mm) + 16.09377 \quad \text{(Eq. 3)}$$

For biomass estimation, the individual mean body weight (W) of 0.285 kg was based on the length-weight equation developed from biological samples collected in this study:

$$W\ (kg) = (1.352604 \times 10^{-7}) \times\ (TL, mm)^{2.544937} \qquad \text{(Eq. 4)}$$

6 ANALYTICAL METHODS

Table 6-1. List of exported analysis variables from Echoview are below with analyzed variables explained.

Variable	Comment
ABC	area backscattering coefficient (m2/m2), primary acoustic metric, see EV help
Area_Backscatter_Strength	
Depth_mean	
Good_samples	
Lat_E	
Lat_M	
Lat_S	
Leg	Survey leg number
Lon_E	
Lon_M	
Lon_S	
NASC	
Ping_E	
Ping_M	
Ping_S	
Region_ID	
Region_bottom_altitude_max	
Region_bottom_altitude_mean	
Region_bottom_altitude_min	
Region_class	
Region_top_altitude_max	
Region_top_altitude_mean	
Region_top_altitude_min	
Sv_max	
Sv_mean	
Sv_min	
Thickness_mean	
Time_E	
Time_M	
Time_S	
date_e	
date_m	

Variable	Comment
date_s	
fish_m2	Areal Fish Density of classified echogram region (Number of fish per square meter) = ABC/($10^{(meanTS/10)}$)
fish_m3	Volumetric Fish Density of classified echogram region (Number of fish per cubic meter) = $10^{(Sv\_mean/10)}$/($10^{(meanTS/10)}$)
kg_m2	Areal Biomass Density of classified echogram region (Kilograms per square meter) = fish_m2 X meanKg
kg_m3	Volumetric Biomass Density of classified echogram region (Number of kilograms per cubic meter) = fish_m3 X meanKg
meanKg	0.285 kg W (kg) = (1.352604×10^{-7}) × (TL, mm)$^{2.544937}$ (this study) where mean TL = 305.4 mm, based on TL (mm) = 1.091998 × (FL, mm) + 16.096377 (this study) where mean FL = 265 mm
meanTS	TS (dB) = 19.1Log10(TL, cm) - 60.58 (at 38 kHz)
region_name	
start_date	Reformatted start date (mm/dd/yy) of echogram region
Volume_shape	Shape of the school volume approximated as a "Dome" if the region (school) extending to seafloor or an "Ellipsoid" if the region is in the water column off seafloor
Volume_m3	Volume in cubic meters of in ideal symmetrical dome or ellipsoid
school_fish	=fish_m3 x volume_m3
school_kg	=kg_m3 x volume_m3
svfile	Individual Echoview export filename

6.1 Volume Calculations

1. Only schools regions classified as **MenhadenRegion** or **MenhadenSchool**
2. **Volume Shape**. Benthic versus midwater/surface schools:

```
if region_bottom_altitude_min <= 0 then Volume_Shape = 'Dome';
if region_bottom_altitude_min >0 then Volume_Shape = 'Ellipsoid';
```

3. **Dome volume.** The tallest pixel with the classified region represent the dome height and is described in the Echoview export as Region_Top_Altitude_Max. A spherical, symmetrical dome approximates the volume of a benthic school with a dome or hump like echo trace. The volume is given $V = \frac{1}{6}\pi h(3r^2 + h^2)$

```
dome_height = region_top_altitude_max;
volume_m3 =(1/6)*constant('PI')*dome_height*((3*(0.5*uncorrected_length)**2)
+ dome_height**2);
```

4. **Ellipsoid volume.** Assume the maximum height of the school in water (height) and assumes in the planar cross-sectional view (i.e., seen from the vessel down onto the school) is a circle (symmetrical) with a radius equivalent to half of the observed school echo trace length (i.e., uncorrected_length). The ellipsoid volume was calculated as:

$$V = \frac{4}{3}\pi\, r_L^2 r_H$$

```
if volume_shape = 'Ellipsoid' then do;

*volume of ideal ellipsoid;
*4/3 x pi x RL^2 x RH;
*where RL = radius or half of observed trace length (uncorrected length);
*where RH = half of the height (tallest dimension);
volume_m3 =
(4/3)*constant('PI')*((0.5*uncorrected_length)**2)*(0.5*(region_top_altitude_
max-region_bottom_altitude_min));

end;
```

7 RESULTS

Biomass and numeric densities and abundance estimates for Atlantic Menhaden were delivered to UMCES with accompanying data deliverable memos. Based on discrete benthic "dome-like" Menhaden schools directly fished, the acoustically derived biomass estimates and trawl catch were often in similar agreement (Figure 7-1).

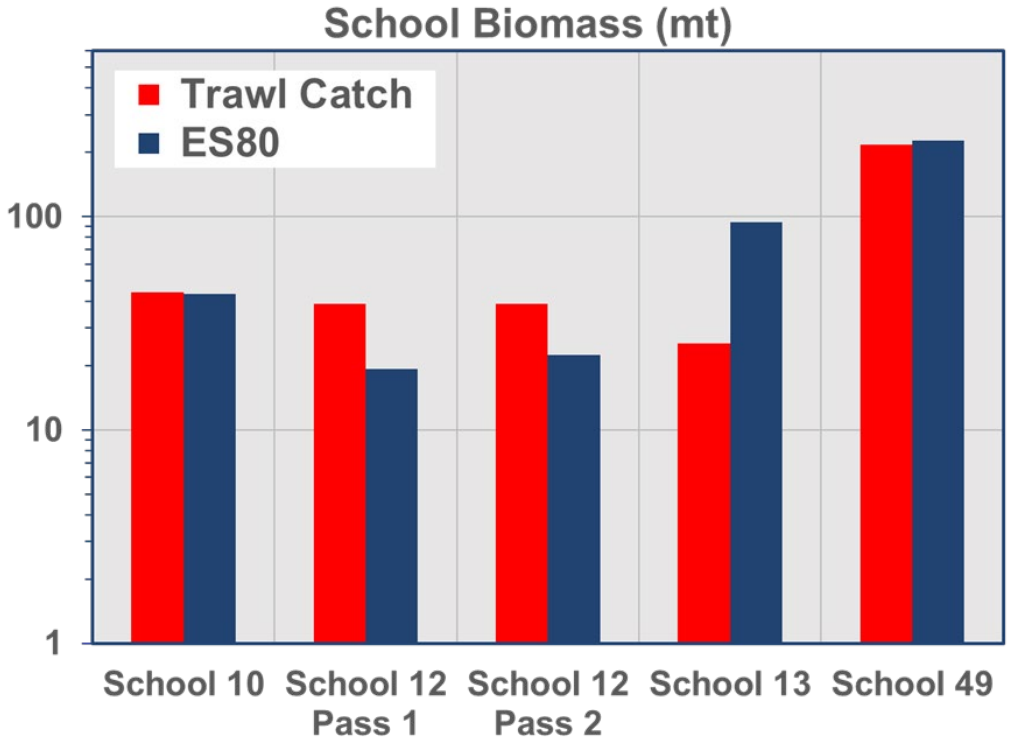

Figure 7-1 **Atlantic Menhaden school biomass estimates by midwater trawl and Simrad ES80 split-beam echosounder. Acoustically-derived density was scaled to biomass (metric tons) based on the ideal dome volume (school height, school length).**

8 LITERATURE CITED

Demer, D. 2015. Calibration of acoustic instruments. ICES Cooperative Research Report No. 326. 133 pp.

Emmrich, M., I.J. Winfield, J. Guillard, A. Rustadbakken, C. Verges, P. Volta, E. Jeppesen, T.L. Lauridsen, S. Brucet, K. Holmgren, C. Argillier, and T. Mehner. 2012. Strong correspondence between gillnet catch per unit effort and hydroacoustically derived fish biomass in stratified lakes. Freshwater Biology 57(12): 2436-2448.

Foote, K. G., H. P. Knudsen, G. Vestnes, D. N. MacLennan, and E. J. Simmonds. 1987. Calibration of acoustic instruments for fish density estimation: A practical guide. ICES Coop. Res. Rep., No. 144. 69 pp.

Liang, D., G. M. Nesslage, and M. J. Wilberg, 2020. A spatial simulation approach to hydroacoustic survey design: A case study for Atlantic menhaden. Fisheries Research 122: 105402. https://doi.org/10.1016/j.fishres.2019.105402

Love, R. H. 1971. Dorsal-aspect target strength of an individual fish. Journal of the Acoustical Society of America 49: 816-823.

Lucca, B. M., and J. D. Warren. 2018. Acoustically measured distribution and abundance of Atlantic Menhaden (*Brevoortia tyrannus*) in a shallow estuary in Long Island, NY. Estuaries and Coasts 41:1436-1447.

Lucca, B.M. and J.D. Warren. 2019. Fishery-independent observations of Atlantic menhaden abundance in the coastal waters south of New York. Fisheries Research 218: 229-236.

Mackenzie, K.V. 1981. Nine-term equation for sound speed in the ocean. Journal of Acoustical Society of America 70: 807-812.

NOAA Fisheries/SWFSC/AST. (National Oceanic and Atmospheric Administration Fisheries /Southwest Fisheries Science Center/Advanced Survey Technologies). 2022. Standard Sphere Target Strength Calculator. https://www.fisheries.noaa.gov/data-tools/standard-sphere-target-strength-calculator

Ryan T. E., Downie R. A., Kloser R. J., Keith G. 2015. Reducing bias due to noise and attenuation in open-ocean echo integration. ICES Journal of Marine Science 72, 2482-2493

Simmonds, J., and D. MacLennan. 2005. Fisheries Acoustics: Theory and Practice, Second edition. Blackwell Science, Oxford, UK.

Appendix A. Reference Target Strength

Advanced Survey Technologies
Southwest Fisheries Science Center

Standard Sphere Target Strength Calculator

Sphere parameters

Material: WC
Diameter: 38.1 mm
Density: 14900 kg/m^3
Longitudinal sound speed: 6853 m/s
Transversal sound speed: 4171 m/s

Water parameters

(●) Temperature: 5.75 °C
Salinity: 35 PSU
Pressure: 20.3 dbar
( ) Sound speed: 1473.81 m/s
Density: 1027.68 kg/m^3

Signal parameters

( ) Center frequency: 38 kHz
Pulse duration: 256 µs
(●) Bandwidth: 38 to 38 kHz
Resolution: 0.04 kHz

Calculate

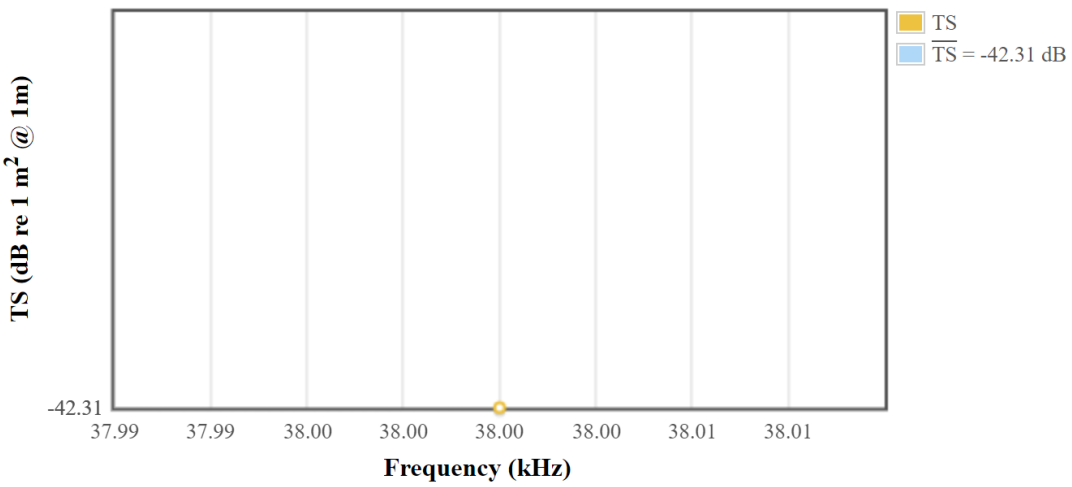

Appendix B. Placeholder

Appendix B

Atlantic Menhaden School Biomass Estimates

Data Collection Period	Date	Mean depth (m)	School biomass (kg)	School biomass (mt)
Survey - Leg 1	2/14/2022	28.16	381.68	0.38
Survey - Leg 1	2/14/2022	28.58	1,379.05	1.38
Survey - Leg 1	2/14/2022	26.43	77,887.39	77.89
Survey - Leg 1	2/14/2022	16.72	499.24	0.50
Survey - Leg 1	2/14/2022	20.12	2,064.57	2.06
Survey - Leg 1	2/14/2022	10.55	937.60	0.94
Survey - Leg 1	2/14/2022	25.55	11,620.19	11.62
Survey - Leg 1	2/15/2022	38.27	2.78	0.00
Survey - Leg 1	2/15/2022	31.27	78,246.04	78.25
Survey - Leg 1	2/15/2022	33.82	28,112.10	28.11
Survey - Leg 1	2/15/2022	32.52	18,150.45	18.15
Survey - Leg 1	2/15/2022	27.32	144,707.01	144.71
Survey - Leg 1	2/15/2022	28.70	462,288.93	462.29
Survey - Leg 1	2/15/2022	20.06	48.24	0.05
Survey - Leg 1	2/15/2022	33.92	46,571.75	46.57
Survey - Leg 1	2/15/2022	14.52	8.26	0.01
Survey - Leg 1	2/15/2022	14.80	1.87	0.00
Survey - Leg 1	2/15/2022	24.63	70,209.34	70.21
Survey - Leg 1	2/15/2022	32.13	219.16	0.22
Survey - Leg 1	2/15/2022	26.72	2,474.88	2.47
Survey - Leg 2	2/20/2022	23.19	3.55	0.00
Survey - Leg 2	2/20/2022	20.94	148.29	0.15
Survey - Leg 2	2/21/2022	16.18	9.88	0.01
Post Survey - Leg 3	3/1/2022	25.40	582,588.46	582.59
Post Survey - Leg 3	3/1/2022	22.67	10,926.57	10.93
Post Survey - Leg 3	3/1/2022	27.12	223.77	0.22
Post Survey - Leg 3	3/1/2022	19.71	5,826.53	5.83
Post Survey - Leg 3	3/1/2022	25.40	582,588.46	582.59
Post Survey - Leg 3	3/1/2022	27.02	22,697.61	22.70
Post Survey - Leg 3	3/1/2022	26.95	130,973.04	130.97
Post Survey - Leg 3	3/1/2022	27.25	55,581.34	55.58
Post Survey - Leg 3	3/1/2022	29.61	2,855.61	2.86
Post Survey - Leg 3	3/1/2022	26.78	126,253.24	126.25
Post Survey - Leg 3	3/3/2022	22.25	749.60	0.75
Post Survey - Leg 3	3/3/2022	26.20	1,112.99	1.11
Post Survey - Leg 3	3/3/2022	25.07	4,555.39	4.56
Post Survey - Leg 3	3/3/2022	29.59	106.87	0.11
Post Survey - Leg 3	3/3/2022	29.97	105.99	0.11
Post Survey - Leg 3	3/3/2022	29.39	318.92	0.32
Post Survey - Leg 3	3/3/2022	25.99	11,253.05	11.25
Post Survey - Leg 3	3/3/2022	27.93	1,685.58	1.69
Post Survey - Leg 3	3/3/2022	29.40	135.54	0.14
Post Survey - Leg 3	3/3/2022	28.35	1,505.24	1.51
Post Survey - Leg 3	3/3/2022	28.44	763.49	0.76

Data Collection Period	Date	Mean depth (m)	School biomass (kg)	School biomass (mt)
Post Survey - Leg 3	3/3/2022	29.31	0.78	0.00
Post Survey - Leg 3	3/3/2022	22.97	2.57	0.00
Post Survey - Leg 3	3/3/2022	28.45	10,461.68	10.46
Post Survey - Leg 3	3/3/2022	22.26	0.02	0.00
Post Survey - Leg 3	3/3/2022	26.18	2,219.64	2.22
Post Survey - Leg 3	3/3/2022	25.27	1,564.54	1.56
Post Survey - Leg 3	3/3/2022	27.33	694.78	0.69
Post Survey - Leg 3	3/3/2022	26.05	14,925.04	14.93
Post Survey - Leg 3	3/3/2022	25.61	19,364.15	19.36
Post Survey - Leg 3	3/3/2022	25.28	8,833.03	8.83
Post Survey - Leg 3	3/3/2022	28.62	744.18	0.74
Post Survey - Leg 3	3/3/2022	19.92	0.78	0.00
Post Survey - Leg 3	3/3/2022	24.56	5,954.29	5.95
Post Survey - Leg 3	3/3/2022	24.67	21,192.19	21.19
Post Survey - Leg 3	3/3/2022	27.54	14,291.16	14.29
Post Survey - Leg 3	3/3/2022	29.07	3,105.40	3.11
Post Survey - Leg 3	3/3/2022	29.20	108.17	0.11
Post Survey - Leg 3	3/3/2022	29.05	59,734.53	59.73
Post Survey - Leg 3	3/3/2022	28.36	23,121.03	23.12
Post Survey - Leg 3	3/3/2022	28.71	2,667.81	2.67
Post Survey - Leg 3	3/3/2022	30.58	15.32	0.02
Post Survey - Leg 3	3/3/2022	29.94	711.83	0.71
Post Survey - Leg 3	3/3/2022	29.49	3,131.96	3.13
Post Survey - Leg 3	3/3/2022	28.50	13,496.06	13.50
Post Survey - Leg 3	3/3/2022	28.55	10,035.22	10.04
Post Survey - Leg 3	3/3/2022	27.30	10,065.23	10.07
Post Survey - Leg 3	3/3/2022	27.92	11,711.95	11.71
Post Survey - Leg 3	3/3/2022	28.58	694.40	0.69
Post Survey - Leg 3	3/3/2022	29.19	293.49	0.29
Post Survey - Leg 3	3/3/2022	27.35	2,359.35	2.36
Post Survey - Leg 3	3/3/2022	26.01	24,611.68	24.61
Post Survey - Leg 3	3/3/2022	26.75	4,533.55	4.53
Post Survey - Leg 3	3/3/2022	25.13	17,761.95	17.76
Post Survey - Leg 3	3/3/2022	25.63	3,706.19	3.71
Post Survey - Leg 3	3/3/2022	25.26	1,079.91	1.08
Post Survey - Leg 3	3/3/2022	28.01	427.69	0.43
Post Survey - Leg 3	3/3/2022	27.59	0.04	0.00
Post Survey - Leg 3	3/3/2022	27.06	11.90	0.01
Post Survey - Leg 3	3/3/2022	25.75	478.05	0.48
Post Survey - Leg 3	3/3/2022	24.56	723.17	0.72
Post Survey - Leg 3	3/3/2022	20.60	2,242.56	2.24
Post Survey - Leg 3	3/3/2022	23.02	604.74	0.60
Post Survey - Leg 3	3/3/2022	20.61	7,285.31	7.29
Post Survey - Leg 3	3/3/2022	10.53	14.71	0.01
Post Survey - Leg 3	3/3/2022	28.92	3,652.10	3.65

Data Collection Period	Date	Mean depth (m)	School biomass (kg)	School biomass (mt)
Post Survey - Leg 3	3/3/2022	28.39	7,185.56	7.19
Post Survey - Leg 3	3/3/2022	28.33	4.79	0.00
Post Survey - Leg 3	3/3/2022	25.78	1,767.94	1.77
Post Survey - Leg 3	3/3/2022	20.50	6,376.42	6.38
Post Survey - Leg 3	3/3/2022	23.36	36,724.80	36.72
Post Survey - Leg 3	3/3/2022	22.98	3,195.59	3.20
Post Survey - Leg 3	3/3/2022	23.64	430.80	0.43
Post Survey - Leg 3	3/3/2022	22.57	5,777.20	5.78
Post Survey - Leg 3	3/3/2022	23.16	5,225.25	5.23
Post Survey - Leg 3	3/3/2022	22.60	2,651.38	2.65
Post Survey - Leg 3	3/3/2022	23.98	2,825.23	2.83
Post Survey - Leg 3	3/3/2022	25.28	351.31	0.35
Post Survey - Leg 3	3/3/2022	27.10	41.91	0.04
Post Survey - Leg 3	3/3/2022	25.73	16,690.06	16.69
Post Survey - Leg 3	3/3/2022	24.31	17,392.12	17.39
Post Survey - Leg 3	3/3/2022	25.93	20,634.05	20.63
Post Survey - Leg 3	3/3/2022	28.82	2,346.98	2.35
Post Survey - Leg 3	3/3/2022	25.33	6,557.40	6.56

Appendix C

2022 Cooperative Winter Atlantic Menhaden Survey

Biomass Estimation Report

2022 Cooperative Winter Atlantic Menhaden Survey
Biomass Estimation Report
Dong Liang

The hydroacoustic survey of Atlantic menhaden in the shelf waters off New Jersey followed a transect design. Six transects were selected using systematic random sampling. Due to the abnormally warm water conditions, possibly related to the disturbance of a storm, the actual survey protocol slightly deviated from the original design. Transects 3 to 6 ("leg 2") were surveyed 5 days after Transects 1 and 2 ("leg 1"), after the storm, when the water column was warmed possibly due to the storm disturbance. The planned trawling of acoustically identified schools was mostly not possible due to the mobility of the population. We applied alternative biomass estimators to account for the potential changes in detectability in the surveys incurred via a model-based approach.

MATERIALS AND METHODS

Hydrographic data: Hydrographic data were collected using a Hydrolab MS5 multi-sonde at the location of each Atlantic Menhaden school encountered along each transect. Additional readings were made at the start and end of each transect as well as locations 10 km apart within each transect to characterize water conditions across the study area. A profile of depth (m), water temperature (ºC), salinity (PSU), and dissolved oxygen concentration (mg/l) was recorded at each location using Hydrolab's Hydras3 LT software. Data collected by this software were exported to a Geographical Information System and interpolated into a raster estimating the contemporary environmental conditions at the centroid of the schools across the study area using inverse distance weighting. The analysis was conducted in ArcMap 10.8.1.

Species distribution modeling: A species distribution model was developed to estimate the changes in detectability driven by the change in seascape conditions, mainly the temperature changes possibly due to the storm effects. We assumed that differences observed in schooling intensity and average biomass (i.e. detectability of the whole schools) at transects 3-6 (i.e. leg 2 of the survey) were entirely due to temperature changes, and these changes did not reflect the actual changes in the spatial distribution of the population. The model used other environmental predictors and geographical coordinates to capture residual spatial trends in the population distribution.

The species distribution model was formulated hierarchically for both school location and biomass. Each school was represented as a point location at the horizontal centroid of the school location. Given the relatively small size of the school to the entire study area, this approximation should have a limited impact on biomass estimation. Models varied by whether or not certain environmental variables were used as predictors of school location and biomass, and the spatial autocorrelation process within a marked point pattern model (Diggle et al. 2010). The schooling distribution follows a log-Gaussian Cox process while the observed biomass follows a log-Gaussian Geostatistical model. We considered shared spatial random effects between the two

model components to enable joint estimation of the spatial process governing both the schooling density and the biomass (Conn et al. 2017, Pennino et al. 2019).

We initially considered all environmental covariates such as bathymetry, salinity, temperature, and dissolved oxygen. The variance inflation factor was computed to identify multi-collinearity between the environmental covariates (Fox 2015). Models for spatially auto-correlated random effects followed a Matérn covariance function and were implemented via a computationally efficient approximation (Lindgren et al. 2011, Simpson et al. 2016). The Geostatistical model was approximated using the Stochastic Partial Differential Equation approach (Lindgren et al. 2011) and implemented using the Integrated Nested Laplace Approximation method (INLA, Rue et al. 2009). We used marginal log-likelihood, as well as mean square errors (MSE) in school intensity and log biomass preschool to estimate the predictive performance of each model.

Detectability estimation: A relative detectability for the leg 2 sampling after the storm was estimated by first predicting the schooling density and average biomass per school at leg 2 transects, based on a hypothetical temperature distribution that was similar in range to the temperature during the leg 1 sampling, accounting for the temperature-driven differences of detectability. These model-based predictions of school intensity and biomass were then compared with the model predictions based on the actual observed temperature. The additional number of schools as well as the increase in log average biomass were estimated. These estimated impacts of relative detectability were applied to the actual biomass and schooling data and expanded using a design-based or ratio-based estimator to the entire study area(Thompson 2012). The design-based uncertainty for these estimates was also quantified using the standard deviation and the ratio-based estimates methods (Thompson 2012). The model framework is described in Appendix C1.

Although additional data were collected during normal fishing operations ("leg 3"), only data on the first two survey legs were included in the detectability estimation because the detectability during leg 3 after the random survey might be subject to the regular fishing process and therefore might differ systematically from those during the random survey and because schools were detected outside and just south of the pre-defined survey area. Post-survey leg 3 data were assumed to represent an upper limit of the school intensity. The observed intensity at leg 3, along with the total biomass were used to derive a prior for the species distribution model. Since only part of the study area was covered by the survey effort, the estimated average log intensity was adjusted upwards by a factor of the ratio between the total study area and the transect area.

Statistical inference was based on approximated Monte Carlo sampling implemented in INLA. All analyses were conducted in R using packages R-INLA (Rue et al. 2009), terra (Hijmans 2023), and sf (Pebesma 2018). To incorporate the uncertainty of both the design-based estimation and the detectability, the design-based errors were randomly sampled from the model-based adjusted transect-specific biomass. Normal approximation was assumed for the design-based error estimates. A Monte Carlo integration was then applied across the approximate posterior sample of adjusted biomass estimates to derive the 90% credible sets for the biomass (Appendix C1). This was necessary because the model estimates were highly right-skewed and

posterior moments were not robust to outliers and could generate unrealistic uncertainty estimates.

RESULTS

Salinity was associated with the largest variance inflation factor (>10) and removed from further modeling (Fox 2015). Twenty-four models were built using the remaining environmental covariates and spatial random effects. Marginal likelihood was estimated for each model to measure their predictive capability (Table 1). Two models generated extreme marginal log-likelihood. The corresponding residual mean squared errors (RMSE) were large, which indicated numerical issues within INLA. The model with only a fixed effect of temperature and shared spatial random effects between the log intensity and average biomass (Figure 1) was best in terms of marginal likelihood, along with a small residual Mean Square Error (MSE). According to the best-fitting model, the temperature had a statistically significant and negative linear effect on both the schooling intensity and the average log biomass per school (Table 2).

The adjusted temperature in leg 2 (transects 3-6) had a similar range as the observed temperature in leg 1, but still exhibited the spatial pattern of the actual temperature observed during the survey (Figure 2). Large uncertainty exists regarding the temperature effects on detectability (Figure 3), possibly due to the small sample size (n=23). More schools on average were expected under the adjusted (and lower) temperature, and larger schools were predicted as well. The relative magnitude of changes in both school intensity and average biomass depends on the assumed changes in the temperature.

Biomass estimates ranged between 8,000 and 11,000 metric tons in the study area (Figure 4, Table 3). Ratio estimates based on the transect area generated 15%-20% lower biomass estimates (Figure 4, Table 3) than the design-based estimates. The design-based estimator expanded to the whole area based on the number of transects, while the ratio estimator expanded based on the ratio of biomass per unit area. The design-based estimator of uncertainty was large because it was based on random sampling, which did not fully incorporate the systematic nature of the sampling. The ratio-based uncertainty estimates were more reasonable. Detectability adjustment led to at most an 18% increase in design-based estimates and a 38% increase in ratio-based estimates.

Eighty schools were observed in a post-survey period leg 3 around an area of 23 km^2. We assume an upper limit of the school intensity of 3.47 schools km^{-2}. The total biomass during leg 3 was 1,844 metric tons, which was assumed as the upper limit of the average biomass per school. Incorporating these limits as prior constraints did not significantly change the original biomass estimates (Supplementary Figure 1).

Table 1: Model comparison of the location and biomass of the Atlantic menhaden, based on marginal log-likelihood, mean squared error (MSE) in schooling intensity and log biomass per school. Random effects include separate spatial random effects for schooling and biomass (spatial), or a shared spatial random effect (joint spatial).

Fixed	Random	Marginal loglik	MSE- school intensity	MSE- log(biomass)
wtemp	None	-61.83	42.16	11.13
wtemp	Spatial	-58.18	30.12	11.08
wtemp	Joint Spatial	**-53.48**	**27.20**	**9.90**
wtemp+oxygen	None	-66.70	42.15	11.43
wtemp+oxygen	Spatial	617.93	>1,000	11.41
wtemp+oxygen	Joint Spatial	-58.26	>1,000	>100
wtemp+bathy	None	-72.76	41.95	11.12
wtemp+bathy	Spatial	-65.81	33.38	11.09
wtemp+bathy	Joint Spatial	-63.87	>1,000	>100
wtemp+bathy+oxygen	None	-77.65	41.98	11.43
wtemp+bathy+oxygen	Spatial	-66.59	60.03	11.39
wtemp+bathy+oxygen	Joint Spatial	-2418.28	20.08	12.13
None	None	-74.39	42.68	14.20
None	Spatial	-62.26	36.40	14.12
None	Joint Spatial	-56.23	34.78	11.91
oxygen	None	-69.98	42.41	14.05
oxygen	Spatial	-61.25	34.22	13.98
oxygen	Joint Spatial	-56.69	33.29	12.30
bathy	None	-82.75	42.57	14.15
bathy	Spatial	-74.09	36.57	14.12
bathy	Joint Spatial	-67.62	>1,000	11.96
bathy+oxygen	None	-81.36	42.42	14.06
bathy+oxygen	Spatial	-73.43	>1,000	13.99
bathy+oxygen	Joint Spatial	-65.80	43.09	14.07

Table 2: Coefficient estimates (posterior median, and limits of the 95% credible sets) of the selected model with respect to the log intensity of the school locations (Intensity) and the average biomass (Biomass). Wtemp denotes water temperature.

Model	Parameter	Estimate	Lower	Upper
Intensity	Intercept	25.67	9.64	46.42
	wtemp	-4.63	-8.27	-1.84
Biomass	Intercept	42.92	12.50	72.12
	wtemp	-6.98	-12.29	-1.45

Table 3: Biomass estimates (metric tons) in terms of posterior median and 90% credit sets according to detectability adjustment and expansion estimators.

	Design-based			Ratio-estimate		
Detectability Adjustment	Estimate	Lower	Upper	Estimate	Lower	Upper
No adjustment	9,460	0	25,065	7,963	5,902	10,024
Adjusted school number	10,042	0	23,422	8,196	6,410	10,432
Adjusted school size	10,076	0	23,441	8,312	6,505	11,434
Adjusted size and number	11,005	0	27,441	8,706	6,703	19,137

Figure 1: The fitted spatial random effects from the selected model, overlaid with school locations as circles and survey transects as lines. Color boundary denotes the study area (with geographic coordinates re-scaled to avoid numerical issues).

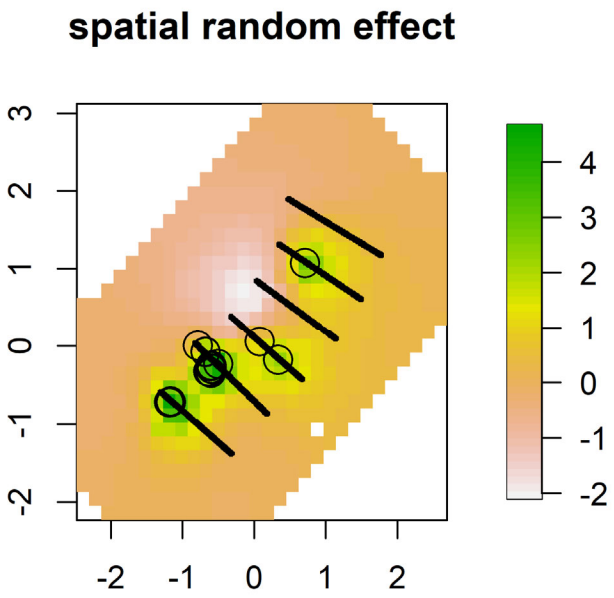

Figure 2: Interpolated water temperature contemporary to the survey in the study area, along with the hypothetical water temperature when the northern areas (leg 2, transects 3-6) were adjusted to maintain the same range as the southern part (leg 1, transects 1-2).

Observed

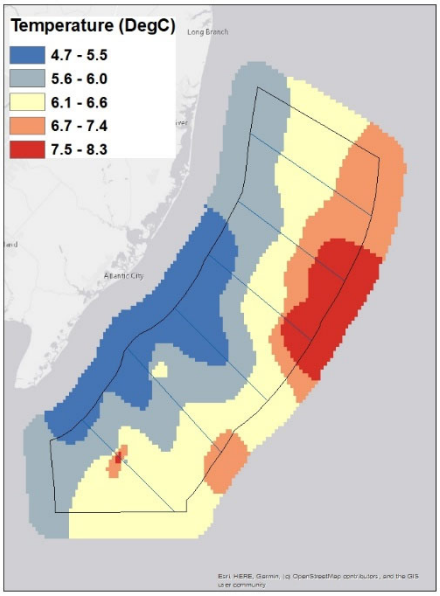

Hypothetical

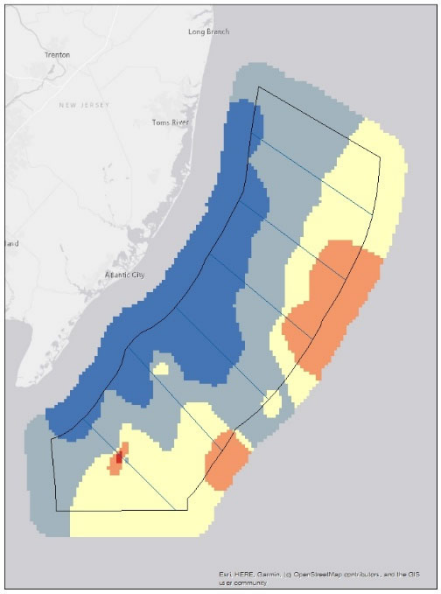

Figure 3: Estimates of temperature effects on (a) school intensity measured as the expected additional number of schools on each transect; and (b) the average biomass per school observed and after the hypothetical temperature change.

(a)

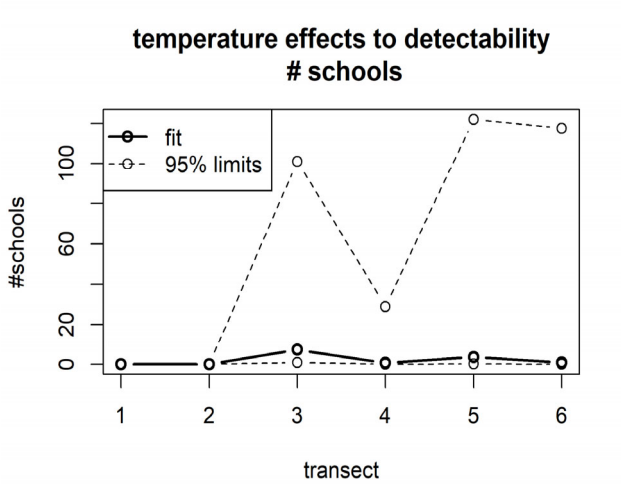

(b)

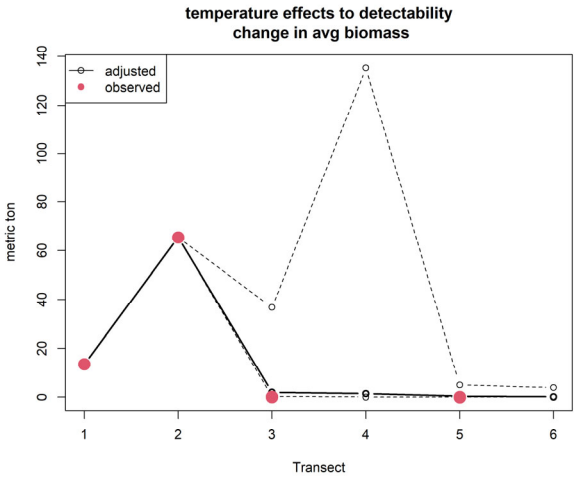

Figure 4: Biomass estimates (metric tons) in terms of posterior median and 90% credit sets according to expansion estimators and detectability adjustment: a) no adjustment, b-d) temperature adjustment to school intensity (b), average biomass (c), and both (d).

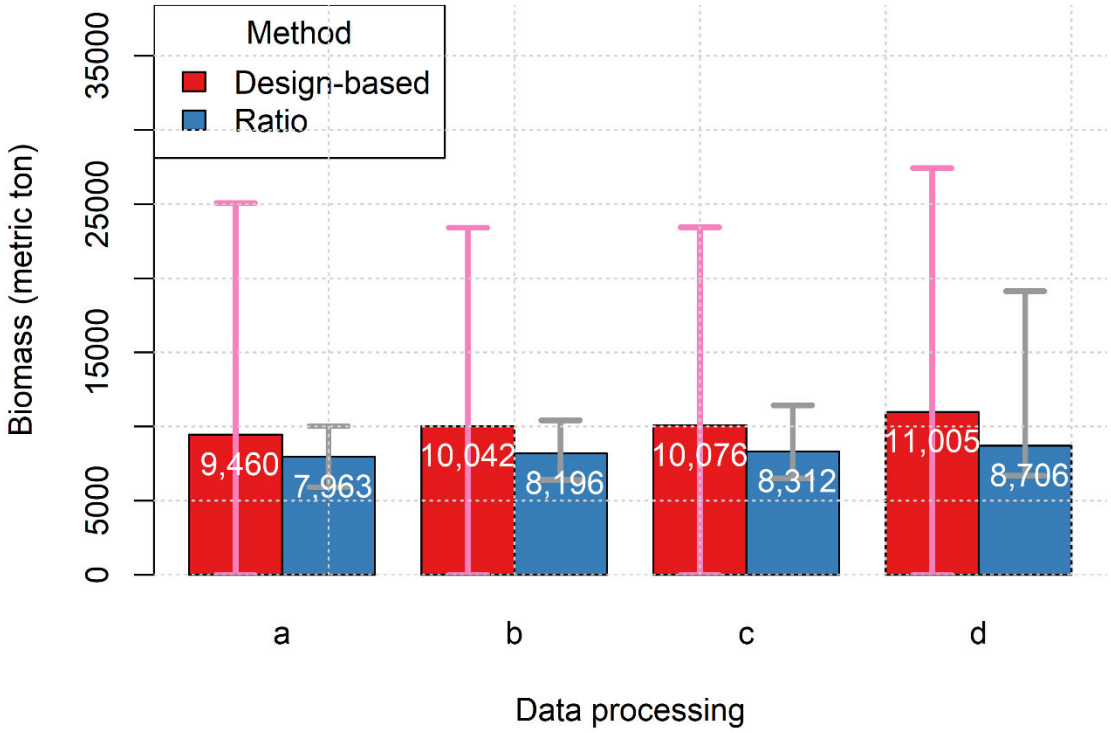

Supplementary Figure 1: Biomass estimates (metric tons) in terms of posterior median and 90% credit sets according to expansion estimators and detectability adjustment: a) no adjustment, b-d) temperature adjustment to school intensity (b), average biomass (c), and both (d). Prior constraints were set based on the observed schooling intensity and biomass.

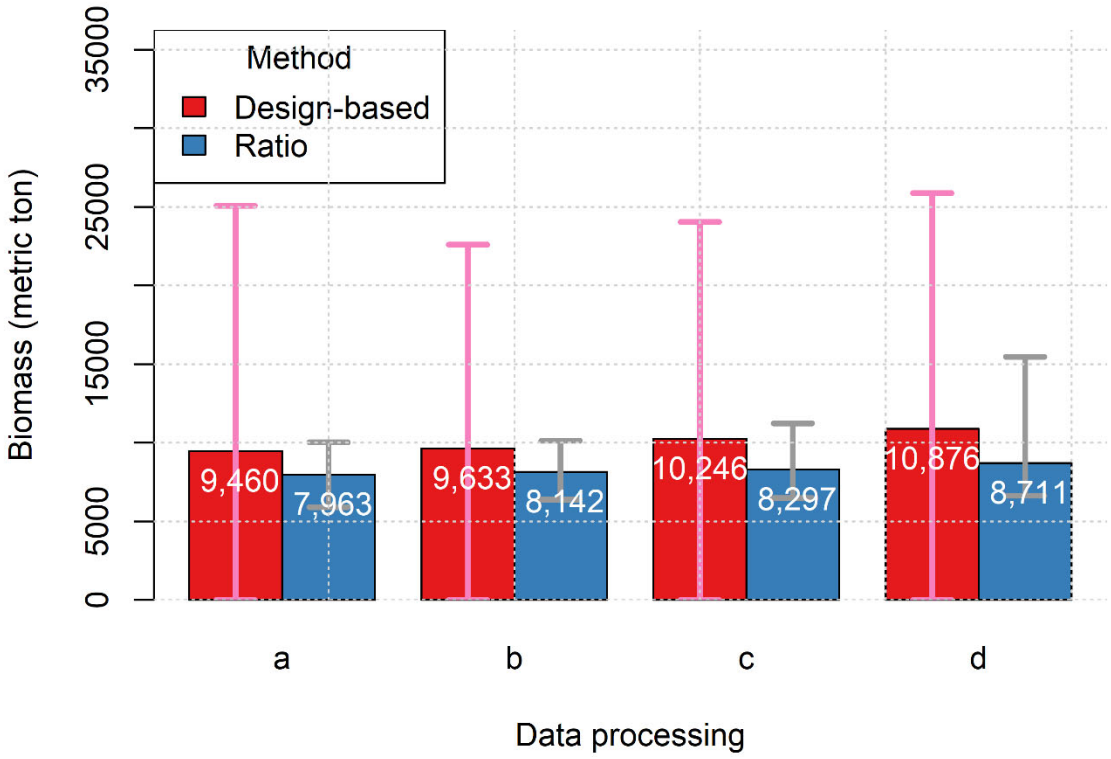

LITERATURE CITED

Conn, P.B., Thorson, J.T. and Johnson, D.S. (2017) Confronting preferential sampling when analysing population distributions: diagnosis and model-based triage. Methods in Ecology and Evolution 8(11), 1535-1546.

Diggle, P.J., Menezes, R. and Su, T.-l. (2010) Geostatistical inference under preferential sampling. Journal of the Royal Statistical Society Series C: Applied Statistics 59(2), 191-232.

Fox, J. (2015) Applied regression analysis and generalized linear models, Sage Publications.

Hijmans, R.J. (2023) terra: Spatial Data Analysis, CRAN, Vienna, Austria.

Lindgren, F., Rue, H. and Lindström, J. (2011) An explicit link between Gaussian fields and Gaussian Markov random fields: the stochastic partial differential equation approach. Journal of the Royal Statistical Society: Series B (Statistical Methodology) 73(4), 423-498.

Pebesma, E.J. (2018) Simple features for R: standardized support for spatial vector data. R Journal 10(1), 439.

Pennino, M.G., Paradinas, I., Illian, J.B., Muñoz, F., Bellido, J.M., López-Quílez, A. and Conesa, D. (2019) Accounting for preferential sampling in species distribution models. Ecology and evolution 9(1), 653-663.

Rue, H., Martino, S. and Chopin, N. (2009) Approximate Bayesian inference for latent Gaussian models by using integrated nested Laplace approximations. Journal of the Royal Statistical Society Series B: Statistical Methodology 71(2), 319-392.

Simpson, D., Illian, J.B., Lindgren, F., Sørbye, S.H. and Rue, H. (2016) Going off grid: Computationally efficient inference for log-Gaussian Cox processes. Biometrika 103(1), 49-70.

Thompson, S.K. (2012) Sampling, John Wiley & Sons.

Appendix C1. Detectability adjustment framework

Model Framework: For each cell denoted by i, let $y_i \sim \text{GPPP}(\lambda_i, \theta_i)$ denote a Geostatistical point pattern process (GPPP) model with λ_i the school per unit area (i.e. intensity) and θ_i the log biomass per school. We adopt the following log-linear models of the intensity and average biomass:

$$l_i = \log(\lambda_i) = \beta_0 + \beta_1 x_i + b_i, \text{and} \quad \theta_i = \gamma_0 + \gamma_1 x_i + \beta b_i \tag{1}$$

The coefficients β_0 and β_1 denote the association between temperature x and intensity, the coefficients γ_0 and γ_1 denote the association between temperature and average biomass, and the random effect b denotes the residual spatial pattern in species distribution. The random effect was shared between the log intensity and log biomass model, with β a scaling parameter linking log intensity and log average biomass. We adopted a Stochastic Partial Differential Equation field on the spatial random effects b_i, with a prior constructed to penalize the complexity of the random field (Fuglstad et al. 2019).

Define x_i^* a novel temperature over which the detectability was estimated. According to model (1)

$$l_i^* = \log(\lambda_i^*) = \beta_0 + \beta_1 x_i^* + b_i, \quad \theta_i^* = \gamma_0 + \gamma_1 x_i^* + \beta b_i \tag{2}$$

Thus the change in the average number of schools per unit area can be estimated as follows.

$$d_i = \exp\{\beta_0 + \beta_1 x_i^* + b_i\} - \exp\{\beta_0 + \beta_1 x_i + b_i\} \tag{3}$$

The change in average biomass per unit area can be estimated as

$$b_i = \exp(l_i^*)\exp(\theta_i^*) - \exp(l_i)\exp(\theta_i) \tag{4}$$

The changes in schools and biomass for a transect can be aggregated across all the unit areas making up the transect. Let a denote the area for each cell.

$$d = a\sum_{i=1}^{n} d_i\,, \quad b = a\sum_{i=1}^{n} b_i \tag{5}$$

The estimates and their uncertainty can be obtained via Monte Carlo Integration.

Monte Carlo Integration: Monte Carlo integration was used to incorporate both design-based uncertainty corresponding to the expansion estimator (i.e. the uncertainty from sampling of transect around the study area), and the uncertainty corresponding to the detectability adjustment according to the GPPP model above. Let $\{b_m, m = 1, \dots, M\}$ denote an approximate Monte Carlo sample of total biomass from the model (1) above representing the uncertainty of detectability adjustment. Let s denote a design-based estimate of standard deviation, we sampled the adjusted biomass from a conditional Normal distribution.

$$\theta_m \sim [\theta | b = b_m] \sim \text{N}(b_m, s) \tag{6}$$

It follows the un-conditional distribution of biomass θ can be obtained by Monte Carlo integration over the samples $\{\theta_m, m = 1, \dots, M\}$.

Appendix C2. Sample analysis R code.

```
rm(list=ls())
## Load packages
library(INLA)
library(terra)
library(rgeos)
library(FNN)
library(sf)
library(ggplot2)
library(foreign)
source("Codes/book_lgcp_geo_2.R")
## parameter: Monte Carlo samples
nMC <- 9999


## data input - UTM
menhaden <- read.dbf("../Data/GIS files/AllSchoolsUpdate.dbf")

## study area
loc1 <- st_read("../Data/GIS files/SurveyAreaUTM.shp")
loc.d.0 <- loc1$geometry[[1]][[1]]
loc.d <- scale(loc.d.0)

## prepare the scale the domain
center_ <- attr(loc.d,"scaled:center")
scale_ <- attr(loc.d,"scaled:scale")

menhaden$POINT_X_2 <- (menhaden$POINT_X-center_[1])/scale_[1]
menhaden$POINT_Y_2 <- (menhaden$POINT_Y-center_[2])/scale_[2]

## subset to legs 1 and 2
menhaden <- subset(menhaden,Survey_Leg<3)

## mesh for the area
mesh <- inla.mesh.2d(loc.domain = loc.d, offset = c(0.25, 0.5),
                     max.edge = c(0.1, 0.2), cutoff = 0.1)


## rescale area to improve numerical stability
source("rscale.R")

wtemp <- rast("../Data/GIS
files/idw_temp_surveyarea_buffered_UTM.tif")
wtemp2 <- rscale(wtemp,center_,scale_)

wtemp.adj <- rast("../Data/GIS
files/idw_temp_surveyarea_buffered_UTM_Adj.tif")
wtemp.adj.2 <- rscale(wtemp.adj,center_,scale_)

covariates <- list(wtemp=wtemp2)
covariates.p <- list(wtemp=wtemp.adj.2)
```

```
## assemble data
xyz <- with(menhaden,cbind(POINT_X_2,POINT_Y_2,log(School_Bio)))

## predictive inference
## survey transects
area <- rast("../Data/GIS files/transectsUTM.tif")
area2 <- rscale(area,center_,scale_)
area_ <- as.points(area)
area_cell <- prod(res(area2))
area_transects <- nrow(area_)*prod(res(area))/1e6 ## in km2
area_study <- 10990.87 ## in km2
#transect area to predict relative detectability
newloc <- data.frame(geom(area_)[,c("x","y")],
                transect=as.integer(unlist(area_[[1]]))+1)
newloc[,1] <- (newloc[,1]-center_[1])/scale_[1]
newloc[,2] <- (newloc[,2]-center_[2])/scale_[2]

## align schools to the nearest transect
library(FNN)
school.cell.fnn <- get.knnx(data=newloc[,1:2],
                            query=xyz[,1:2],k=1)
## some schools are far away from the transect
## just assume they are close and aligned with the nearest cell
newloc$n <- 0
table.school <- table(school.cell.fnn$nn.index[,1])
newloc$n[as.integer(names(table.school))] <- as.vector(table.school)

## average biomass per school per cell.
newloc$b <- NA ## no biomass if number of school is zero
biomass.school <- tapply(menhaden$School_Bio,
                         school.cell.fnn$nn.index[,1],
                         mean)
newloc$b[as.integer(names(biomass.school))] <-
as.vector(biomass.school)


## temperature difference at transects
wtemp.adj.2s <- resample(wtemp.adj.2,wtemp2,method="near")
dwtemp0 <- wtemp2-wtemp.adj.2s
dwtemp <- dwtemp0[cellFromXY(dwtemp0,newloc[,1:2])]$lyr.1
## model
res <- book.LGCP.geo(
  xyz=xyz,mesh=mesh,domain=loc.d,
  prior.range=c(2,0.01),prior.sigma=c(1,0.01),
  rast=covariates,newrast = covariates,
  newloc = as.matrix(newloc[,1:2]),spde_in = T,copy = T
)
## approximate posterior samples
set.seed(12345)
sam <- inla.posterior.sample(n=nMC,result=res)
```

```
## recover the predicted values
library(stringr)
tmp_ <- str_split(dimnames(sam[[1]]$latent)[[1]],pattern="\\:")
table(sapply(tmp_,function(elmt) elmt[1]))

fitted_index <- grep("Predictor",dimnames(sam[[1]]$latent)[[1]])
## environmental impacts to intensity

## adjust the intensity according the survey area
log_area_ratio <- log(area_study/area_transects)

## total number of schools
nschool <- tapply(newloc$n,newloc$transect,sum)

## additional schools expected on each transect
dhat <- sapply(sam,function(elmt){
  ## current log lambda
  li <- elmt$latent[fitted_index,1][res$DLindPred$pp]
  ## adjusted for survey area
  li.area <- li+log_area_ratio
  ## changed log lambda
  li.area.star <- li.area+elmt$latent[,1]["wtemp.pp:1"]*(-1*dwtemp)
  ## changed in lambda
  di <- exp(li.area.star)-exp(li.area)
  ## changed school expected per transect
  tapply(di*area_cell,newloc[,"transect"],sum)

})
## additional biomass expected per transect
bhat.lst <- lapply(sam,function(elmt){
  ## current log lambda
  li <- elmt$latent[fitted_index,1][res$DLindPred$pp]
  ## adjusted for survey area
  li.area <- li+log_area_ratio
  ## changed log lambda
  li.area.star <- li.area+elmt$latent[,1]["wtemp.pp:1"]*(-1*dwtemp)
  ## current log avg biomass
  mi <- elmt$latent[fitted_index,1][res$DLindPred$resp]
  ## changed log avg biomass
  mi.star <- mi+elmt$latent["wtemp.y:1",1]*(-1*dwtemp)
  ## change in biomass:
  ### only change in lambda
  delta1 <- area_cell*(exp(li.area.star)-exp(li.area))*exp(mi)
  ### only change in avg biomass
  delta2 <- area_cell*exp(li.area)*(exp(mi.star)-exp(mi))
  ## changes in lambda and avg biomass
  delta3 <- area_cell*(exp(li.area.star+mi.star)-exp(li.area+mi))
  ## aggregate over transects
  cbind(
    tapply(delta1,newloc$transect,sum),
    tapply(delta2,newloc$transect,sum),
    tapply(delta3,newloc$transect,sum)
```

```
  )
})
## total biomass before the adjustment
y2 <- with(newloc,tapply(n*b,transect,sum,na.rm=T))
id <- as.integer(names(y2))
# Design based----
## Design based estimates of total biomass
frame <- st_read("../Data/GIS files/SurveyAreaUTMLine.shp")

source(file="R/sys_utils_3.R")
Y0 <- esys(s=id,id=frame$Id,y=y2/1e3) ## mt
R0 <- esys.ratio(s=id,id = frame$Id,y = y2/1e3,w = frame$Area)
## extract total biomass estimates Monte Caro
model_est <- function(col,b0,ratio=F){
  ##col: column from the bhat.lst entries
  ##   indicating scenario of modeling
  ## ratio: whether to conduct ratio estimation
  lst <- lapply(bhat.lst,function(entry){entry[,col]})
  if(ratio){
    bio <- sapply(lst,function(delta){
      esys.ratio(s=id,id=frame$Id,y=(b0+delta)/1e3,w=frame$Area)
    })
  }else{
    bio <- sapply(lst,function(delta){
      esys(s=id,id=frame$Id,y=(b0+delta)/1e3)
    })
  }
  t(bio)
}
## only change in lambda
bio1 <- model_est(1,y2,ratio=F)
bio1r <- model_est(1,y2,ratio=T)

## only change in avg biomass
bio2 <- model_est(2,y2,ratio = F)
bio2r <- model_est(2,y2,ratio = T)

## changes in both
bio3 <- model_est(3,y2,ratio=F)
bio3r <- model_est(3,y2,ratio = T)
## Monte carlo integartion estimates of biomass
## estimate, standard error and components of the variance
mc_integ <- function(bio,alpha=0.10){
  ## assume Normal distribution given biomass
  ## adjustment
  err <- rnorm(nrow(bio),sd=bio[,2])

  bio.design <- bio[,1]+err
  lwr2 <- quantile(bio.design,prob=alpha/2)
  fit2 <- quantile(bio.design,prob=0.5)
  upr2 <- quantile(bio.design,prob=1-alpha/2)
```

```
  c(fit=fit2,lwr=lwr2,upr=upr2)
}
set.seed(123456)
## Adjusted for intensity ----
Y1 <- mc_integ(bio1)
R1 <- mc_integ(bio1r)

## Adjusted for biomass ----
Y2 <- mc_integ(bio2)
R2 <- mc_integ(bio2r)

## Adjusted for intensity and biomass ----
Y3 <- mc_integ(bio3)
R3 <- mc_integ(bio3r)
```

LITERATURE CITED

Fuglstad, G.-A., Simpson, D., Lindgren, F. and Rue, H. (2019) Constructing priors that penalize the complexity of Gaussian random fields. Journal of the American Statistical Association 114(525), 445-452.

Appendix D

2022 Cooperative Atlantic Menhaden Winter Survey
Ageing Exchange Report

2022 Cooperative Atlantic Menhaden Winter Survey
Ageing Exchange Report

Prepared for the ASMFC Atlantic Menhaden Ageing Workshop
November 14-15, 2023

Ageing Team
Jameson Gregg - Virginia Institute of Marine Science
Jamie Darrow - New Jersey Department of Environmental Protection
Amanda Rezek - NOAA Fisheries Southeast Fisheries Science Center Beaufort Laboratory

Principal Investigator
Geneviève Nesslage (UMCES Chesapeake Biological Laboratory)

Co-Principal Investigators
James Gartland & Robert Latour (Virginia Institute of Marine Science)
Christopher Gurshin (Normandeau Associates, Inc.)
Dong Liang (UMCES Chesapeake Biological Laboratory)

Industry Collaborators
Stefan Axelsson & Leif Axelsson (H&L Axelsson Inc.)
Wayne Reichle & Jeff Kaelin (Lund's Fisheries, Inc.)

Field Team
Chief Scientist - Dustin Gregg (Virginia Institute of Marine Science)
Survey Team - Charlie Jordan, Matt Farnham, and Chris Bonzek (Virginia Institute of Marine Science)

Federal & State Partners
Michael Jech (NOAA Fisheries Northeast Fisheries Science Center)
Ray Mroch (NOAA Fisheries Southeast Fisheries Science Center Beaufort Laboratory)
Jeffrey Brust (New Jersey Department of Environmental Protection)

INTRODUCTION

Atlantic menhaden (*Brevoortia tyrannus*) supports the largest commercial fishery by volume on the U.S. East Coast (NMFS 2022). Management of Atlantic menhaden is supported by a statistical catch-at-age model that estimates fishing mortality and stock abundance primarily using information on the change in age composition of the stock over time (SEDAR 2020). Thus, accuracy of assessment model estimates relies heavily on accuracy of the ages assigned to fish sampled dockside from the reduction and bait fisheries by NOAA Fisheries and state agencies.

Atlantic menhaden exhibit size-based migration along the East Coast such that larger, older fish are more frequently encountered in the northern portion of their range (SEDAR 2020). Despite

the fact that Atlantic menhaden are thought to reach age-10 (SEDAR 2020), few ageing studies have focused on larger fish found in the northern portion of their range due to the fact that majority of the fishery occurs in the Chesapeake Bay region such that sampling efforts do thoroughly encompass the full extent of the fish's range. Most fishery-independent surveys that collect menhaden scales and otoliths are sampling in the spring to fall in estuarine or nearshore areas where smaller fish are typically encountered. Thus, there has been limited opportunity to study ageing precision for Atlantic menhaden from the northern portion of their range due to relatively low sample size.

A new opportunity to conduct an ageing exchange arose in February-March 2022 when a cooperative acoustic survey of the overwintering resident stock of Atlantic menhaden was conducted offshore of the New Jersey coast to generate estimates of local stock biomass, structure, and habitat use. A subset of schools detected were trawled and Atlantic menhaden samples were collected from each school for laboratory analysis, including the determination of age, size, sex, and maturity. Additional opportunistic samples were collected by the survey team at sea for five days after the survey and at port throughout the remainder of the winter menhaden fishing season.

An ageing exchange of scales and otolith samples was conducted post-survey to quantify ageing uncertainty. The exchange involved project collaborators with ageing programs, namely the Virginia Institute of Marine Science (VIMS), New Jersey Department of Environmental Protection (NJDEP), and the NOAA Fisheries Southeast Fisheries Science Center Beaufort Laboratory (Beaufort). The objectives of this ageing exchange was to:

1) quantify intralab and interlab paired age agreement, when possible,
2) quantify scale vs otolith paired age agreement, and
3) identify patterns, if present, in paired age agreement by sex and size.

Although validated ages were not available to assess accuracy (age estimates compared with true ages), intralab and interlab estimates of precision (repeatability of age estimates by the same or among different readers), and bias (systematic differences in age estimates) can be used to improve ageing methodology, ensure greater consistency among ageing programs, and inform stock assessment uncertainty (Campana et al. 1995, Morison et al. 2005).

METHODS

Data Collection

Biological samples were collected from each trawled school to provide information on school structure. VIMS scientists subsampled the catch from the vessel's net pump using NEFOP's Catch Composition Technique for purse seine and midwater trawl operations. Once the cod end had been brought alongside the vessel, the chief scientist asked the captain for an estimate of pumping time for that haul. The estimated pumping time was divided by 10 to yield the sampling interval (e.g., estimated pumping time = 20 minutes, sampling interval = 2 minutes, yield = 10 baskets of sample). From each basket collected, 3 individual fish received full processing, which included the following elements: fork length (mm), total length (mm), whole weight (g), eviscerated weight (g), macroscopic sex (male/female/unknown), macroscopic maturity stage (immature/mature-resting/ mature-ripe /mature-spent). For female menhaden, both ovaries were removed, weighed, and preserved in Normalin for later reproductive evaluation. A scale patch

(~50 scales) was also collected, stored in labeled vials, and frozen. The head was removed and frozen for later extraction and preparation of both sagittal otoliths for ageing. Once 10 menhaden from each basket had been sampled in this manner, individual length (fork and total) and individual whole weight were recorded for the remaining menhaden specimens.

A total of 2,133 menhaden were sampled for fork length, total length, and whole weight during the survey (Table 1). Of those survey samples, 81 were selected for additional data collection, including sex, maturity, eviscerated weight, and age (both scale- and otolith-based reads). Additional opportunistic samples were collected at sea by the VIMS team during Atlantic menhaden fishing operations for five days after completion of the survey. An additional 155 schools were spotted and 94 schools were ensonified. Two extremely large schools were sampled post-survey, providing an additional 2,016 menhaden size samples (Table 1). Of those samples collected at sea post-survey, 72 were sampled for additional data (10 from each basket), including sex, maturity, eviscerated weight, and age (both scale- and otolith-based reads). Once the VIMS team had returned to land, Lund's Fisheries continued port sampling throughout the remainder of the winter menhaden fishing season, collecting an additional 150 fish at port (three 10-fish samples/trip collected over five additional trips), and all 150 samples received full workups.

Ageing exchange

Sample processing

All samples collected in the field for full workups were first transported to VIMS for processing using standard VIMS survey protocols and procedures. VIMS fish ageing protocols were established from procedures developed by NEFSC, Old Dominion University, and VIMS validated and published research developed by NEFSC, Old Dominion University, and VIMS (Bonzek et al. 2017, VanderKooy 2020). VIMS standard ageing protocols have been verified, collaborated, and referenced annually at the ASMFC Fish Ageing QA/QC Workshop (ASMFC 2023).

Scale samples were thawed and lightly scrubbed in a soap and water solution to remove debris and excess slime. Six of the cleanest, undamaged scales from each scale patch were selected, thoroughly dried, and pressed between two glass microscope slides. Many samples included regenerated scales. When possible, replacement scales were found, but some samples included a few regenerated samples on the slides. One sample (fish Specimen ID #75) contained all regenerated samples with no replacements and was omitted from analysis. Both sagittal otoliths from each sample were extracted, thoroughly dried, and cleaned as necessary.

Ageing Methods

Each ageing lab followed their own standard protocols for ageing Atlantic menhaden as described below. VIMS prepared scale samples and evaluated them using a microfiche reader using VIMS Atlantic menhaden protocols (attached). Paired whole otoliths were evaluated in water under a stereo dissecting microscope at 50x magnification with transmitted light. One reader, Jameson Gregg, read each hard part twice using VIMS protocols for scale (June and Roithmayr 1960) and otolith ageing (Deegan and Thompson 1987, Warlen 1988, Warlen 1992,

Ahrenholz 1994) of menhaden. In cases where the two reads differed, info on size or location and date of capture was used to inform the final age assignment based on expected timing of mark formation. Upon completion, all samples were mailed to NJDEP.

At NJDEP, two readers, Jamie Darrow (Reader 1) and Alissa Wilson (Reader 2), read each hard part once. Beaufort Laboratory ageing protocols were used to age scales and VIMS protocols were used to age otoliths as detailed in the attached protocols. Prepared scale samples were evaluated using a Microfiche reader. Paired whole otoliths were evaluated in water under a stereo dissecting microscope using reflected light. Upon completion, all samples were mailed to Beaufort.

At Beaufort, one reader, Amanda Rezek, read each hard part once. Prepared scale samples were evaluated using a stereo microscope (10X magnification) with transmitted light and cellSens imaging software to measure. Scales were aged using Beaufort Laboratory scale ageing protocols (attached). Paired whole otoliths were evaluated in 70% ethanol under a stereo dissecting microscope (20X magnification) with transmitted light using VIMS ageing protocols. Upon completion, all samples were archived at Beaufort Laboratory for use in future studies.

Statistical Analyses

Of the 303 samples for which full workups were conducted, 302 were suitable for inclusion in the ageing comparison. In the absence of validated ages, ageing agreement was evaluated. For labs that aged each hard part more than once (VIMS and NJDEP), consistency between two reads by the same reader, and among two different readers was quantified. For the two interlab comparisons, the most experienced ager at the NJDEP lab (Darrow – Reader 1) and VIMS's second read were used.

To quantify ageing agreement within and among ageing labs, the following indices were calculated: percent agreement (PA), average percent error (APE), and Chang's average coefficient of variation (ACV). To evaluate bias within and among ageing labs, the following tests of symmetry were conducted: McNemar's (McNemar; McNemar 1947) and Evans & Hoenig (EvansHoenig; Evans and Hoenig 1998). Although frequently used in other ageing studies, Bowker's test of symmetry (Bowker 1948) was not used here given the overall large number of samples, high variability in age reads, and pattern of decreasing sample size with age would likely generate false positives indicating bias when it is not actually present (Nesslage et al. 2022). Age-bias plots were generated for each comparison and for each comparison with results separated by the sex of each sample. All indices were calculated and tests of symmetry performed using the FSA package (Ogle DH 2023) for R Version 0.9.4 (R Core Team 2023).

RESULTS

Intralab precision was high for VIMS and low for NJDEP. VIMS demonstrated high agreement among reads (Table 2, Fig. 1) for both scales (PA=89%) and otoliths (PA=92%), although scale-based reads were slightly biased such that second reads of scales tended to be older than first reads. Agreement between the two NJDEP readers was low for otoliths (PA=36%), and very low for scales (PA=2%; Table 2, Fig. 2); both sets of intralab NJDEP age comparisons demonstrated significant bias.

Among labs, there was greater agreement in paired ages between VIMS and Beaufort (Fig. 3) for both scales (PA=66%) and otoliths (PA=59%) than between VIMS and NJDEP (Fig. 4) or between Beaufort and NJDEP (Fig. 5), which ranged in PA from 36-48% (Table 2). VIMS Read 2 age determinations were consistently older than that of Beaufort's for younger fish and vice versa for older fish. Although ACV for otolith-based age comparisons between VIMS Read 2 and Beaufort was greater than seven, the overall difference among reads was statistically unbiased (Fig. 3). NJDEP Reader 1 age determinations were typically older than that of VIMS Read 2 and Beaufort regardless of hard part examined (Figs. 4-5).

VIMS demonstrated good agreement between paired scale and otolith ages (PA=82%). Paired age agreement between hard parts was lower for Beaufort (54%) and NJDEP (PA=41%). Scale-otolith comparisons for both VIMS and NJDEP were biased, but Beaufort was not. When comparing scale- vs otolith-based age determinations, all three labs demonstrated a pattern of assigning an older age to younger fish and a younger age to older fish when aging scales.

Overall, evaluation of paired age agreement by sex did not reveal significant differences potentially due to sexually dimorphic growth (Figs. 7-12). Although sample size was low at older ages, VIMS and Beaufort ages agreed more closely for female than male samples (Fig. 9).

DISCUSSION

This ageing exchange study was novel in several ways. First, this was one of the largest interlab Atlantic menhaden ageing exchange study to date (302 paired scales and otoliths), and this was the only ageing study focused solely on Atlantic menhaden samples collected during a season (winter) and region (offshore NJ) that is sparsely sampled. Previous interlab ageing exchanges focused primarily on port samples collected from the large reduction fishery in Reedville, VA, with no samples examined from January or February (ASMFC 2015). Fish encountered in the 2022 winter cooperative survey were on average larger in size than what is typically encountered in the reduction fishery port samples or inshore state surveys (Table 3, Fig. 13). The only comparable samples aged on a regular basis are the winter bait fishery port samples collected annually. Thus, some of the agers in this study may have been unaccustomed to ageing overwintering adult Atlantic menhaden collected early in the year.

Another way in which this Atlantic menhaden ageing study differed from previous ageing exchanges is that it included a scale vs otolith paired age comparison. Most ageing of Atlantic menhaden is conducted using scales through the extensive reduction and bait fishery menhaden ageing program at the Beaufort Lab spanning 1955 to the present (Chester and Waters 1985, Smith 1991). Yet, previous comparisons of Atlantic menhaden scale vs whole otoliths age determinations at the Beaufort Laboratory resulted in low APE (4.2%; Wilburn et al. unpublished). VIMS regularly ages Atlantic menhaden with otoliths as part of their multispecies monitoring program (NEAMAP and ChesMMAP surveys), which may explain the good agreement between scales and otoliths for that lab. We reiterate the 2015 exchange workshop recommendation that an ageing validation study comparing scales and otolith across all ages using radio isotope analysis of archived scales would be extremely valuable. When possible, paired scales and otoliths should be collected across the stock's range to support this type of

research.

In this study, the same person aged each hard part twice at VIMS, allowing for comparison with a previous intralab ageing study conducted in 2009 at Beaufort (SEDAR 2015). In the 2009 study, in a total of 3,711 Atlantic menhaden scales collected in 2008 were re-aged by the lab's one menhaden ager at the time, Ethel Hall. Agreement among paired scale ages by the same reader at Beaufort was approximately 80%, and thus was similar to that of VIMS in this study (89%; Table 2). The 2009 Beaufort study found that precision varied with age such that precision was relatively high for age-0s (95.2%), age-1s (74.5%), age-2s (87.0%), and age-3s (74.4%), but declined to 51.9% for age-4 and 19.1% for age-5 fish. When ages determinations disagreed, most disagreements were within one year for age-1 through age-3, but discrepancies increased with age. In contrast, VIMS scale read comparisons did not demonstrate such a steep a decline in precision above age-3.

Interlab agreement among the VIMS, NJDEP, and Beaufort ageing labs in this study was much lower than that of the 2015 Atlantic Menhaden scale ageing exchange (ASMFC 2015). In the 2015 study, scale age agreement was >80% among all three labs compared with percent agreement in this study which ranged from 36%-66% (Table 2). Similarly, ACV was low among the three labs in the 2015 study, but consistently exceeded the threshold of 7 in this study (range 7.8-14.97). Systematic differences among labs were also identified in this study with the high proportion of significant tests of symmetry for interlab comparisons vs the lack of bias evident in the previous ageing exchange. Lack of agreement among labs in this study may be due to the focus on larger, older fish, the early time of year during which samples collected, and the quality of the samples collected given the gear used.

CONCLUSIONS

TBD – after discussion post-workshop.

ACKNOWLEDGEMENTS

This study was a collaboration between fishing industry members and federal, state, private, and academic scientists funded by the Saltonstall-Kennedy Program award NOAA Grant NA20NMF4270163. Additional support for survey operations was provided by the Atlantic States Marine Fisheries Commission.

REFERENCES

Ahrenholz, D. 1994. Confidence of otolith ageing through the juvenile stage for Atlantic menhaden (Brevoortia tyrannus). Fishery Bull. **93**:209-216.

ASMFC. 2015. Atlantic Menhaden Ageing Workshop Report. ASMFC, Arlington, VA.

ASMFC. 2023. Report of the Quality Assurance/Quality Control Fish Ageing Workshop St. Petersburg, Florida March 7-9, 2023. Arlington, VA.

Bonzek, C. F., J. Gartland, D. J. Gauthier, and R. J. Latour. 2017. Northeast Area Monitoring and Assessment Program (NEAMAP) 2016 data collection and analysis in support of single and multispecies stock assessments in the Mid-Atlantic: Northeast Area Monitoring and Assessment Program Near Shore Trawl Survey. Virginia Institute of Marine Science, William & Mary. https://doi.org/10.25773/7206-KM61.

Bowker, A. H. 1948. A test for symmetry in contingency tables. Journal of the American

statistical Association **43**:572-574.
Campana, S. E., M. C. Annand, and J. I. McMillan. 1995. Graphical and statistical methods for determining the consistency of age determinations. Transactions of the American Fisheries Society **124**:131-138.
Chester, A. J., and J. R. Waters. 1985. Two-Stage Sampling for Age Distribution in the Atlantic Menhaden Fishery, with Comments on Optimal Survey Design. North American Journal of Fisheries Management **5**:449-456.
Deegan, L. A., and B. A. Thompson. 1987. Growth Rate and Life History Events of Young-of-the-Year Gulf Menhaden as Determined from Otoliths. Transactions of the American Fisheries Society **116**:663-667.
Evans, G. T., and J. M. Hoenig. 1998. Testing and viewing symmetry in contingency tables, with application to readers of fish ages. Biometrics:620-629.
June, F. C., and C. M. Roithmayr. 1960. Determining age of Atlantic menhaden from their scales. US Fish and Wildlife Service.
McNemar, Q. 1947. Note on the sampling error of the difference between correlated proportions or percentages. Psychometrika **12**:153-157.
Morison, A., J. Burnett, W. McCurdy, and E. Moksness. 2005. Quality issues in the use of otoliths for fish age estimation. Marine and Freshwater Research **56**:773-782.
Nesslage, G., A. M. Schueller, A. R. Rezek, and R. M. Mroch III. 2022. Influence of sample size and number of age classes on characterization of ageing error in paired-age comparisons. Fisheries Research **249**:106255.
NMFS. 2022. Fisheries of the United States, 2020. U.S. Department of Commerce, NOAA Current Fishery Statistics No. 2020 Available at: https://www.fisheries.noaa.gov/national/sustainable-fisheries/fisheries-united-states.
Ogle DH, D. J., Wheeler AP, Dinno A 2023. FSA: Simple Fisheries Stock Assessment Methods. R package version 0.9.5, https://fishr-core-team.github.io/FSA/.
R Core Team. 2023. R: A language and environment for statistical computing. R Foundation for Statistical Computing, Vienna, Austria. URL https://www.R-project.org/.
SEDAR. 2020. SEDAR 69 – Atlantic Menhaden Stock Assessment Report. SEDAR, North Charleston SC. 691 pp. available online at: http://sedarweb.org/sedar-69. North Charleston, SC
Smith, J. W. 1991. The Atlantic and gulf menhaden purse seine fisheries: Origins, Harvesting technologies, biostatistical monitoring, recent trends in fisheries statistics, and forecasting. Marine Fisheries Review **53**:28-41.
VanderKooy, S. 2020. A practical handbook for determining the ages of Gulf of Mexico and Atlantic coast fishes. Gulf States Marine Fisheries Commission: Ocean Springs, MS, USA.
Warlen, S. M. 1988. Age and growth of larval gulf menhaden, Brevoortia patronus, in the northern Gulf of Mexico. Fishery Bulletin **86**:77-90.
Warlen, S. M. 1992. Age, Growth, and Size Distribution of Larval Atlantic Menhaden off North Carolina. Transactions of the American Fisheries Society **121**:588-598.

TABLES

Table 1. Schools sampled and samples collected pre- and post-survey at sea and at port.

	Schools sampled	Fish sampled: fork length, total length, whole weight	Full workups: sex, maturity, eviscerated weight, age (scale & otolith)
Survey (at sea)	5	2,133	81
Post-survey (at sea)	2	2,016	72
Post-survey (port)	-	150	150
Total		4,299	303

Table 2. Ageing comparison indices of agreement and tests of symmetry. R=Read (VIMS) or Reader (NJDEP), PA= percent agreement, APE = average percent error, ACV = Average Coefficient of Variation, McNemar = p-value for McNemar's test of symmetry, EvansHoenig = p-value for Evans and Hoenig test of symmetry. Gray shading indicates either ACV > 7 (indicating low precision), or test of symmetry p-value was significant ($\alpha = 0.05$; indicating bias).

Lab	Hard Part	Comparison	PA	APE	ACV	McNemar	EvansHoenig
VIMS	Scales	R1 vs R2	89%	1.64	2.32	*0.00026*	*0.00026*
NJDEP	Scales	R1 vs R2	2%	42.61	*60.26*	*0.00000*	*0.00000*
Interlab	Scales	VIMS R2 vs NJDEP R1	44%	8.27	*11.70*	*0.00000*	*0.00000*
Interlab	Scales	Beafort vs VIMS R2	66%	5.52	*7.80*	*0.00013*	*0.00058*
Interlab	Scales	Beafort vs NJDEP R1	36%	10.59	*14.97*	*0.00000*	*0.00000*
VIMS	Otoliths	R1 vs R2	92%	1.32	1.87	0.41422	0.68321
NJDEP	Otoliths	R1 vs R2	36%	12.03	*17.02*	*0.00000*	*0.00000*
Interlab	Otoliths	VIMS R2 vs NJDEP R1	48%	8.72	*12.34*	*0.00000*	*0.00000*
Interlab	Otoliths	Beafort vs VIMS R2	59%	6.64	*9.38*	0.08897	0.17260
Interlab	Otoliths	Beafort vs NJDEP R1	45%	9.47	*13.40*	*0.00000*	*0.00000*
VIMS	Both	R2 Scales vs Otoliths	82%	2.72	3.85	*0.00000*	*0.00000*
NJDEP	Both	R1 Scales vs Otoliths	41%	9.04	*12.78*	*0.00097*	*0.00182*
Beaufort	Both	Scales vs Otoliths	54%	8.00	*11.32*	0.16339	0.44192

FIGURES

Figure 1. Paired age comparisons among reads by the same reader at VIMS for scales (top) and otoliths (bottom). Dots and lines represent mean and 95% confidence intervals, respectively, for the y-axis age relative to the x-axis age. Red indicates the difference among reads is significantly different from 0.

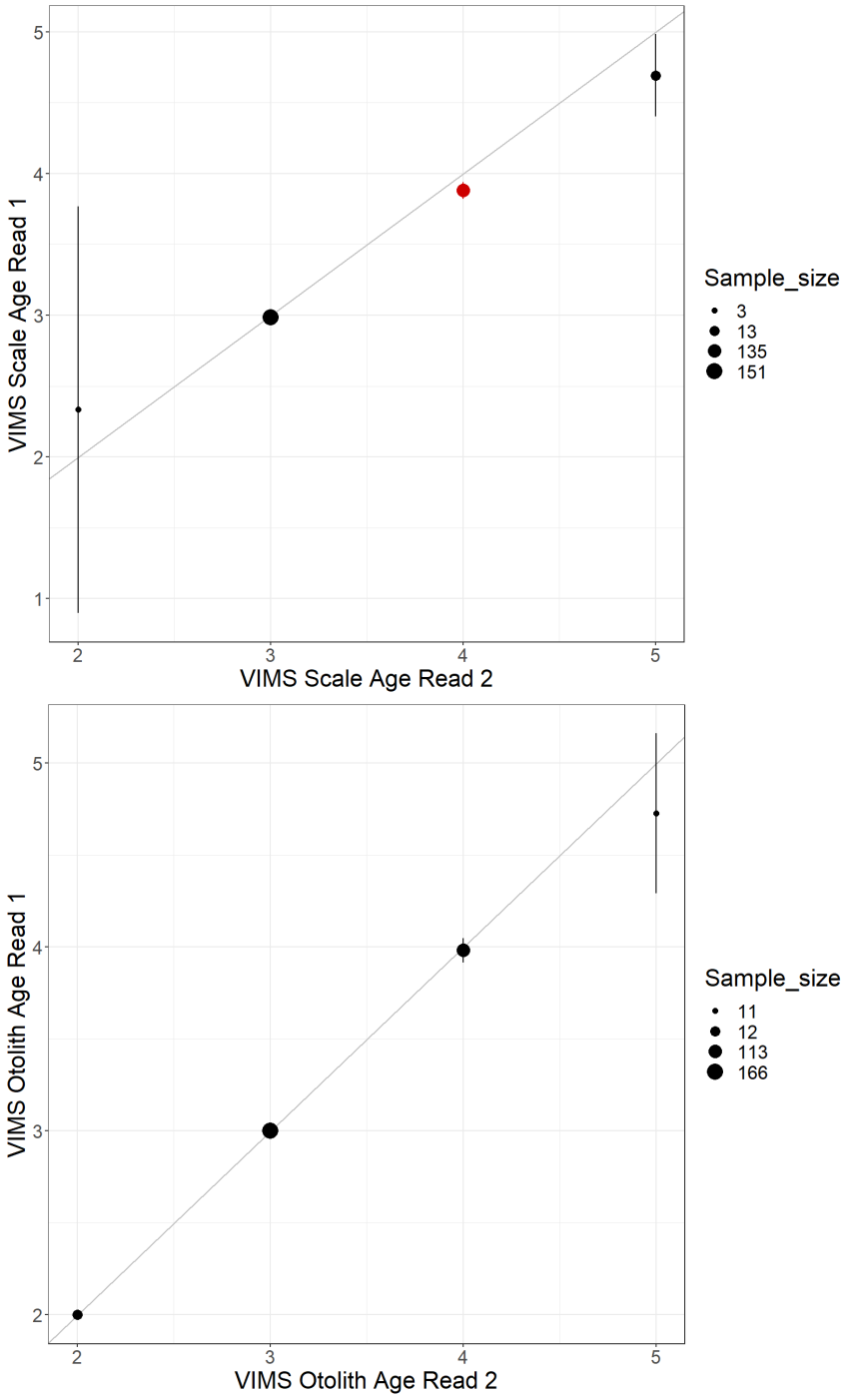

Figure 2. Paired age comparisons among NJDEP readers for scales (top) and otoliths (bottom). Dots and lines represent mean and 95% confidence intervals, respectively, for the y-axis age relative to the x-axis age. Red dots indicate the difference among reads is significantly different from 0.

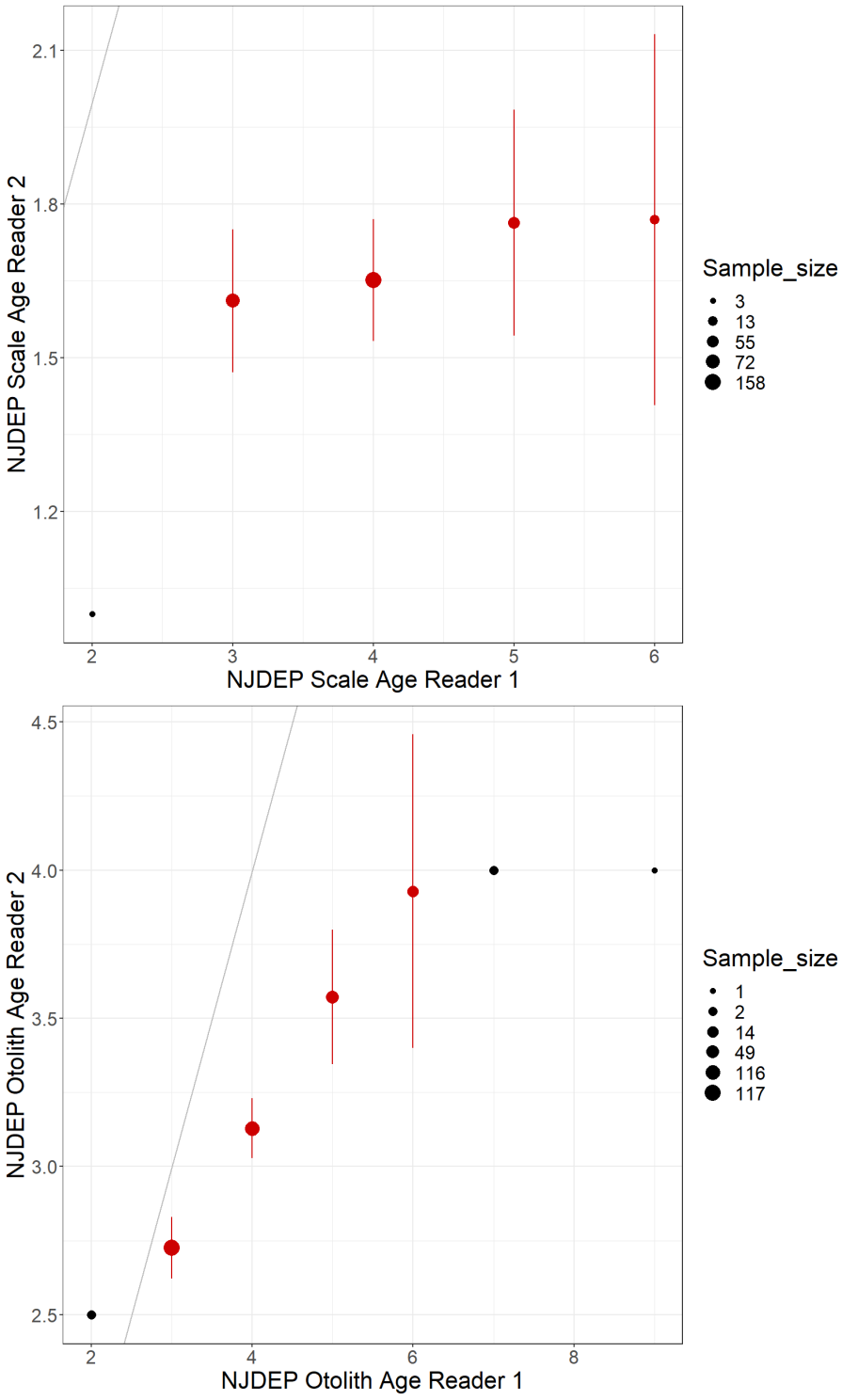

Figure 3. Paired age comparisons between Beaufort and VIMS Read 2 for scales (top) and otoliths (bottom). Dots and lines represent mean and 95% confidence intervals, respectively, for the y-axis age relative to the x-axis age. Red dots indicate the difference among reads is significantly different from 0.

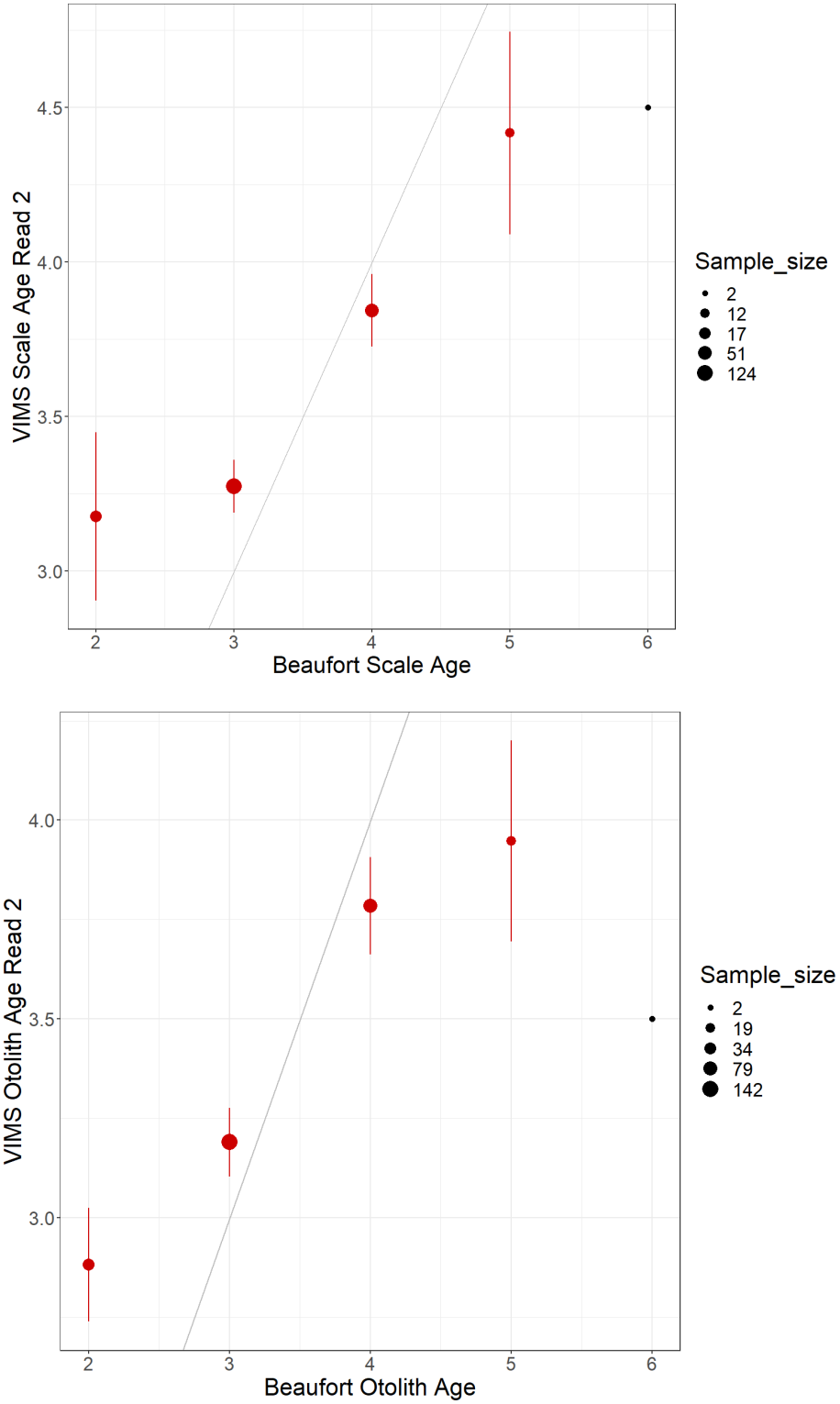

Figure 4. Paired age comparisons between VIMS Read 2 and NJDEP Reader 1 for scales (top) and otoliths (bottom). Dots and lines represent mean and 95% confidence intervals, respectively, for the y-axis age relative to the x-axis age. Red dots indicate the difference among reads is significantly different from 0.

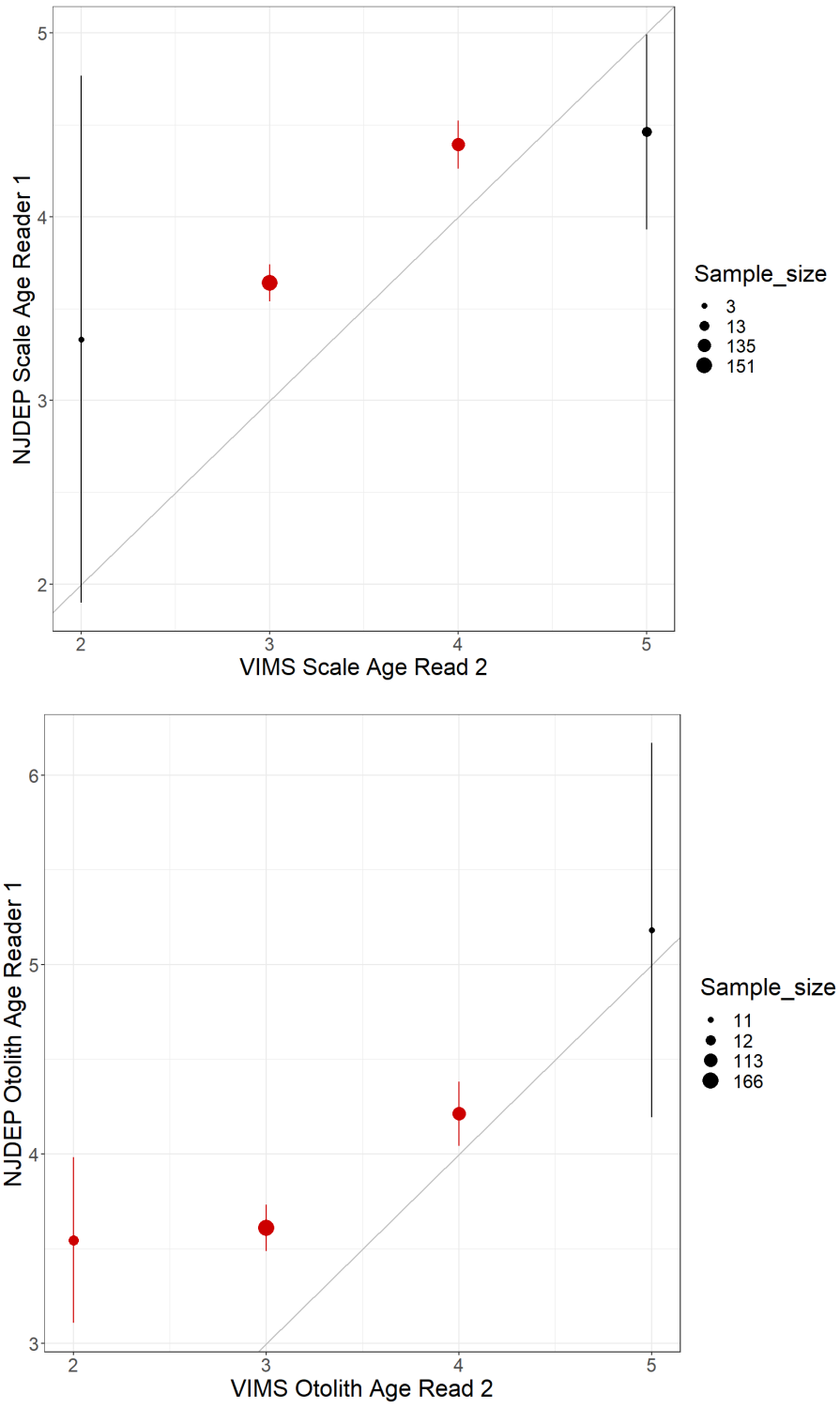

Figure 5. Paired age comparisons between Beaufort and NJDEP Reader 1 for scales (top) and otoliths (bottom). Dots and lines represent mean and 95% confidence intervals, respectively, for the y-axis age relative to the x-axis age. Red dots indicate the difference among reads is significantly different from 0.

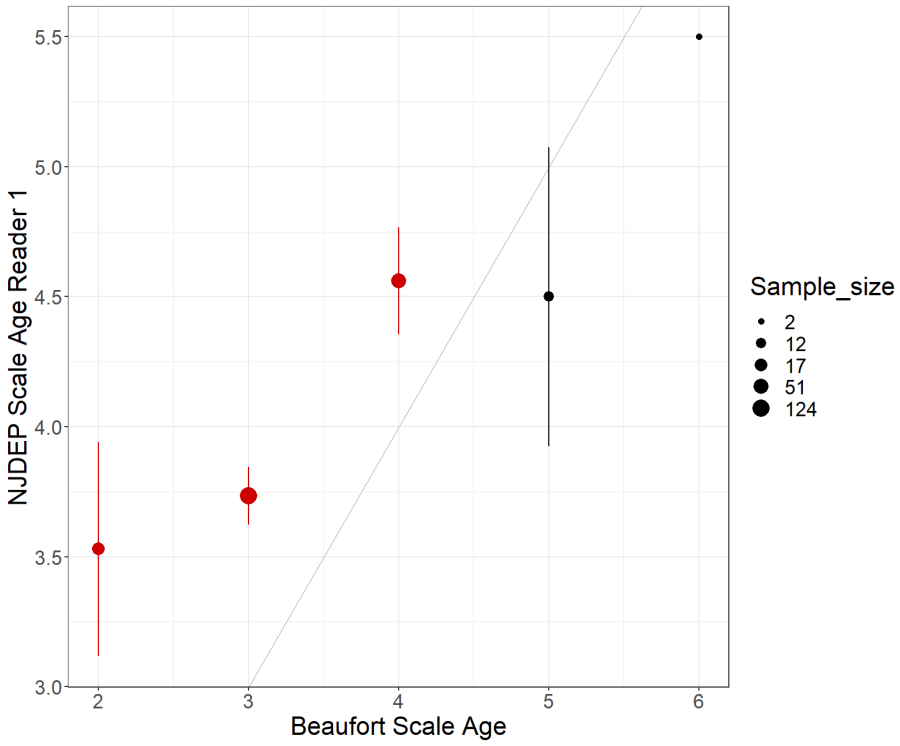

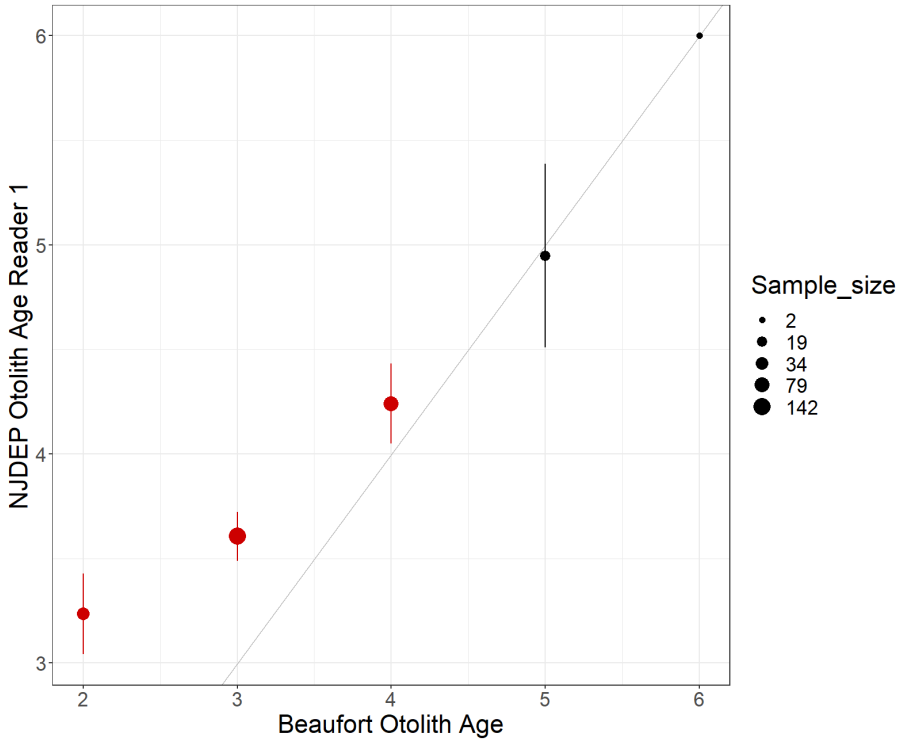

Figure 6. Scale vs otolith paired age comparisons for VIMS Read 2 (top left), NJDEP Reader 2 (top right), and Beaufort (bottom). Dots and lines represent mean and 95% confidence intervals, respectively, for the y-axis age relative to the x-axis age. Red dots indicate the difference among reads is significantly different from 0.

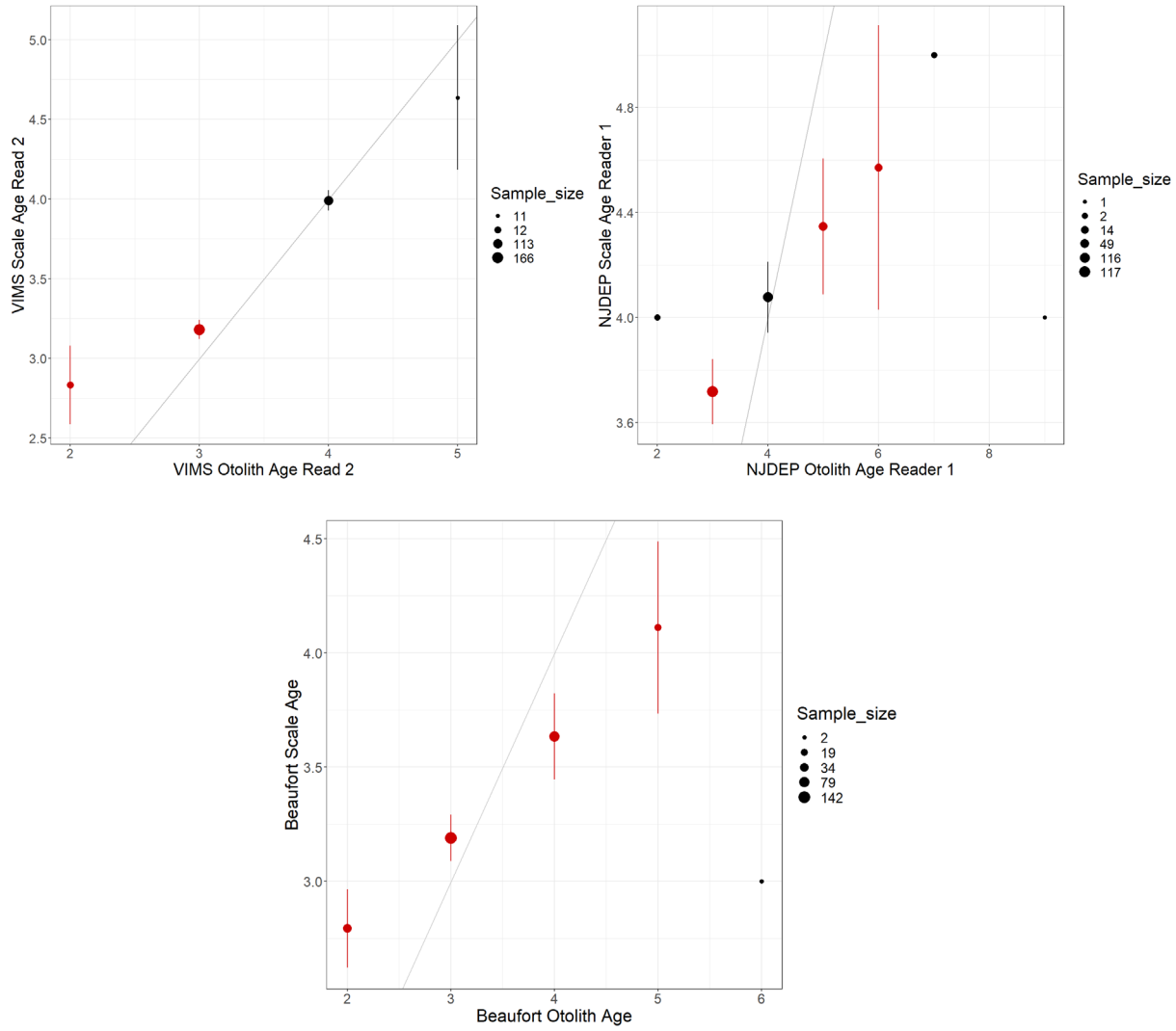

Figure 7. Paired age comparisons among reads by the same VIMS reader for scales (top) and otoliths (bottom) by sex. Dots represent mean and lines represent 95% confidence intervals for the difference between ages relative to the reference (x-axis) age.

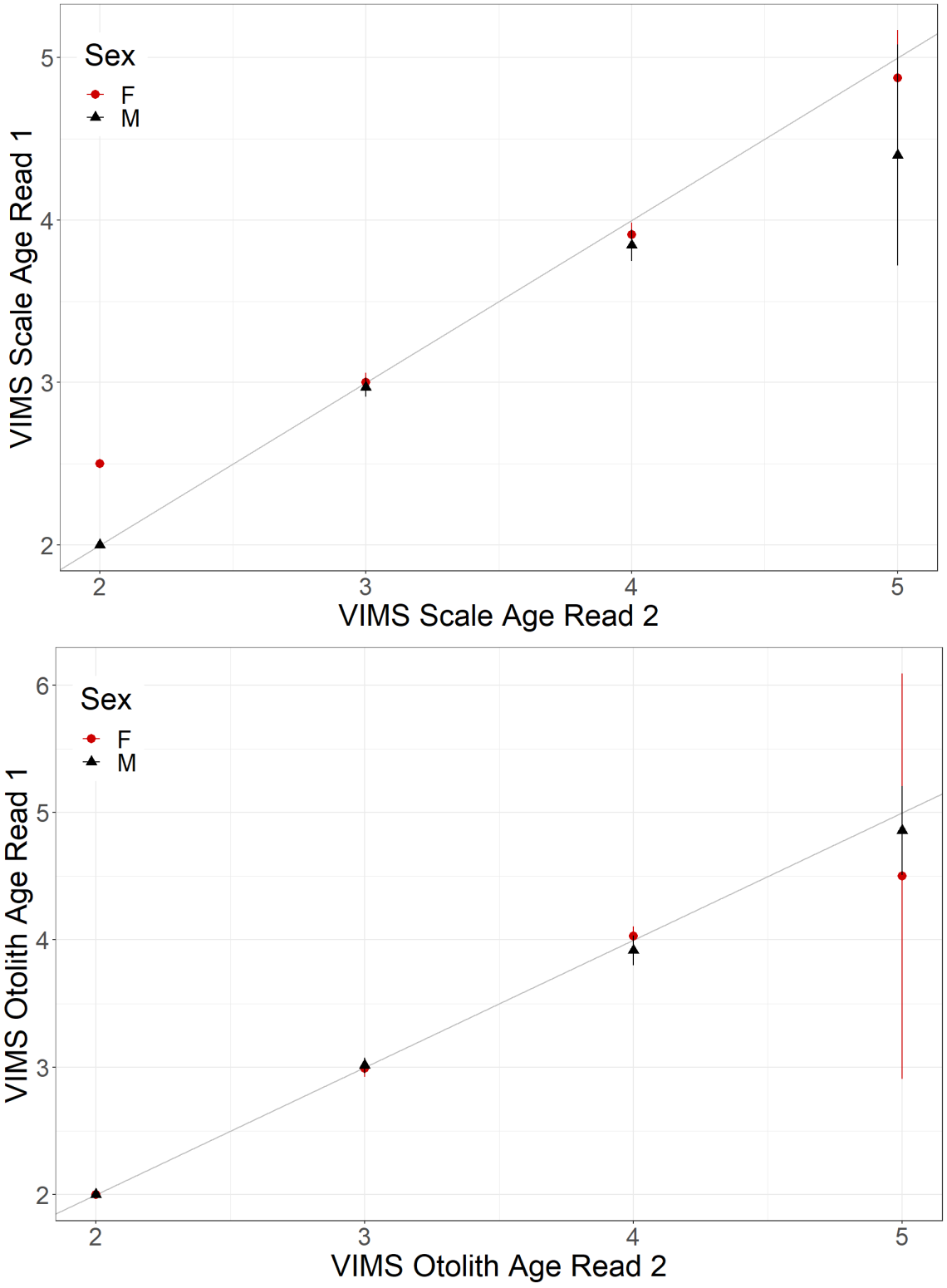

Figure 8. Paired age comparisons among reads by the same NJDEP Reader 1 for scales (top) and otoliths (bottom) by sex. Dots represent mean and lines represent 95% confidence intervals for the difference between ages relative to the reference (x-axis) age.

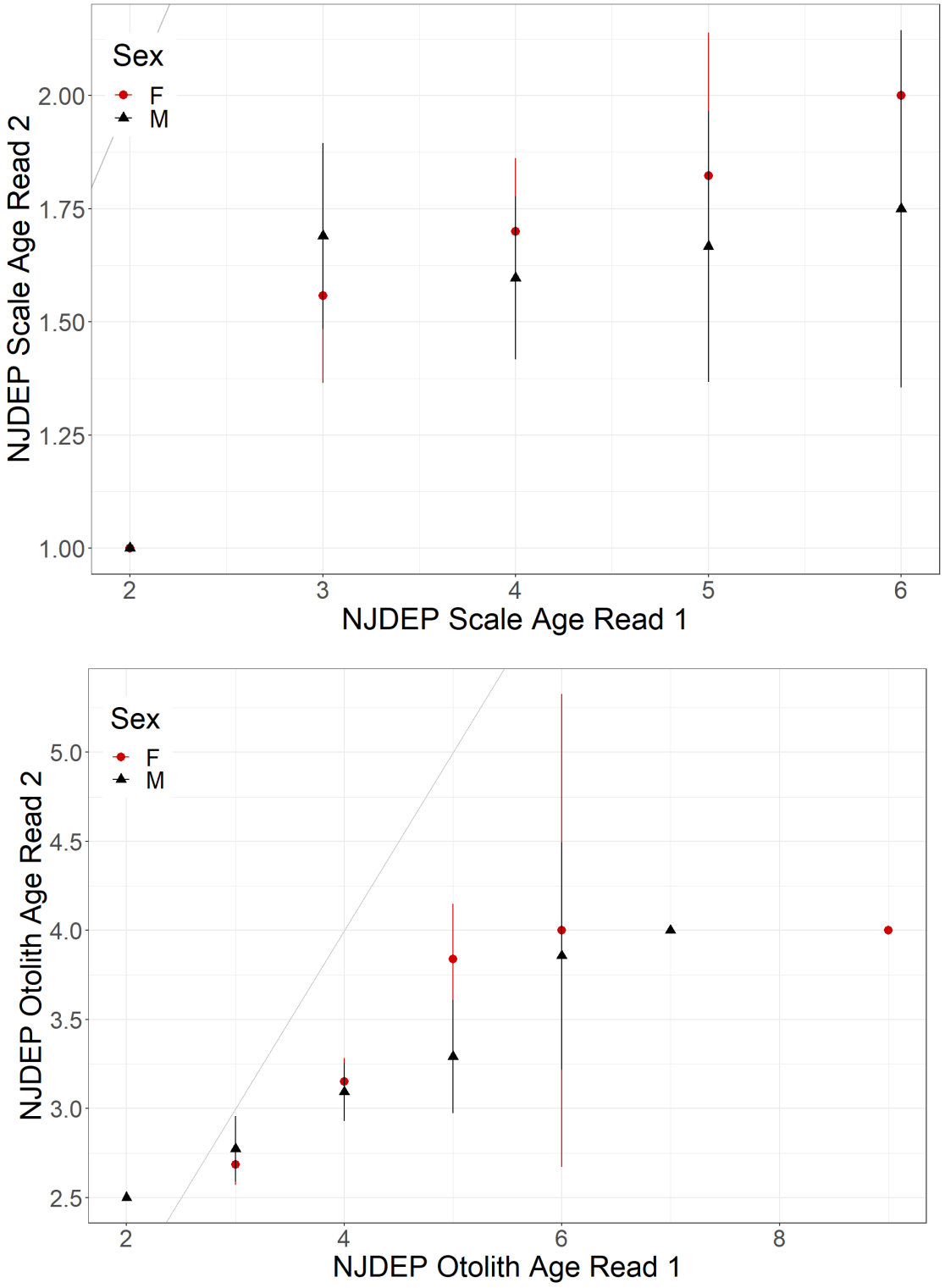

Figure 9. Paired age comparisons between Beaufort and VIMS Read 2 for scales (top) and otoliths (bottom) by sex. Dots represent mean and lines represent 95% confidence intervals for the difference between ages relative to the reference (x-axis) age.

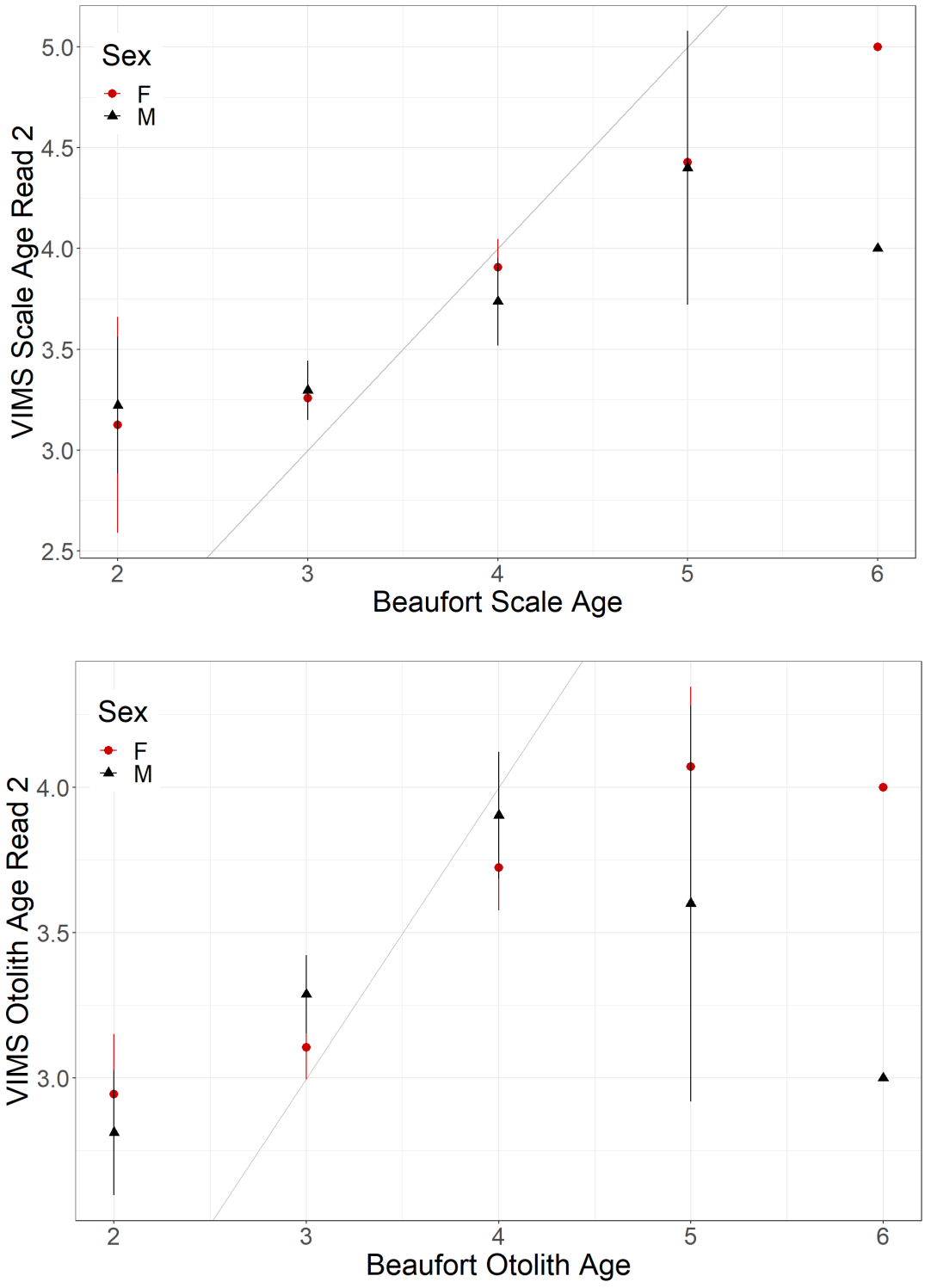

Figure 10. Paired age comparisons between NJDEP Reader 1 and VIMS Read 2 for scales (top) and otoliths (bottom) by sex. Dots represent mean and lines represent 95% confidence intervals for the difference between ages relative to the reference (x-axis) age.

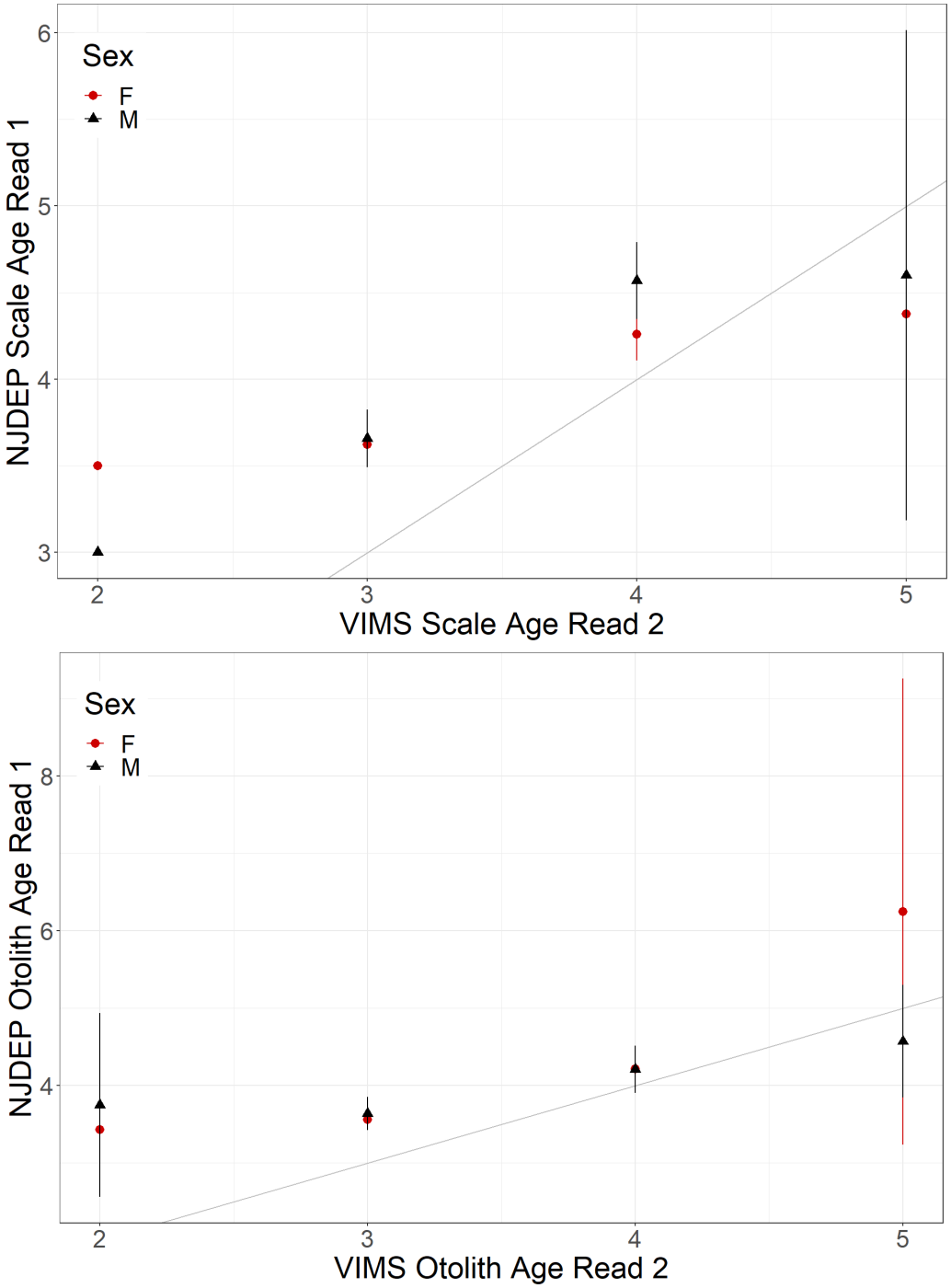

Figure 11. Paired age comparisons between NJDEP and Beaufort for scales (top) and otoliths (bottom) by sex. Dots represent mean and lines represent 95% confidence intervals for the difference between ages relative to the reference (x-axis) age.

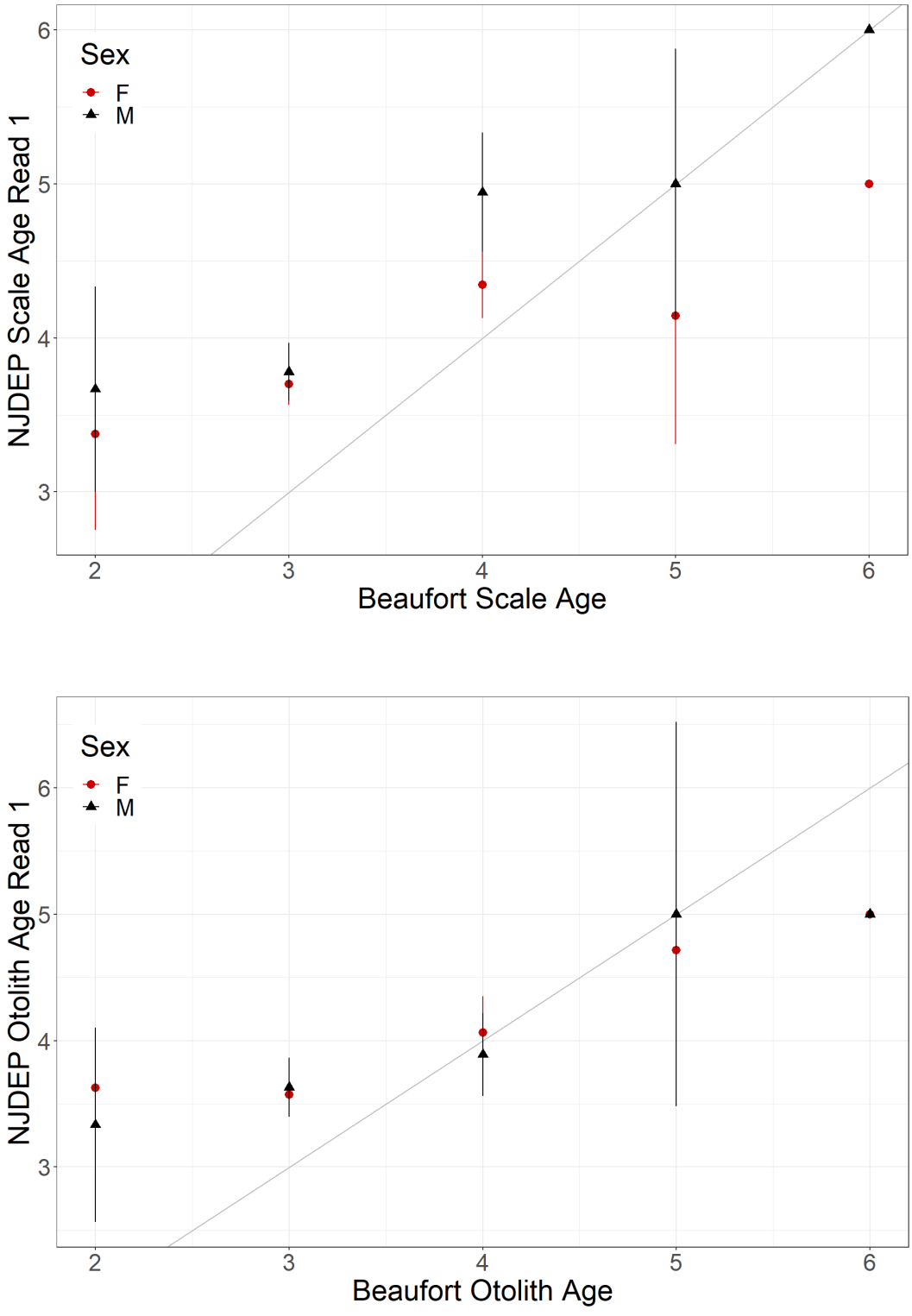

Figure 12. Scale vs otolith paired age comparisons for VIMS Read 2 (top left), NJDEP Reader 2 (top right), and Beaufort (bottom) by sex. Dots represent mean and lines represent 95% confidence intervals for the difference between ages relative to the reference (x-axis) age.

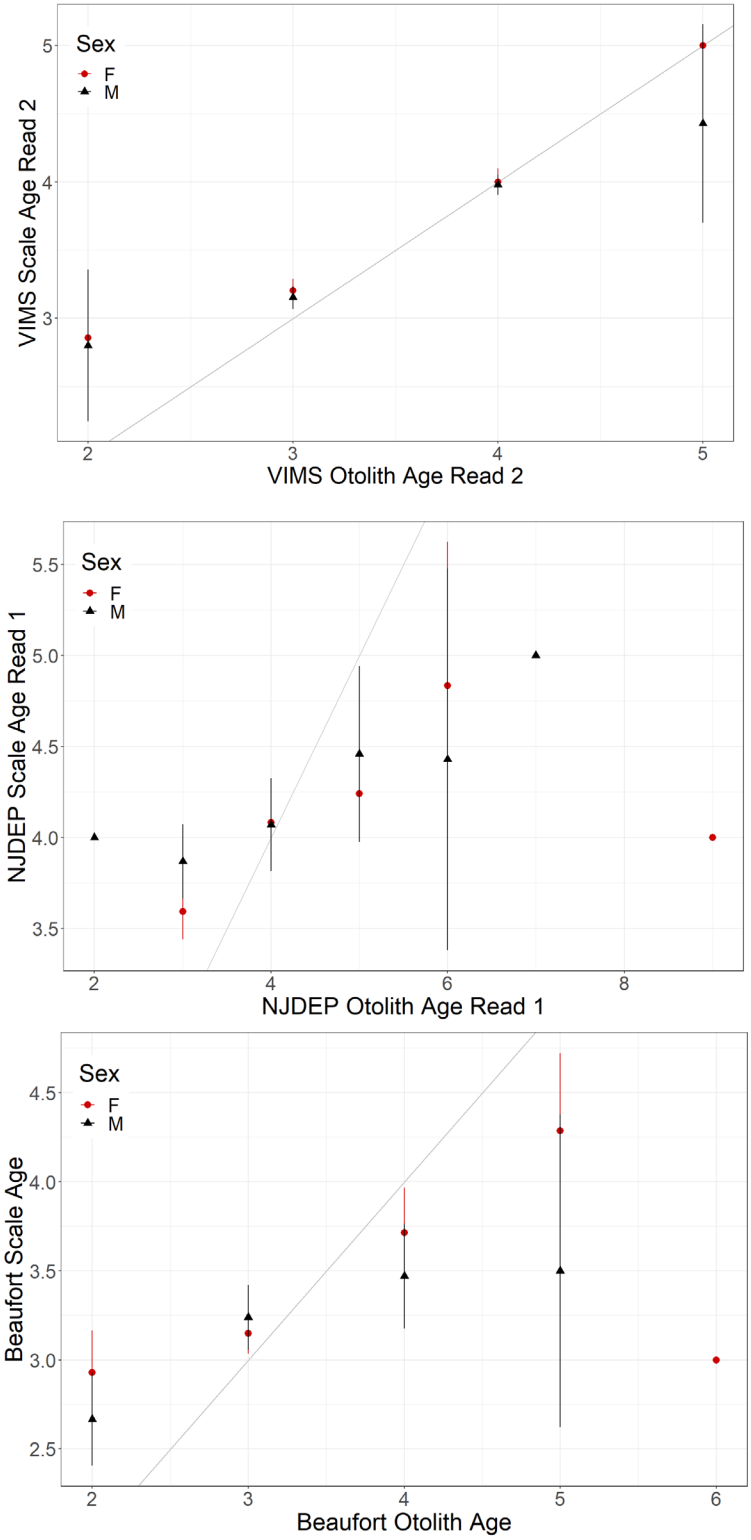

Figure 13. Size distribution of Atlantic menhaden samples used in ageing exchange. All samples were collected either at sea or at port in February 2022.

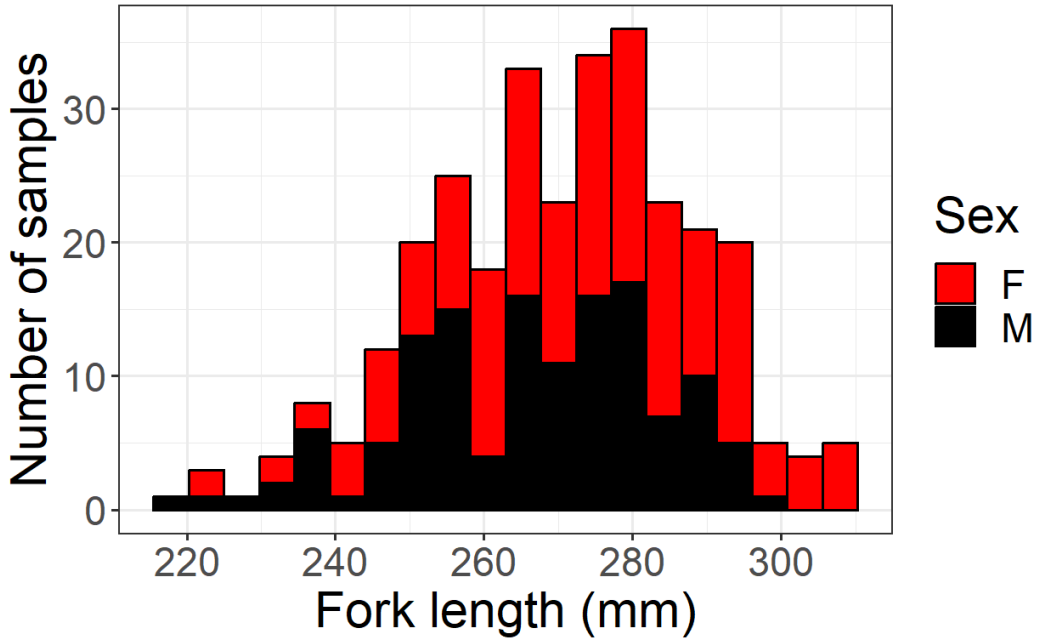

Ageing Atlantic Menhaden Scales (Beaufort lab)
12/15/22
A. Rezek

Reading scales to assign age

1- Note scale sample's fork length (FL), weight (Wt.) and capture date.
2- Using a stereo microscope with transmitted light, look at all mounted scales to see which are readable (clean, uniform, not torn, have distinct rings) and which rings are common among scales.
3- After finding the best scale, with ctenii pointed downward, locate the focus for a starting point (middle of the reading plane) and count annuli straight up the middle of the scale to the edge. Assign and record final age.
4- If the scale is questionable/unreadable, assign an age of 40, which indicates "unageable".

Identifying true annuli

- 1st annulus usually occurs ≥ 1.2 mm from focus.
- A true annulus will appear as a consistent dark line and is roughly parallel to the edge of the scale.
- A true annulus will hold up in the "shoulders" of the scale and cross the reading plane on both sides.
- Each consecutive annulus is ~ ½ the distance of previous annuli. If ring spacing does not make sense but ring follows other "rules" and is seen in most/all other scales, consider FL/Wt. May count questionable annulus as true.
- You may have a false annulus if it has black dashes ("stiches"), is inconsistent, looks smudged or is right next to another annulus. In some instances, a band of close rings may be counted as one annulus.

Assigning fish to the correct cohort

5- Pre June 1st: A virtual annulus is added to the seen annulus count if the scale has a wide margin (distance from last annulus to edge) where you expect to see an annulus soon and the fish was captured before June 1st. (=bumping age). Annuli should be deposited by June 1st for the spring cohort.
6- Post June 1st: Do not count an annulus near or on the edge, especially in the fall. Closely spaced annuli may be seen near the edge in older fish, so marginal increments vary.

Radius measurements to annuli and edge of the scale

7- Measure from the focus to each annulus and to the edge, up the middle of the scale and record. Do not measure scales with a virtual annulus (see Item 5).

Tips

- Generally, the smaller the scale, the younger the fish. The longer the ctenii, the older the fish.
- Ages 0-5 are seen in currently received bait and reduction fishery samples. [Reduction fishery samples May-October]

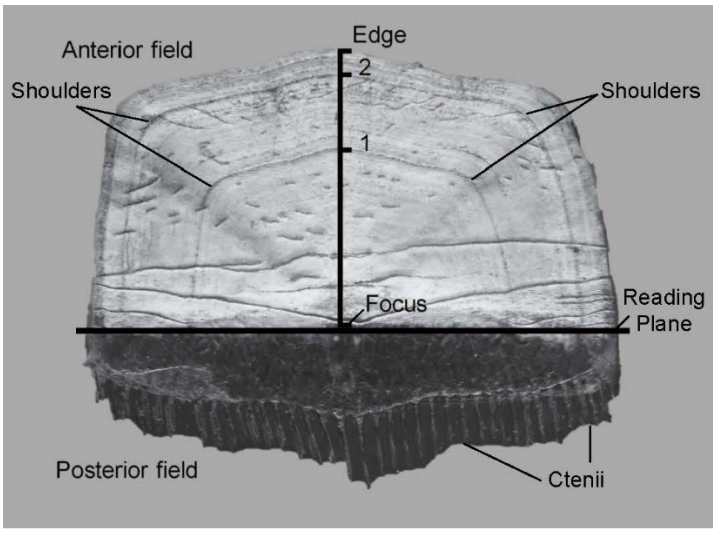

2 year old Atlantic menhaden scale

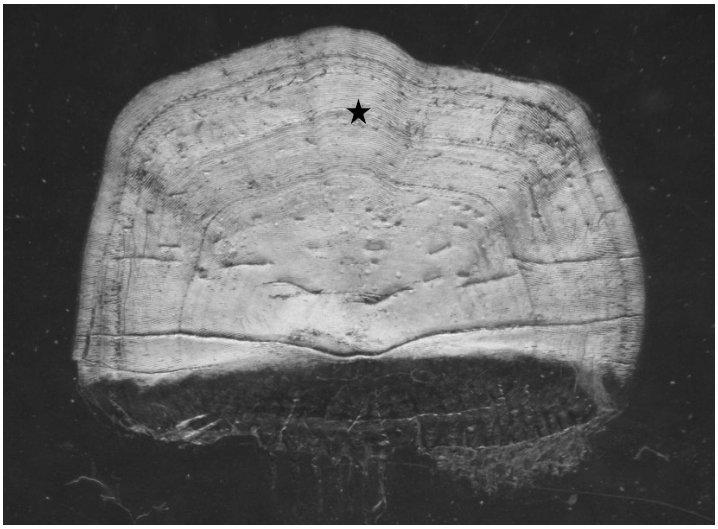
False annulus between 2 true annuli

VIMS MRG Atlantic Menhaden Ageing

Sample collection-

Atlantic Menhaden is a "Priority" species for its two major trawl surveys, NEAMAP and ChesMMAP. Priority species means that length, weight, sex, maturity state, stomach, and otoliths are collected for 5 individuals from each length bin on each tow. Paired otolith and scale samples were collected from the NEAMAP fisheries-independent trawl survey from 2015-2018. As otoliths are the preferred hard part for ageing other species, menhaden otoliths have been collected and aged from 2008 to present. Additionally, smaller grant funded projects and collaborations have paired scales and otoliths in 2018-2019 and again in 2022. The total number of whole otoliths that have been aged from the NEAMAP and ChesMMAP Trawl Surveys to date is 4,897 (NM 2,116, CM 2,781).

Scales-

Paired Atlantic menhaden scales and otolith samples will be removed from specimens at sea. Approximately 30-50 scales will be removed from each specimen. After collection, these scales are properly labeled and stored in capped vials in the freezer for later cleaning and processing in the laboratory. By freezing the scales rather than drying them, the scales will less likely be damaged. At the laboratory the scales will be thawed and lightly scrubbed in a soap and water solution to remove any debris and excess slime. Six of the best scales will be selected, thoroughly dried and pressed between two glass microscope slides with the sides of the slides taped closed on the ends. Due to variations in the scales, six samples are selected to provide the most accurate age for each specimen. Scale sample slides are preferably read using a microfiche reader. If no microfiche is available, then a stereo dissecting scope with transmitted light will suffice. Additionally, if the stereo microscope has imaging capabilities, larger images can be displayed to mimic the microfiche.

Whole Otoliths-

Atlantic menhaden sagittal otoliths are removed in the field as part of full specimen workup for up to 5 individuals of each size group from each station (sampling site). Both otoliths are extracted by making a shallow cut to the dorsal surface of the head of the menhaden with a serrated knife. In this case, shallow is defined as 0.25cm to 1cm, depending on the size of the individual. The otic capsule is located relatively close to the top of the skull. Otoliths can then be extracted using a pair of forceps. To assist in extraction, the otolithic membrane can be removed from the otic capsule, which often also removes the sagittal otoliths with it. The otoliths can then be carefully removed from the otolithic membrane for collection. Alternatively, the whole head of each menhaden sample can be removed with a serrated knife behind the operculum, labeled and frozen in storage bags to later have their delicate otoliths removed back at the laboratory. Due to the size and fragile nature of menhaden otoliths, careful extraction can more easily occur at the stable laboratory setting.

After otolith extraction, samples are dried and stored in small vials. Otoliths are read whole in a petri dish full of water or ethanol (Ethanol dries quickly and samples can be sealed back in storage vials more quickly), under a stereo dissecting microscope with transmitted light for the best contrast. Depending on the clarity and size of the otolith 25x zoom should be used with the otolith viewed in a watch glass full of 70% EtOH. This will assure no "clearing" (loss of visible annuli) will occur if the otoliths are dried, then stored. Wet stored otoliths straight from the otic cavity, read in water or read in ethanol can cause

clearing if sealed in a vial before drying. Sometimes a combination of reflected and transmitted light is necessary to distinguish annuli separation and boundaries.

The core of the otolith will appear as a circular, hollow shape in the center of the otolith. The core has a dark/opaque outline. This outline will be called the core boundary. The core boundary extends away from the core slightly up both the rostrum (long point) and antirostrum ("thumb") of each otolith. Figure 1.

The first annulus is often a thicker, darker band. Establishing the first annulus is critical to proper age assignment. The first annulus will often not have a lot of separation from the core boundary. The clearest separation to identifying the first annulus will occur on the rostrum.

Similar to the first annulus, any of the additional annuli will be best identified on the rostrum of the otolith. Starting with the first annulus, the annuli will gradually get thinner and lighter as the fish grows older. The best and clearest annuli can be traced all the way around the otolith. More difficult annuli can be checked by observing annuli on both the rostrum and antirostrum. Annuli are often less visible on the antirostrum, however the annuli often morphometrically visible by raised bumps along the inner edge of the antirostrum. Additionally, these raised bumps can be seen as layers of the otolith (like a typographical map). These layers can be traced to individual annuli around the otolith and are usually most visible on fish exhibiting more than one annulus.

Age Determination-

Spawning has been observed year-round with a concentration across fall and winter, October through March. Atlantic menhaden annuli deposition typically occurs from February to June depending on the latitude of the capture location. Annulus formation occurs post-spawn. The annulus formation on scales will usually be visible prior to the visible annulus formation on the otoliths.

Specimens caught by the VIMS ChesMMAP and NEAMAP surveys are randomly numbered to reduce bias. No specimen biological information is included with the three reads. Additionally, only the survey cruise is included with the random specimen number to serve as a capture date for final age determination. To reduce the subjective classification of margin codes, VIMS uses a simplified in-house version of margin coding. VIMS readers use the survey cruise number coupled with annulus formation proximity to the outer edges of the structure to assign either a Light or Dark "Edge Code", simply L or D. (The terms Light and Dark are used due to the nature of the otolith structure when read with transmitted light. The opaque banding of the annuli appears as a darker color with the transmitted light from the microscope). The larger translucent banding is observed as Light.

Typically, specimens caught during or around spawning will often have a new annulus forming on the edge of the structure, and these specimens will be observed with a Dark edge. Specimens caught prior to annuli deposition will be observed with the number of annuli present. These specimens will have their final age "bumped" +1 to account for the near-future deposition. The same Light and Dark edge code method can be applied to scale structure age determination as well.

There are three readers at VIMS and the mode age for each sample (both scales and otoliths) is provided as the final age. If there is no mode from the initial read, the readers reread the sample and if there is still no mode, they examine the sample together and come to a consensus age. If a consensus age cannot be determined the sample is discarded. Very few samples are discarded. Precision tests are

preformed within each reader (multiple reads of the same sample) and between readers. VIMS uses similar precision and symmetry tests to the NEFSC.

Figure 1. (NM1604, final Age-2. VIMS recorded as 2 D).